

NASA Contractor Report 187578

1N-36

26658

P204

**Energy Transfer Processes Between
Tm³⁺ and Ho³⁺ in LiYF₄**

(NASA-CR-187578) ENERGY TRANSFER PROCESSES
BETWEEN Tm(3+) AND Ho(3+) IN LiYF₄ Ph.D.
Thesis Final Report (Boston Coll.) 204 p
CSCL 20E

N91-27530

Unclas

63/36 0026658

Gönül Özen

BOSTON COLLEGE
Chestnut Hill, Massachusetts

Grant NAG1-955
July 1991

NASA

National Aeronautics and
Space Administration

Langley Research Center
Hampton, Virginia 23665-5225

ABSTRACT

This work consists of a detailed study of the spectroscopic properties of the crystal LiYF_4 doped with Thulium (Tm) and Holmium (Ho) ions. The purpose of this study is to understand the basic processes that regulate the transfer of energy between these two ions in this crystal. In this system Tm is considered the donor ion and Ho the acceptor ion.

Spectral data were obtained on three samples available: $\text{LiYF}_4:\text{Tm}^{3+}$ (.5%), $\text{LiYF}_4:\text{Ho}^{3+}$ (1%), and $\text{LiYF}_4:\text{Tm}^{3+}$ (5%), Ho^{3+} (.2%). These data, which include absorption, luminescence, excitation and the response to pulsed excitation in a wide range of temperatures, have allowed us to look at the dynamics of the energy transfer processes by considering the kinetic evolution of the emission of the two ions (donor and acceptor) involved in the process and the basic spectroscopic properties related to them. This inclusive approach has led to the validation of our physical model.

It was of great interest to find that the energy transfer processes between the $^3\text{F}_4$ spectral manifold of the Tm ion and the $^5\text{I}_7$ spectral manifold of the Ho ion cause a thermal equilibration of the excitation in these two manifolds. This fact has important implications for the laser applications of this system.

ACKNOWLEDGEMENTS

I would like to express my sincere gratitude to Professor Baldassare Di Bartolo for his support, patience, advice and encouragement during the entire period of my graduate work.

Special thanks to Professors B. Di Bartolo and M. Graf for their critical reading of this manuscript, and to Dr. C. W. Struck for his comments and suggestions.

I wish to thank Professors B. Di Bartolo, R. Uritam, M. Graf, and A. M. Buoncristiani for serving on my thesis committee.

My thanks are also directed to the members of the Physics Department, especially Ms. Sherley Lynch, for their friendship and encouragement. I also would like to thank Mr. Everett Casey for his help in the preparation of the experiments in the solid state physics laboratory.

I would like to acknowledge the support of NASA Grant NAG - 1 - 955 and the Laser Technology and Applications Branch of the Flight Electronics Division of the Langley Research Center of Hampton, Virginia for technical assistance and for providing me with the opportunity of using their spectroscopy laboratory. I am especially grateful to Addison T. Inge for his help during the experiments and the measurements made at the laboratory.

I wish to thank Drs. G. Armagan and John Collins for their help and support in my first years at Boston College.

I extend very special words of thanks to Professor Özcan Öktü, Professor Önder Pekcan, Francis Xavier, Stevan Radojev, Emel Hadzipasic, Birsen Alaçakır, Laurie Ortyl, Melissa Pereira, Sam and Beth Perry, and Indrani Bhattacharya for their friendship, support and encouragement.

Finally I would like to express my deepest appreciation for my parents, *Emin* and *Türkan Özen*, for my sisters *Güler* and *Sevgi*, and for my brother *Tevfik* whose love, encouragement and inspiration made it all possible.

TABLE OF CONTENTS

	Page
ABSTRACT.....	i
ACKNOWLEDGEMENTS.....	ii
TABLE OF CONTENTS.....	iv
LIST OF TABLES.....	vii
LIST OF FIGURES.....	x
1. INTRODUCTION.....	1
References.....	4
2. THEORY OF ENERGY TRANSFER AMONG IONS IN SOLIDS.....	6
2.1 Nonradiative Energy Transfer.....	8
2.1.1 Resonant Energy Transfer.....	8
2.1.2 Nonresonant Energy Transfer.....	12
2.2 Radiative Energy Transfer.....	14
2.3 Statistical Treatment of Energy Transfer processes.....	15
References.....	19
3. EXPERIMENTAL APPARATUS.....	22
3.1 Absorption Spectrometer.....	23
3.2 Continuous Luminescence Apparatus.....	24
3.2.1 The Exciting System.....	24
3.2.2 The Analyzing System.....	24
3.2.3 The Detecting and Amplifying System.....	25
3.2.4 The Recording System.....	26
3.2.5 The Temperature Regulating Devices.....	27
3.3 Pulsed Luminescence Apparatus.....	29
3.3.1 The Exciting System.....	29
3.3.2 The Analyzing System.....	29
3.3.3 The Detecting System.....	29
3.3.4 The Recording System.....	30
3.3.5 The Temperature Regulating System.....	30

TABLE OF CONTENTS
(continued)

	Page
4. SAMPLES EXAMINED.....	42
4.1 Optical and Physical Properties of the Host Lattice, LiYF ₄	43
4.2 The Rare Earth Ions in a Crystalline Solid.....	44
4.3 Optical Properties of Tm ³⁺ in LiYF ₄	46
4.4 Optical Properties of Ho ³⁺ in LiYF ₄	47
References.....	49
5. EXPERIMENTAL RESULTS I. ABSORPTION AND LUMINESCENCE MEASUREMENTS.....	57
5.1 LiYF ₄ : Tm ³⁺ (.5%).....	57
5.2 LiYF ₄ : Ho ³⁺ (1%).....	59
5.3 LiYF ₄ : Tm ³⁺ (5%), Ho ³⁺ (.2%).....	60
6. EXPERIMENTAL RESULTS II. EXCITATION MEASUREMENTS.....	98
6.1 LiYF ₄ : Tm ³⁺ (.5%).....	98
6.2 LiYF ₄ : Ho ³⁺ (1%).....	99
6.3 LiYF ₄ : Tm ³⁺ (5%), Ho ³⁺ (.2%).....	100
7. EXPERIMENTAL RESULTS III. LIFETIME MEASUREMENTS.....	113
7.1 LiYF ₄ : Tm ³⁺ (.5%).....	114
7.2 LiYF ₄ : Ho ³⁺ (1%).....	116
7.3 LiYF ₄ : Tm ³⁺ (5%), Ho ³⁺ (.2%).....	117
8. DISCUSSION OF RESULTS I.ABSORPTION, LUMINESCENCE AND EXCITATION.....	155
8.1 LiYF ₄ : Tm ³⁺ (.5%).....	155
8-2 LiYF ₄ : Ho ³⁺ (1%).....	157
8-3 LiYF ₄ :Tm ³⁺ (5%), Ho ³⁺ (.2%).....	158

TABLE OF CONTENTS
(continued)

	Page
9. DISCUSSION OF RESULTS II. DECAY PATTERNS AND (Tm) ³ F ₄ ↔ (Ho) ⁵ I ₇ ENERGY TRANSFER.....	170
9-1 Considerations on Luminescence Decay Patterns.....	171
9-2 LiYF ₄ : Tm ³⁺ (.5%).....	174
9-3 LiYF ₄ : Ho ³⁺ (1%at.).....	175
9-4 LiYF ₄ :Tm ³⁺ (5%), Ho ³⁺ (.2%).....	176
10. CONCLUSIONS.....	185

List of Tables

Table		Page
3.1	Specifications of the Lexel Model 526 Ar-Ion laser.....	31
3.2	Specifications of Quantel Model TDL-51 dye laser.....	32
3.3	Specifications of Quantel Model 660A-10 YAG : Nd ³⁺ laser.....	33
3.4	Specifications of EG&G dye laser.....	34
4.1	Optical, physical and mechanical properties of LiYF ₄	51
5.1	Absorption spectrum of LiYF ₄ : Tm ³⁺ (.5%) at 300K.....	61
5.2	Optical luminescence spectrum of LiYF ₄ : Tm ³⁺ (.5%) at 300K.....	63
5.3	Infrared luminescence spectrum LiYF ₄ : Tm ³⁺ (.5%).....	64
5.4	Temperature dependence of Tm ³⁺ optical luminescence in LiYF ₄	65
5.5	Temperature dependence of Tm ³⁺ 1.9 μm luminescence in LiYF ₄	66
5.6	Absorption spectrum of LiYF ₄ : Ho ³⁺ (1%) at 300K.....	67
5.7	Optical luminescence spectrum of LiYF ₄ : Ho ³⁺ (1%) at 300K.....	71
5.8	Infrared luminescence spectrum LiYF ₄ : Ho ³⁺ (1%).....	73
5.9	Temperature dependence of Ho ³⁺ 2.1 μm luminescence in LiYF ₄	74
5.10	Absorption spectrum of LiYF ₄ : Tm ³⁺ (5%), Ho ³⁺ (.2%) at 300K.....	75
5.11	Optical luminescence spectrum of LiYF ₄ : Tm ³⁺ (5%), Ho ³⁺ (.2%) at 300K.....	78

List of Tables

(continued)

Table		Page
5.12	Infrared luminescence spectrum of LiYF ₄ : Tm ³⁺ (5%) Ho ³⁺ (.2%).....	80
6.1	Excitation spectrum of LiYF ₄ : Tm ³⁺ (.5%) at 300K (1.7 μm luminescence monitored).....	101
6.2	Excitation spectrum of LiYF ₄ : Ho ³⁺ (1%) at 300K (2.1 μm luminescence monitored).....	103
6.3	Excitation spectrum of LiYF ₄ : Tm ³⁺ (5%), Ho ³⁺ (.2%) at 300K (1.7 μm luminescence monitored).....	105
6.4	Excitation spectrum of LiYF ₄ : Tm ³⁺ (5%), Ho ³⁺ (.2%) at 300K (2.1 μm luminescence monitored).....	107
7.1	Temperature dependence of Tm ³⁺ (³ H ₄ level) lifetime in LiYF ₄ :Tm ³⁺ (.5%at.).....	118
7.2	Decay times of the infrared emission of LiYF ₄ : Tm ³⁺ (.5%) at various wavelengths for T=300, 77 and 8K.....	119
7.3	Temperature dependence of Tm ³⁺ (³ F ₄ level) lifetime in LiYF ₄ : Tm ³⁺ (.5% at.).....	120
7.4	Temperature dependence of Ho ³⁺ (⁵ I ₇ level) lifetime in LiYF ₄ : Ho ³⁺ (1%at.).....	122
7.5	Decay times of the infrared emission of LiYF ₄ : Tm ³⁺ (5%), Ho ³⁺ (.2%) at various wavelengths for T=300, 77 and 8K.....	124
7.6	Temperature dependence of Tm ³⁺ and Ho ³⁺ (³ F ₄ and ⁵ I ₇ levels) lifetimes in LiYF ₄ : Tm ³⁺ (5%), Ho ³⁺ (.2%) (³ H ₄ level is excited).....	125

List of Tables
(continued)

Table		Page
7.7	Temperature dependence of Tm^{3+} and Ho^{3+} lifetimes in $LiYF_4 : Tm^{3+}(5\%)$, $Ho^{3+}(.2\%)$ (5S_2 level is excited).....	127
8.1	The temperature dependence of the absorption coefficient integral of 5I_7 level of Ho^{3+} in $LiYF_4$	159
8.2	The temperature dependence of R^6_o , $C^{(6)}$, and the reciprocal lifetime of 3F_4 level of Tm^{3+} in $LiYF_4$	160

List of Figures

Figure		Page
2.1	Typical sequences of events for energy transfer from one excited ion to other unexcited ion.....	20
2.2	The initial and the final states of two-atom system.....	21
2.3	Nonresonant energy transfer from one excited ion to other unexcited ion.....	21
3.1	Block diagram of the continuous luminescence apparatus.....	35
3.2	Photocathode spectral response characteristics of the RCA Model C31034 photo-tube.....	36
3.3	Dewar (Model 8DT "SuperVaritemp").....	37
3.4	Block diagram of the pulsed luminescence apparatus.....	38
3.5	Transmission spectra of the filters.....	39
	(a) : central wavelength is 1.8 μm	
	(b) : central wavelength is 1.9 μm	
	(c) : central wavelength is 2.1 μm	
3.6	Preamplifier circuit for InAs infrared detector.....	40
4.1	Energy levels of Tm^{3+} and Ho^{3+} in LiYF_4	52
4.2	The phase diagram of the $\text{LiF} - \text{YF}_3$	53
4.3	Refractive indices of LiYF_4 crystal.....	54
4.4	Transmission limits of LiYF_4	54

List of Figures

(continued)

Figure		Page
4.5	Energy levels of the rare earths in LaCl_3	55
4.6	The decay channels and the lifetimes of Ho^{3+} (Ho concentration is 1% at.; $^5\text{S}_2$ level is excited).....	56
5.1 (a)	The absorption spectrum of Tm^{3+} in LiYF_4 in optical region.....	82
5.1 (b)	The absorption spectrum of Tm^{3+} in LiYF_4 in infrared region.....	83
5.2	The optical luminescence spectra of Tm^{3+} in LiYF_4 at 300K.....	84
5.3 (a)	The infrared luminescence spectra of Tm^{3+} in LiYF_4 at 78 and 300K (luminescence detected in the direction of the c-axis of the sample.....	85
5.3 (b)	The infrared luminescence spectra of Tm^{3+} in LiYF_4 at 78 and 300K (luminescence detected at 90° to the c-axis of the sample.....	86
5.4	Temperature dependence of Tm^{3+} luminescence in LiYF_4 ($^3\text{H}_4$ level).....	87
5.5	Temperature dependence of Tm^{3+} luminescence in LiYF_4 ($^3\text{F}_4$ level).....	88
5.6 (a)	The absorption spectrum of Ho^{3+} in LiYF_4 in optical region.....	89
5.6 (b)	The absorption spectrum of Ho^{3+} in LiYF_4 in infrared region	90
5.7	The optical luminescence of Ho^{3+} in LiYF_4 at 300K.....	91
5.8	The infrared luminescence of Ho^{3+} in LiYF_4 at 78 and 300K.....	92

List of Figures

(continued)

Figure		Page
5.9	Temperature dependence of Ho ³⁺ 2.1μm luminescence in LiYF ₄	93
5.10 (a)	The absorption spectrum of LiYF ₄ : Tm ³⁺ , Ho ³⁺ in optical region.....	94
5.10 (b)	The absorption spectrum of LiYF ₄ : Tm ³⁺ , Ho ³⁺ in infrared region.....	95
5.11	The optical luminescence spectrum of LiYF ₄ : Tm ³⁺ , Ho ³⁺ at 300K.....	96
5.12	The infrared luminescence spectrum of LiYF ₄ : Tm ³⁺ , Ho ³⁺ at 300K...	97
6.1	The excitation spectra of 1.7 μm Tm ³⁺ luminescence in LiYF ₄	109
6.2	The excitation spectra of 2.1 μm Ho ³⁺ luminescence in LiYF ₄	110
6.3 (a)	The excitation spectra of LiYF ₄ : Tm ³⁺ , Ho ³⁺ at 300K (luminescence is monitored at 1.7 μm).....	111
6.3 (b)	The excitation spectra of LiYF ₄ : Tm ³⁺ , Ho ³⁺ at 300K (luminescence is monitored at 2.1 μm).....	112
7.1	Temperature dependence of lifetime of optical luminescence from 3H ₄ level of Tm in LiYF ₄ (Excitation into the 3F ₃ level).....	129
7.2 (a)	Decay pattern of 1.6 μm emission of LiYF ₄ : Tm ³⁺ (.5%) at T = 300K.....	130
7.2 (b)	Decay pattern of 1.6 μm emission of LiYF ₄ : Tm ³⁺ (.5%) at T = 77K.....	131
7.2 (c)	Decay pattern of 1.6 μm emission of LiYF ₄ : Tm ³⁺ (.5%) at T = 8K.....	132
7.3 (a)	Decay pattern of 1.8 μm emission of LiYF ₄ : Tm ³⁺ (.5%) at T = 300K.....	133
7.3 (b)	Decay pattern of 1.8 μm emission of LiYF ₄ : Tm ³⁺ (.5%) at T = 77K.....	134

List of Figures

(continued)

Figure		Page
7.3 (c)	Decay pattern of 1.8 μm emission of $\text{LiYF}_4 : \text{Tm}^{3+}(.5\%)$ at $T = 8\text{K}$	135
7.4 (a)	Beginning of the decay patterns of the infrared emission of $\text{LiYF}_4 : \text{Tm}^{3+}(.5\%)$ at $T = 300\text{K}$	136
7.4 (b)	Beginning of the decay patterns of the infrared emission of $\text{LiYF}_4 : \text{Tm}^{3+}(.5\%)$ at $T = 77\text{K}$	137
7.4 (c)	Beginning of the decay patterns of infrared emission of $\text{LiYF}_4 : \text{Tm}^{3+}(.5\%)$ at $T = 8\text{K}$	138
7.5	Temperature dependence of Tm^{3+} infrared luminescence lifetime in LiYF_4 (Excitation into the $^3\text{H}_4$ level).....	139
7.6 (a)	Decay pattern of 2.1 μm emission of $\text{LiYF}_4 : \text{Ho}^{3+}(.2\%)$ at $T = 300\text{K}$	140
7.6 (b)	Decay pattern of 2.1 μm emission of $\text{LiYF}_4 : \text{Ho}^{3+}(.2\%)$ at $T = 77\text{K}$	141
7.7	Temperature dependence of Ho^{3+} infrared luminescence lifetime in LiYF_4 (Excitation into the $^5\text{S}_2$ level).....	142
7.8 (a)	Decay pattern of 1.6 μm emission of $\text{LiYF}_4 : \text{Tm}^{3+}(5\%), \text{Ho}^{3+}(.2\%)$ at $T = 300\text{K}$	143
7.8 (b)	Decay pattern of 1.6 μm emission of $\text{LiYF}_4 : \text{Tm}^{3+}(5\%), \text{Ho}^{3+}(.2\%)$ at $T = 77\text{K}$	144

List of Figures

(continued)

Figure		Page
7.8 (c)	Decay pattern of 1.6 μm emission of $\text{LiYF}_4 : \text{Tm}^{3+}(5\%)$ $\text{Ho}^{3+}(.2\%)$ at $T = 8\text{K}$	145
7.9 (a)	Decay pattern of 2.1 μm emission of $\text{LiYF}_4 : \text{Tm}^{3+}(5\%)$ $\text{Ho}^{3+}(.2\%)$ at $T = 300\text{K}$	146
7.9 (b)	Decay pattern of 2.1 μm emission of $\text{LiYF}_4 : \text{Tm}^{3+}(5\%)$ $\text{Ho}^{3+}(.2\%)$ at $T = 77\text{K}$	147
7.9 (c)	Decay pattern of 2.1 μm emission of $\text{LiYF}_4 : \text{Tm}^{3+}(5\%)$ $\text{Ho}^{3+}(.2\%)$ at $T = 8\text{K}$	148
7.10 (a)	Beginning of the decay patterns of the infrared emission of $\text{LiYF}_4 : \text{Tm}^{3+}(5\%), \text{Ho}^{3+}(.2\%)$ at $T = 300\text{K}$	149
7.10 (b)	Beginning of the decay patterns of the infrared emission of $\text{LiYF}_4 : \text{Tm}^{3+}(5\%), \text{Ho}^{3+}(.2\%)$ at $T = 77\text{K}$	150
7.10 (c)	Beginning of the decay patterns of infrared emission of $\text{LiYF}_4 : \text{Tm}^{3+}(5\%), \text{Ho}^{3+}(.2\%)$ at $T = 8\text{K}$	151
7.11	Temperature dependence of $\text{LiYF}_4 : \text{Tm}^{3+}(5\%), \text{Ho}^{3+}(.2\%)$ infrared luminescence lifetime (Excitation into the $^3\text{H}_4$ level of Tm).....	152
7.12	Temperature dependence of $\text{LiYF}_4 : \text{Tm}^{3+}(5\%), \text{Ho}^{3+}(.2\%)$ infrared luminescence lifetime (Excitation into the $^5\text{S}_2$ level of Ho).....	153

List of Figures
(continued)

Figure		Page
7.13	Temperature dependence of LiYF ₄ : Tm ³⁺ (5%at.),Ho ³⁺ (.2%at.) 2.1 μm luminescence lifetime.....	154
	(a) ³ H ₄ energy level of Tm is excited.	
	(b) ⁵ S ₂ energy level of Ho is excited.	
8.1	The absorption spectrum of ³ F ₄ level of Tm ³⁺ in LiYF ₄	161
	(a) at T=300K.	
	(b) at T=78K.	
8.2	Comparison of the temperature dependence of the integrated intensity and the lifetime of the ³ H ₄ level of Tm in LiYF ₄	162
8.3	Comparison of the temperature dependence of the integrated intensity and the lifetime of the ³ F ₄ level of Tm in LiYF ₄	163
8.4	The absorption spectrum of ⁵ I ₇ level of Ho ³⁺ in LiYF ₄	164
	(a) at T=300K.	
	(b) at T=78K.	
8.5	The temperature dependence of the absorption coefficient integral of ⁵ I ₇ level of Ho ³⁺ in LiYF ₄	165
8.6	Comparison of the temperature dependence of the integrated intensity and the lifetime of the ⁵ I ₇ level of Ho in LiYF ₄	166
8.7	The spectral overlap between normalized emission spectrum of ³ F ₄ level of Tm ³⁺ and the absorption spectrum of Ho ³⁺ in LiYF ₄	167
8.8	The temperature dependence of the overlap integral between the emission spectrum of ³ F ₄ level of Tm ³⁺ and the absorption spectrum oh ⁵ I ₇ level of Ho ³⁺ in LiYF ₄	168

List of Figures

(continued)

Figure		Page
8.9	The temperature dependence of $R^6_0 C^{(6)}$, and the reciprocal lifetime of 3F_4 level of Tm^{3+} in $LiYF_4$	169
9.1	Three level system with two metastable states.....	180
9.2 (a)	Emission patterns at early times of the decay of the infrared emission of $LiYF_4 : Tm^{3+}(5\%at.), Ho^{3+}(.2\%at.)$ at various wavelengths at $T = 8K$ (excitation is into the 3H_4 level of Tm).....	181
9.2 (b)	Emission patterns at early times of the decay of the infrared emission of $LiYF_4 : Tm^{3+}(5\%at.), Ho^{3+}(.2\%at.)$ at various wavelengths at $T = 77K$ (excitation is into the 3H_4 level of Tm).....	182
9.2 (c)	Emission patterns at early times of the decay of the infrared emission of $LiYF_4 : Tm^{3+}(5\%at.), Ho^{3+}(.2\%at.)$ at various wavelengths at $T = 300K$ (excitation is into the 3H_4 level of Tm).....	183
9.2 (d)	Emission patterns at early times of the decay of the infrared emission of $LiYF_4 : Tm^{3+}(5\%at.), Ho^{3+}(.2\%at.)$ at various wavelengths at $T = 500K$ (excitation is into the 3H_4 level of Tm).....	184

1. INTRODUCTION

Energy transfer processes are very important in solid state laser systems because they can provide an enhancement of the luminescence emission and a consequent reduction of the laser threshold. This is usually achieved by the introduction of an ion of a different type, called sensitizer or donor, into the laser host material in addition to the ion, called activator or acceptor, responsible for the laser emission. The donor ion absorbs strongly where the pumping source emits, and transfers its excitation energy to the acceptor.

Most of the research on LiYF_4 - based crystals has addressed problems such as the laser threshold, output energy versus input energy curve, laser pulse characteristics etc. [1-10]. Chickles et al. [2] observed high efficiency pulsed laser action in alphabet (doped with Er^{3+} , Tm^{3+} , and Ho^{3+}) LiYF_4 at a wavelength of 2.06 microns at room temperature for the first time in 1971. Ho^{3+} lasing action assisted by energy transfer has also been observed in Ho^{3+} doped alphabet yttrium aluminum garnet [11], glass [12], yttrium iron garnet [13], ErO_3 [14] as well as other materials.

Johnson et al. [15] reported energy transfer between Er^{3+} and Tm^{3+} , and Er^{3+} and Ho^{3+} in CaMoO_4 . CaMoO_4 has the same crystal structure as LiYF_4 . They found that the enhancement of infrared emission from Tm^{3+} and Ho^{3+} ions is due to the energy transfer from Er^{3+} ions. Jenssen et al. studied some of the characteristics of various rare earth lasers [16], and reported the energy levels and the laser wavelengths for Ce^{3+} , Pr^{3+} , Nd^{3+} , Tb^{3+} , Ho^{3+} , Er^{3+} and Tm^{3+} ions in LiYF_4 .

In order to optimize the performance of a sensitized laser, it is necessary to know in detail what energy transfer steps are involved, their rates, and dependences on temperature and concentrations of the different ions. Bernier et al. [17,18] considered the sensitization of the 2 micron emission of Ho^{3+} by the Er^{3+} ions in LiYF_4 , and described the $\text{Er}^{3+} \rightarrow \text{Ho}^{3+}$ energy transfer by using rate equations. They measured the decay pattern and the lifetime of $\text{Ho}^{3+} 5I_7$ energy level as a function of the Er^{3+} excitation level and of the Ho^{3+} concentration. They found that the lifetime of the $5I_7$ level increases with increasing Ho^{3+} concentration. The same group also studied the excited state dynamics of the Tm^{3+} ions and the $\text{Tm}^{3+} \rightarrow \text{Ho}^{3+}$ energy transfer in LiYF_4 at room temperature [19,20]. They showed that when Tm^{3+} ions are excited in their $3H_4$ level three relaxation channels have to be considered: relaxation to the ground state, a cross-relaxation process within the Tm^{3+} system and energy transfer from Tm^{3+} to Ho^{3+} . They reported that the $\text{Tm}^{3+} \rightarrow \text{Ho}^{3+}$ energy transfer is dominant for high Ho^{3+} concentrations.

The energy levels of rare earth ions are not strongly effected by the host material. However, the nature of the host material is relevant to the energy transfer process for a number of reasons. First, in many cases the energy transfer process needs the assistance of phonons, whose frequency and population at a certain temperature depend on the nature of the material. Second, one complicated effect is due to the influence of the thermal vibrations on the kinetics of the excitation and deexcitation of the relevant levels of sensitizer and activator. Finally, thermal vibrations may also effect the positions and width of sharp levels; even if such effects are small, they may be important in the case of resonant transfer. The temperature is extremely important for

these processes, and may provide a key to the full understanding of the energy transfer mechanism.

In this research, the temperature dependence of the energy transfer from Tm to Ho (both are rare earths) in LiYF_4 (called YLF) was studied in a systematic way. Ho is known to lase in the 2 micron region, and Tm at slightly shorter wavelengths. LiYF_4 crystals have some advantages over the other laser hosts. For example they have a scheelite structure, and so rare earth ions can be substitute in the Y^{3+} sites without charge compensation. It also has a lower phonon energy cut off than $\text{Y}_3\text{Al}_5\text{O}_{12}$, called YAG, which is a well known host material for rare earths.

The outline of this thesis is as follows: The theory of energy transfer processes is presented in Chapter 2. Chapter 3 deals with the experimental set-ups and the detailed design of the system. The samples were examined and their optical properties are presented in Chapter 4. The Chapters 5, 6 and 7 contain the experimental results obtained. The results are discussed in Chapters 8 and 9. The final chapter gives the conclusions of this study.

REFERENCES (Chapter 1)

- 1) R. L. Remski, L. T. James, Jr., K. H. Gooen, B. Di Bartolo, and Linz, IEEE J. Quantum Electron., Vol. QE-5, 214 (1969).
- 2) E. P. Chicklis, C. S. Naiman, and R. C. Folweiler, Apply. Phys. Lett. Vol.19, 119 (1971).
- 3) E. P. Chicklis, C. S. Naiman, R. C. Folweiler, and J. C. Doherty, IEEE J. Quantum Electron., Vol. QE-8, 225 (1972).
- 4) E. P. Chicklis, R. C. Folweiler, C. S. Naiman, D. R. Gabbe, A. Linz, and H. P. Jenssen, Tech. Report ECOM-73-0066-E (1974).
- 5) E. P. Chicklis, C. S. Naiman, L. Esterowitz, and R. Allen, IEEE J. Quantum Electron., Vol. QE-13, 893 (1977).
- 6) M. G. Knights, W. F. Wing, J. W. Baer, E. P. Chicklis, and H. P. Jenssen, IEEE J. Quantum Electron., Vol. QE-18, 163 (1982).
- 7) H. Hemmati, Tech. Report, Contractor: Jet Propulsion Laboratory, NASA Case No. NPO-17282-1-CU (1988).
- 8) Y. Kalisky, J. Kagan, H. Lotem and D. Sagie, Optics Commun., Vol.65, 359 (1988).
- 9) R. C. Eckardt, Esterowitz and Y. P. Lee, IEEE Quantum Electron., Vol. QE-12, 380 (1976).
- 10) N. P. Barnes, D. J. Levinos, and J. E. Griggs, SPIE (LASL Optics Conference), Vol.190, 297 (1979).
- 11) L. F. Johnson, J. E. Geusic, and L.G. Van Uitert, Appl. Phys. Lett., Vol.8, 200 (1966).

- 12) H. W. Gandy, R. J. Ginther, and J. F. Weller, Appl. Phys. Lett., Vol. 21, 37 (1966).
- 13) R. H. Hoskins and B. H. Soffer, IEEE J. Quantum Electron., Vol. QE-2, 253 (1966).
- 14) L. F. Johnson, J. P. Remeika, and J. F. Dillon, J. Phys. Lett., Vol. 21, 37 (1966).
- 15) L. F. Johnson, L. G. Van Uitert, J. J. Rubin, and R. A. Thomas, Phys. Rev., Vol. 133, A494 (1964).
- 16) H. P. Jenssen, D. R. Gabbe, A. Linz, and C. S. Naiman, IEEE J. Quantum Electron., Vol. QE-13, 735 (1977).
- 17) J. Rubin, A. Brenier, R. Moncorge and C. Pedrini, J. of Luminescence, Vol. 36, 39 (1986).
- 18) J. Rubin, A. Brenier, R. Moncorge and C. Pedrini, J. Physique, Vol. 48, 1761 (1987).
- 19) A. Brenier, J. Rubin, R. Moncorge and C. Pedrini, in Proceedings of the International School on Excited States of Transition Metal Elements. (Wroclaw, Poland, June 20 - 25, 1988), (World Science Company 1988), p.120.
- 20) A. Brenier, J. Rubin, R. Moncorge and C. Pedrini, J. Physique, Vol. 50 1463 (1989).

2. THEORY OF ENERGY TRANSFER AMONG IONS IN SOLIDS

The transfer of energy from an excited ion called sensitizer (or donor, D,) to an unexcited ion called activator (or acceptor, A,) is generally the second step in a series of three steps that often take place in luminescent systems (see Fig. 2.1) :

- 1) absorption of a photon by D,
- 2) energy transfer from D to A, and
- 3) emission of a photon by A.

The time required for the energy transfer in step (2) depends on the distance between the donor and the acceptor. If the distance is too large one of the following processes may occur :

i) Radiative transition: The donor may relax to a lower energy state by emitting a photon. The photon emitted may be absorbed by A. The process depends on the absorption coefficient and the total number of A.

The photon emitted may also be absorbed by another D. In this case the absorption depends on the spectral overlap between the absorption and the emission bands of D and the number of D in the crystal.

ii) Migration of energy: Without emission of a photon, another D ion may be excited to a higher energy level. This process depends on the concentration of D and the spectral overlap between the absorption and the emission bands of D.

iii) **Nonradiative relaxation:** D may decay to its ground state through a nonradiative transition. Here the energy is given to the phonon bath. Reviews of relaxation processes in luminescent materials have been given by several authors [1-3].

Di Bartolo [4] and Grant [5] have given comprehensive reviews of the energy transfer processes. This chapter is mostly a summary of Di Bartolo's article.

Energy transfer can be of two types; nonradiative and radiative. The nonradiative energy transfer process provides an additional decay mechanism to the donor and therefore, when it is present, the lifetime of the donor is shorter. It arises from the van der Waals' interaction between the two ions involved; since this interaction is weak, no relevant changes in the energy levels of either donor or acceptor are observed.

In the case of radiative transfer the photon emitted by the sensitizer is absorbed by the acceptor. The lifetime of the donor is not affected by this type of transfer. In this case for an effective energy transfer the acceptor must have a strong absorption band in the spectral region where the donor emits.

2.1 Nonradiative Energy Transfer

The process can be of two types : resonant and nonresonant.

2.1.1 Resonant Energy Transfer

Resonant energy transfer was first studied by Förster in 1948 [6]. He formulated the energy transfer rate for electric dipole - dipole interaction between organic molecules. A few years later Dexter [7] generalized Förster's formula to include transfer by means of forbidden transitions, and applied the theory to energy transfer between dopant ions in inorganic solids.

In the case of resonant energy transfer process an excited donor ion decays to the ground state by giving its energy to an unexcited acceptor ion without creation or annihilation of photons or phonons. Since the transfer occurs between one donor ion and one acceptor ion, we can study the system by using a two-atom model. The initial and the final states of the system are described by the wave function Ψ_I and Ψ_F respectively. (see Fig. 2.2). Ψ_I and Ψ_F can be written as follows:

$$\begin{aligned}\Psi_I &= \frac{1}{\sqrt{2}} \left[\psi'_D(\vec{r}_1) \psi_A(\vec{r}_2) - \psi'_D(\vec{r}_2) \psi_A(\vec{r}_1) \right] \\ \Psi_F &= \frac{1}{\sqrt{2}} \left[\psi_D(\vec{r}_1) \psi'_A(\vec{r}_2) - \psi_D(\vec{r}_2) \psi'_A(\vec{r}_1) \right]\end{aligned}\tag{2.1.1}$$

where

ψ'_D = wave function of donor when it is in its excited state

ψ_A = wave function of acceptor when it is in its ground state,

ψ_D = wave function of donor when it is in its ground state, and

ψ'_A = wave function of acceptor when it is in its excited state

The transition probability per unit time is given by the Fermi Golden rule:

$$W_{DA} = \frac{2\pi}{\hbar} \rho_E |\langle \psi_I | H_{DA} | \psi_F \rangle|^2 \quad (2.1.2)$$

where

\hbar is Planck's constant,

ρ_E is density of states, and

H_{DA} is the interaction Hamiltonian between the donor and the acceptor given by $H_{DA} = e^2/r_{12}$. The relevant matrix element is then given by

$$\langle |H_{AB}| \rangle = \left\langle \psi'_D(\vec{r}_1) \psi_A(\vec{r}_2) \left| \frac{e^2}{r_{12}} \right| \psi_D(\vec{r}_1) \psi'_A(\vec{r}_2) \right\rangle - \left\langle \psi'_D(\vec{r}_1) \psi_A(\vec{r}_2) \left| \frac{e^2}{r_{12}} \right| \psi'_A(\vec{r}_1) \psi_D(\vec{r}_2) \right\rangle \quad (2.1.3)$$

where the first term is called the direct term and the second term the exchange term. The exchange term can be neglected if the multipole interactions are strong. In case of rare earths the distance between ions is large enough to ignore this term.

The rate of the energy transfer depends on the square of the matrix element which can be expressed in a multipolar expansion as follows :

$$|\langle |H_{AB}| \rangle|^2 = \frac{C^{(6)}}{R^6} + \frac{C^{(8)}}{R^8} + \frac{C^{(10)}}{R^{10}} + \dots \quad (2.1.4)$$

where the first term corresponds to dipole - dipole, the second term corresponds to dipole - quadrupole, and the third term corresponds to quadrupole-quadrupole interactions, respectively.

In case of a dominant multipolar interaction the transfer rate can be written as

$$W_{DA}(R) = \frac{C^{(n)}}{R^n} \quad (2.1.5)$$

In the formula above R is the distance between the acceptor and the donor; and $C^{(n)}$ is called the microscopic interaction parameter and represents the energy transfer rate from the donor to the acceptor when the distance between them is equal to 1 cm.

We define energy transfer radius, R_0 , as the distance between the donor and the acceptor at which the energy transfer rate is equal to the decay rate of the donor in the absence of the acceptor :

$$W_{DA}(R) = \frac{C^{(n)}}{R^n} = \frac{1}{\tau_D} \left(\frac{R_0}{R} \right)^n \quad (2.1.6)$$

where τ_D is the intrinsic lifetime of the donor. The parameter $C^{(n)}$ is then given by

$$C^{(n)} = \frac{R_0^n}{\tau_D} \quad (2.1.7)$$

In the dipole - dipole case [8] R_0 can be expressed in terms of the overlap integral

$$R_0 = \left[\epsilon f_A \frac{3\pi e^2 c^3 h^5}{4m\pi^5} \int g_D(E)g_A(E) \frac{dE}{E^4} \right]^{1/6} \quad (2.1.8)$$

where

$g_D(E)$, $g_A(E)$ = normalized spectral functions of the donor and the acceptor,

ϵ = quantum efficiency of the donor luminescence in the absence of the acceptor, given by

$$\epsilon = \frac{\text{rate of radiative decay}}{\text{rate of radiative decay} + \text{rate of nonradiative decay}} = \frac{\tau_{\text{rad}}^{-1}}{\tau_D^{-1}}$$

where τ_{rad} is the radiative lifetime of A.

The oscillator strength, f_A is derived from the absorption data as

$$f_A = \frac{m c n}{2\pi^2 e^2 c_A} \int \alpha_A(\omega) d\omega \quad (2.1.9)$$

where

c_A = concentration of A, $\alpha_A(\omega)$ = absorption coefficient of A, and n = index of refraction. In the dipole - dipole case the energy transfer rate is then given by

$$W_{DA}(R) = \frac{1}{\tau_D} \left(\frac{R_0}{R} \right)^6 \quad (2.1.10)$$

2.1.2 Nonresonant Energy Transfer

In this process the mismatch of energy between the energy levels of the donor and the acceptor is compensated by the simultaneous emission or absorption of one or more phonons as shown in Fig. 2.3. Phonon assisted energy transfer processes have been studied by Fonger and Struck [9]. They presented a model of phonon coupling to transitions based on Condon's quantum - mechanical treatment of the Frank - Condon principle. Miyakawa and Dexter [10] related the phonon sidebands to the multiphonon relaxation of excited states and the phonon assisted energy transfer between ions in solids. Yamada et al. [11] studied phonon assisted energy transfer between trivalent rare earth ions in Y_2O_3 . They found a good agreement between experimental results and the theory of Miyakawa and Dexter.

The transition probability per unit time of the energy transfer process accompanied by the production of a phonon is given by

$$W_{DA} = \frac{2\pi}{\hbar} \left| \langle \psi_D'(\vec{r}_1) \psi_A(\vec{r}_2) | H_{DA} | \psi_D(\vec{r}_1) \psi_A'(\vec{r}_2) \rangle \right|^2 S[n(\omega) + 1] \int g_D(E) g_A(E - \hbar\omega) dE \quad (2.1.11)$$

where S = ion- vibrations coupling parameter, $n(\omega)$ = phonon occupation numbers, and $\hbar\omega = \Delta E$.

If a phonon is destroyed in the process;

$$W_{DA} = \frac{2\pi}{\hbar} \left| \langle \psi_D(\vec{r}_1) \psi_A(\vec{r}_2) | H_{DA} | \psi_D(\vec{r}_1) \psi_A'(\vec{r}_2) \rangle \right|^2 S[n(\omega)] \int g_D(E) g_A(E + \hbar\omega) dE \quad (2.1.12)$$

When $\Delta E \gg h\omega_m$ where ω_m is the maximum phonon frequency, energy transfer is assisted by more than one phonons and the transition probability per unit time [10] is given by

$$W_{DA}(\Delta E) = W_{DA}(0)e^{-\beta\Delta E} \quad (2.1.13)$$

where β is a temperature dependent parameter.

2.2 Radiative Energy Transfer

Radiative transfer of energy consists of two stages:

- 1) a donor ion in an excited energy level decays to the ground state by emitting a photon, and
- 2) an acceptor absorbs the photon emitted by the donor.

The quantum yield for the transfer is given by [7]

$$\bar{\eta}_T(E) = Av \int f_D(E) [1 - e^{-c^+ c_A \sigma_A(E)}] dE \quad (2.2.1)$$

where the average is taken over the linear dimension ℓ , $v = (3/4)\pi R^3$ and

$f_D(E)$ = normalized line shape of the donor's transition,

$\sigma_A(E)$ = absorption cross section of the activator,

c^+ = density of available activator sites, and

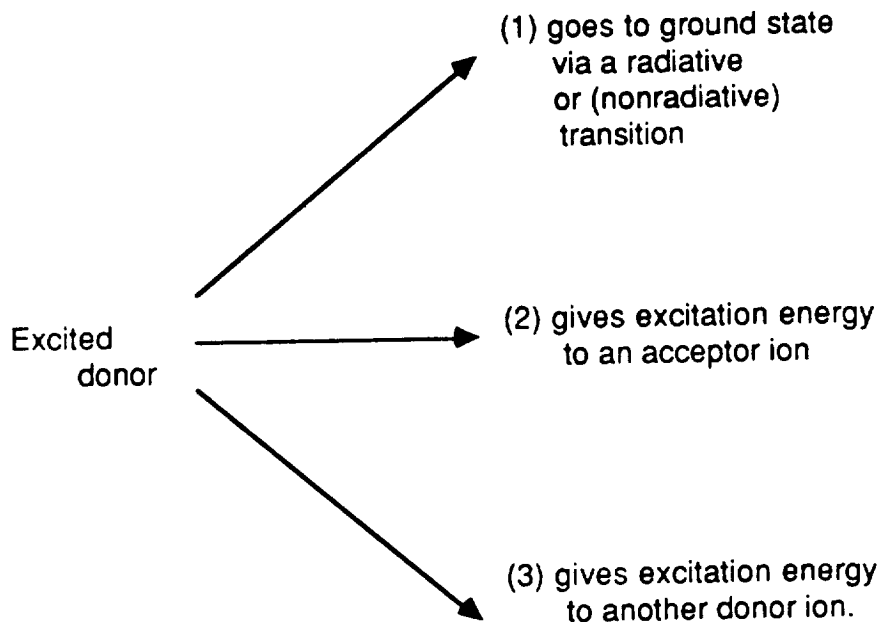
c_A = concentration of the activator ions.

As it can be seen from the equation above, the probability of radiative transfer depends on the concentration of the acceptor ions, and the size and the shape of the system as well as on the strength of the donor emission and the acceptor absorption.

The transfer may occur between the donor ions in the host lattice. It may lead to trapping of the radiation and to an increase of the measured lifetime. In such case the lifetime may depend on the size and the shape of the sample.

2.3 Statistical Treatment of Energy Transfer

An excited donor can decay to its ground state by one of the following processes:



The process of donor to acceptor energy transfer can be studied by considering three limiting cases :

- 1) energy transfer from donor to acceptor without diffusion,
- 2) energy transfer from donor to acceptor with diffusion limited transfer, and
- 3) energy transfer from donor to acceptor with fast diffusion among donors.

Effect of diffusion on energy transfer by resonance has been studied by Yokoda et al. [12]. Weber [13] examined the time dependence of the luminescence following pulsed excitation from Cr^{3+} doped europium phosphate glass. Here Cr^{3+} acts as the donor and Eu^{3+} as the acceptor.

Three cases are of interest :

1) Energy transfer without diffusion among donor ions: When acceptor ions are present, the donors further away from the acceptors decay with their intrinsic lifetime. In this case the donor decay is presented by a function

$$\rho(t) = \exp(-t / \tau_D) \quad (2.3.1)$$

The donor ions close to the acceptors decay by transferring their excitation energy to acceptor ions. The energy transfer rates for different donor - acceptor pairs generally decreases rapidly with the separation. If the probability for direct energy transfer to an acceptor at distance R from the donor is $w_{DA}(R)$, then

$$\rho(t) = \exp[-t / \tau_D - w_{DA}(R)t] \quad (2.3.2)$$

If the interaction between the donor - acceptor coupling is the multipolar interaction the decay rate is given by the Förster formula [8]

$$\rho(t) = \exp\left[-\frac{t}{\tau_D} - \frac{c_A}{c_0} \Gamma \left(1 - \frac{3}{n}\right) \left(\frac{t}{\tau_D}\right)^{3/n}\right] \quad (2.3.3)$$

where $c_0^{-1} = \frac{4\pi R_0^3}{3}$

$n = 6$ for electric dipole - dipole interactions,

8 for electric dipole - quadrupole interactions,

10 for electric quadrupole - quadrupole interactions, and

c_A = concentration of acceptor ions.

2) Diffusion - Limited case: When the diffusion rate of energy among the donor ions to the acceptor ion is slow but comparable to the intrinsic decay rate of the donor ion, the decay of the total donor system is composed of several competing processes.

A donor in the vicinity of an acceptor decays predominantly by direct energy transfer to the acceptor. A donor far away from an acceptor must first diffuse the excitation energy into the vicinity of an acceptor before energy transfer can occur. The time evaluation for the donor decay can be obtained by solving the equation

$$\frac{\partial \rho(\vec{r}, t)}{\partial t} = D \nabla^2 \rho(\vec{r}, t) - \sum w_{DA}(\vec{r} - \vec{r}_n) \rho(\vec{r}, t) - \frac{1}{\tau_D} \rho(\vec{r}, t) \quad (2.3.4)$$

where D is the diffusion constant and $w_{DA}(\vec{r} - \vec{r}_n)$ is the probability for energy transfer from an excited donor to the acceptor at position r_n . We define $t^* = \frac{C_D A}{D^{3/2}}$

as a boundary between energy transfer without diffusion among donor ions and energy transfer with diffusion among them.

For $t \ll t^* \rightarrow \bar{\rho}(t)$ is the same as for the case of no -diffusion.

For $t \gg t^* \rightarrow \bar{\rho}(t) \approx e^{-\frac{t}{\tau_D} - K_D t}$

where $K_D = 4\pi D C_A R_D$, and

$$R_D = \left(\frac{C_D A}{D} \right)^{1/4}$$

3) Fast Diffusion among the donor ions: When the donor concentration is high or the average donor separation is small and the probability for resonant energy transfer is large, energy diffusion can be very rapid. In this case variations in the transfer rate is averaged out and the donor system shows an exponential decay.

REFERENCES (Chapter 2)

- 1) L. A. Riseberg and M. J. Weber, in Progress in Optics, vol.14, edited by E. Wolf (North Holland, New York, 1976), p.91.
- 2) R. K. Watts in Optical Properties of Ions in Solids, edited by B. Di Bartolo (Plenum Press, New York, 1975), p.307.
- 3) G. Blasse, in Prog. Solid St. Chem., Vol.18, 79 (1988).
- 4) B. Di Bartolo, in Energy Transfer Processes in Condensed Matter, edited by B. Di Bartolo (Plenum Press, New York, 1983), p.103.
- 5) W. J. C. Grant, Phys. Rev.B, Vol.4, 648 (1971).
- 6) T. Förster, Ann. Physik, Vol.2, 55 (1948).
- 7) D. L. Dexter, J. Chem.Phys. Vol.21, 836 (1953).
- 8) M. Inokuti and H. Hirayama, J. Chem. Phys. Vol.43, 1978 (1965).
- 9) W. H. Fonger and C. W. Struck, in Radiationless Processes, edited by B. Di Bartolo (Plenum Press, New York 1979), p.471.
- 10) T. Miyakawa and D. L. Dexter, Phys. Rev.B, Vol.1, 2961 (1970).
- 11) N. Yamada, S. Shionoya and T. Kushida, J. Phys. Soc. Japan, Vol.32, 1577 (1972).
- 12) M. Yokota and O. Tanimoto, J. Phys. Soc. Japan, Vol.22, 779 (1967).
- 13) M. J. Weber, Phys. Rev.B, Vol.4, 2932 (1971).

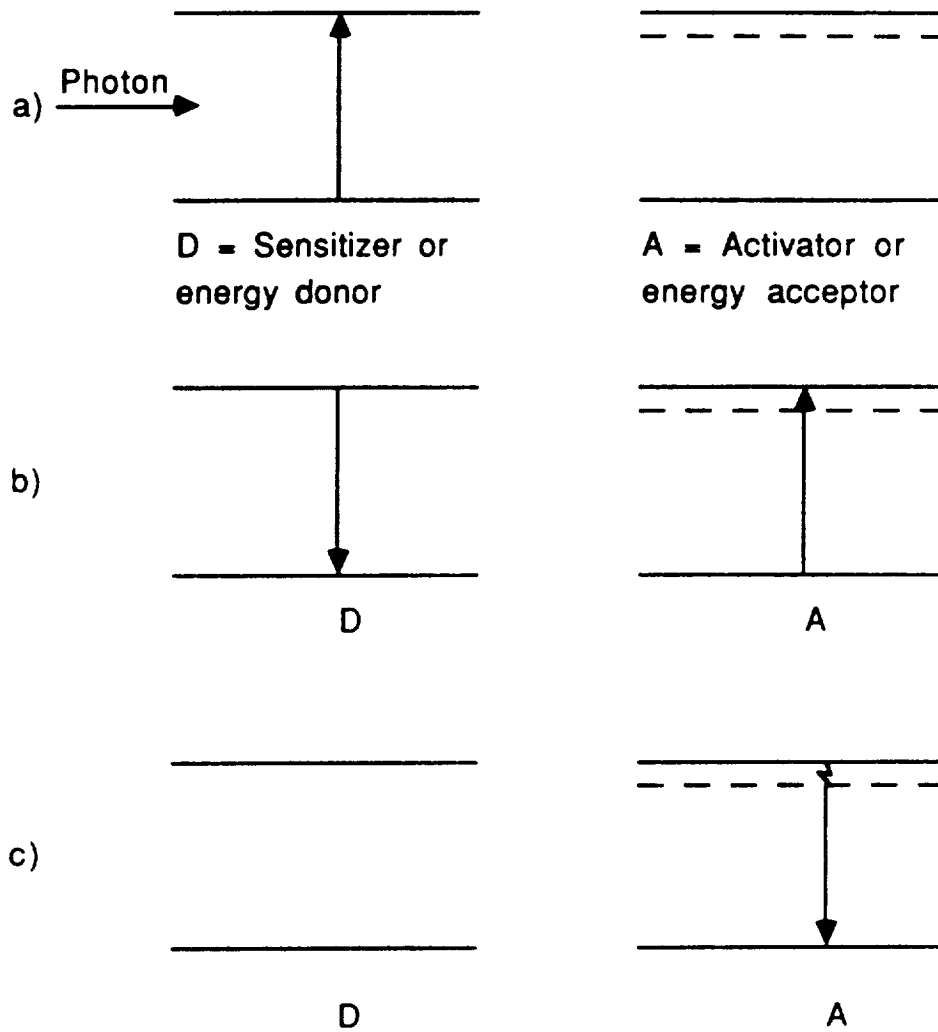


Fig. 2.1 Typical sequences of events for energy transfer from one excited ion to other unexcited ion

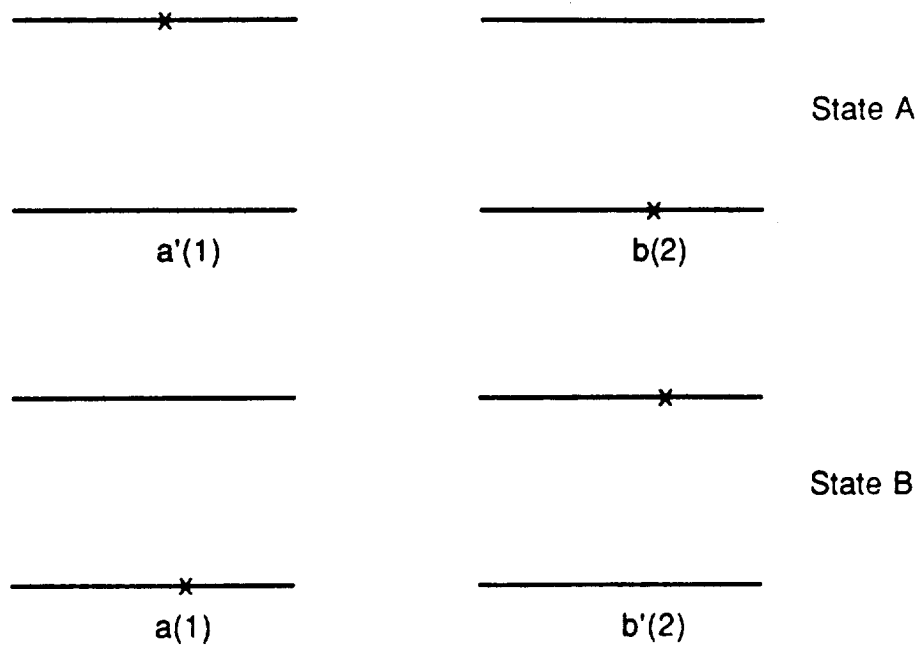


Fig. 2.2 The initial and the final states of two - atom system.

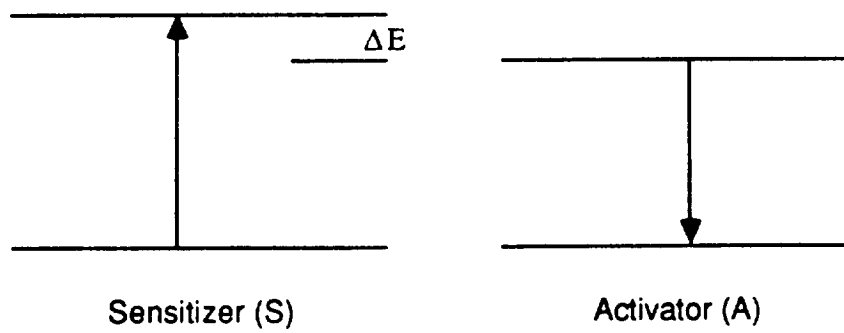


Fig. 2.3 Phonon assisted energy transfer from S to A.

3. EXPERIMENTAL APPARATUS

The experiments that we performed were optical absorption, continuous luminescence, excitation and pulsed luminescence.

The equipment used consists of:

- 1) The absorption spectrophotometer,
- 2) The continuous luminescence apparatus, and
- 3) The pulsed luminescence apparatus.

An absorption spectrum gives the information about the energy level structure and the energy storage capability of the sample. What is measured with the absorption spectrophotometer is the absorbance or the transmittance of the sample. The absorbance is measured in terms of the optical density (O.D.) defined as $O. D. = \text{Log}_{10} (I_i / I_o)$, where I_i is the intensity of the incident light, and I_o the intensity of the light after it travels through the sample.

If an ion or an atom is excited to an upper energy level by some mechanism (for example by absorbing a photon), the atom may decay back to the ground state via different decay paths. The information about these paths can be obtained from the continuous emission spectra of the sample. Continuous luminescence spectra also give information about additional energy levels that are not seen in absorption.

The response of an energy level to a pulsed excitation is studied in order to understand the decay kinetics of the level.

3.1 The Absorption Spectrophotometer

A PERKIN-ELMER Model LAMDA-9 spectrophotometer was used for absorption measurements at room temperature. The instrument has an access to a microcomputer with a video display and a soft key operating system. The usable wavelength range is 185 - 3200 nm with the accuracy of 0.2 nm for the ultraviolet/visible (UV/VIS) range and 0.8 nm for the infrared (IR) range. The slit width is selectable from 0.05 - 5 nm with 0.01nm increments in the UV/VIS range, and self adjusted in the IR range. The instrument provides the light sources :

- 1) a deuterium lamp for UV range,
- 2) a tungsten-halogen lamp for VIS and IR ranges

and the detectors:

- 1) a side window photomultiplier for UV/VIS range,
- 2) a lead sulfide (PbS) detector for NIR (near IR) range.

The light sources and the detectors can be changed automatically or manually at a selected wavelength.

3.2 Continuous Luminescence Apparatus

This apparatus consists of the following (Fig. 3.1) :

- 1) The exciting system,
- 2) The analyzing system,
- 3) The detecting and amplifying system,
- 4) The recording system, and
- 5) The temperature regulating systems.

3.2.1 The Exciting System

This system consists of a Jarrell Ash 30 W tungsten-halogen lamp in a housing and a focusing lens on the same optical axis or a coherent Lixel Model 526 Argon-Ion laser. The specifications for the Argon-Ion Laser are given in Table 3.1.

3.2.2 The Analyzing System

The analyzing system consists of a lens, and either a Spex Model 1269 1.26 m or Spex Model 1681B 0.22 m scanning monochromator. The model 1681B has an internal drive circuitry that couples directly to a computer (Spex Model DM1B) described in section 3.2.4. The Model 1269 scanning monochromator is driven by a Spex mini-step driver that couples directly to the DM1B.

The gratings used with both monochromators are:

- 1) 1200 groove/mm grating set to the first order, blazed at 500 nm, and
- 2) 600 groove/mm grating set to the second order, blazed at 1.25 μm .

The luminescence emitted by the material is observed at 90° with respect to the direction of the excitation, focused by a lens onto the slit of the monochromator, and chopped.

3.2.3 The Detecting and Amplifying System

The detecting system consists of a Lead Sulfide (PbS) infrared detector or an RCA Model C31034 photomultiplier, a Photon Technology International (PTI) Model 03-OC4000 light chopper, and a Stanford Research Systems Model SR510 Lock-in amplifier.

A Spex Model 1428 PbS detector was used for the detection of the infrared luminescence. It fits in the Spex Model 1427 infrared detector housing. An RCA C31034 photomultiplier (having a GaAs photocathode) cooled by a HAKEE K1 refrigerator was used for detection of the optical luminescence. The photocathode spectral response characteristics of this tube are shown in Fig. 3.2. This phototube has high sensitivity, low noise and fast response time characteristics throughout its entire spectral range.

A Photon Technology International Model 03-OC4000 chopper was used. It consists of a chopper head, a controller unit, and a disk. The chopper can be operated under internal or external control by means of a switch. If it is operated under internal control, then the speed can be set by speed control dial on the front panel. In the case of external frequency control, an analog signal must be fed to the back connector. A linear increase in frequency can be achieved by varying the voltage from 0 to 4 V. Frequency can be varied from 0 to 4000 Hz. For the continuous luminescence measurements the chopper was set to 150 Hz to modulate the luminescence output which was then detected

and amplified by a Stanford Research Systems Model SR510 "Lock-in" amplifier. This method of phase sensitive detection rejects a large amount of background noise. The output circuit of the phase sensitive detector may have different time constant ($\tau = 0.001$ to 100 sec), and corresponding noise bandwidth.

3.2.4 The Recording System

The recording system is composed of a Spex Model DM103M Voltage Input Module (VIM), a Spex Model DM1B spectrophotometer controller and data processor, and a Houston Instrument Model HILOT DMP-29 multi-pen plotter.

The DM103M converts a bipolar voltage from an external device such as a detector, into a digital signal. Two signals can be applied providing selectable output options to collect one signal, invert the other or take the difference of them.

The DM1B provides data and program storage, and eight data files. Once the data are stored, they can be processed in fifteen different data acquisition modes to subtract away background, take ratios, integrate or convert to logarithms for absorption measurements.

The raw data or processed results can be displayed on a non-glare CRT or plotted by a digital plotter or an X-Y analog recorder.

3.2.5 The Temperature Regulating System

This system consists of a Janis Helium Research Dewar Model 8DT combined with a "SuperVaritemp" device and a Lake Shore Cryotronics Model DRC-80C digital thermometer/controller for low temperature measurements.

The dewar provides a vacuum insulated sample chamber. The sample is cooled by means of a flowing helium (or nitrogen) vapor. The helium vapor is vented ordinarily to the atmosphere. The temperature of the sample can be varied from 2K to 300K (from 78 to 300K if liquid nitrogen is used). The speed of the sample temperature change can be adjusted by changing the helium supply flow (see Fig. 3.3).

The model DRC-80C digital thermometer/ controller is used to increase and control the sample temperature. This instrument is designed to be used with the Model DT-500CU-DRC-36 silicon diode sensors manufactured by the same company. Two 10 mA constant current sources are used to excite the dual sensor inputs. These inputs enable two silicon diode sensors to be used concurrently. The DRC-80C provides a direct digital readout in Kelvin temperature units. The temperature is controlled by direct analog comparison between the sensor voltage and an analog equivalent of the digital temperature set point. Two heater output levels are selectable. The HI mode provides up to 25 watts of heater power while the LO mode keeps output power to a nominal 10 watts. The specified range of operation is 4.0 to 380K. In this temperature range, the diode sensor has a uniform characteristics.

For the temperatures higher than 300K, a 40 watts iron heater was used. The heater is powered by an LFE Model 232 voltage A.C. power supply and

controller. The temperature was measured and readout by using an iron-constantan thermocouple connected to a FLUKE Model 2190A digital thermometer.

3.3 Pulsed Luminescence Apparatus

The pulsed luminescence apparatus consists of (Fig. 3.4) :

- 1) The exciting system,
- 3) The analyzing system,
- 3) The detecting system, and
- 4) The storing and processing system.
- 5) The temperature regulating systems

3.3.1 The Exciting System

The exciting system consists of either a Quantel Model TDL-51 tunable dye laser pumped by a Quantel Nd³⁺: YAG (Yttrium Aluminum Garnet) Model 660A-10 laser or an EG&G Princeton Applied Research Model 2100 tunable dye laser pumped by a nitrogen laser. The specifications of these lasers are given in Tables 3.2, 3.3, and 3.4.

3.3.2 The Analyzing System

The analyzing system consists of a lens and an interference filter that can be replaced by a high resolution Spex Model 1269 monochromator. The axis of the lens is either at 90° or 45° with respect to the incident radiation. The transmission spectra of some filters used are shown in Fig. 3.5.

3.3.3 The Detecting System

The detecting system consists of an RCA Model C31034 photomultiplier for the detection of optical signals, and a Judson Infrared Inc. Model J12TE2 InAs detector for the detection of infrared signal. The detector is combined with a Judson Infrared Inc. Model TC200 cooling system and a preamplifier circuit

(see Fig. 3.6). The signal was amplified by using an Analogic Data Precision Model D1000 dual amplifier.

3.3.4 The Recording System

The recording system consists of an Analogic Data Precision Model Data 6000 waveform analyzer, and a Macintosh computer. The signal is processed and stored by the waveform analyzer and then transferred to the computer.

The amplitude of the signal generally decreases as Ce^{-V/τ_F} , where τ_F is the luminescence lifetime. τ_F is derived from the best exponential fit to the signal by using Cricket-Graph software.

3.3.5 The Temperature Regulating System

This system consists of a Helix CTI-Cryotronics Model SC-21 compressor unit connected to a cold head. The temperature was changed from 10K to 300K by passing a current through a nichrome heater wire wound around the cold head. The temperature was measured by means of a type - T Copper/Constantan thermocouple wire attached to the sample and was read by using a Laser Analytics Inc. Model 5720 Cryogenic Temperature Stabilizer.

Table 3.1. Specifications of the Lexel Model 526 Ar- Ion Laser

Tuning range.....	457.9 - 528.7 nm.
Beam Diameter.....	1.1 mm.
Beam Divergence (full angle).....	0.7 mrad.
Power (multiline).....	0.5 Watt

Amplitude power stability :

in light control.....	<± 0.2%
in current control.....	<± 2.0%

Optical noise (10 Hz. to 2 MHz) :

Typical in light control.....	<0.5% rms.
Maximum ripple in current control.....	<1.5
Typical high frequency component.....	<0.3
Typical high frequency with etalon.....	<0.15
Input voltage range.....	190-245 volts
Cooling water requirements.....	5.6 Liter/min. at 1 Atm.

Table 3.2 Specifications of Quantel Model TDL-51 Dye Laser

Energy (mJ)	
532 nm pump-peak of R590 ($\approx 560\text{nm}$).....	150
355 nm pump-peak of Coumarin 500 ($\approx 515\text{nm}$).....	27
532 nm pump peak of R590, mixed ($\approx 368\text{ nm}$).....	48
532 nm pump-Rhodamine 590, doubled ($\approx 280\text{ nm}$).....	36
532 nm pump-peak of R590, doubled and mixed ($\approx 222\text{ nm}$)....	6
Pulse length (FWHM)	
Fundamentals.....	7 to 9 ns
Harmonics.....	6 to 8 ns
Wavelength Characteristics	
Tuning range	
Without wavelength conversion accessories (nm).....	420 -740
With wavelength conversion accessories (nm).....	191-5000
Linewidth (560 nm)	
Without NBP-2*.....	$< 0.8\text{ cm}^{-1}$
With NBP-2.....	$< 0.08\text{cm}^{-1}$
With BBP-2**.....	$> 90\text{cm}^{-1}$
Nominal beam diameter.....	5.00mm

* narrow bandwidth package

** broad bandwidth package

Table 3.3 Specifications of Quantel Model 660A-10 YAG : Nd³⁺ Laser

Energy (mJ)	
1064 nm.....	250
532 nm.....	100
355 nm.....	45
266 nm.....	15
Pulse width (ns)	
1064 nm.....	5-7
532 nm.....	4-6
355 nm.....	4-6
266 nm.....	3-5
Divergence (mrad).....	0.5
Jitter (ns).....	0.5
Energy stability (%).....	
1064 nm.....	3.0
532 nm.....	5.0
355 nm.....	5.0
266 nm.....	N/A
Repetition rate (Hz.).....	10

Table 3.4. Specifications of EG&G Dye Laser

A) Nitrogen Laser:

Output Pulse Duration:.....1.2 ns.
Output Pulse Energy:..... ≥ 0.55 mJ.
Output Peak Power (337 nm).... ≥ 0.4 μ W.

B) Dye Laser:

Output Pulse Duration:.....1.0 ns
Output Pulse Energy..... ≥ 30 μ J.
Output Peak Power (590 nm).... ≥ 25 kW.
Spectral Linewidth (590 nm)..... ≤ 0.04 nm.
Tuning Range.....360 to 800 nm.
Polarization.....100 : 1 horizontal

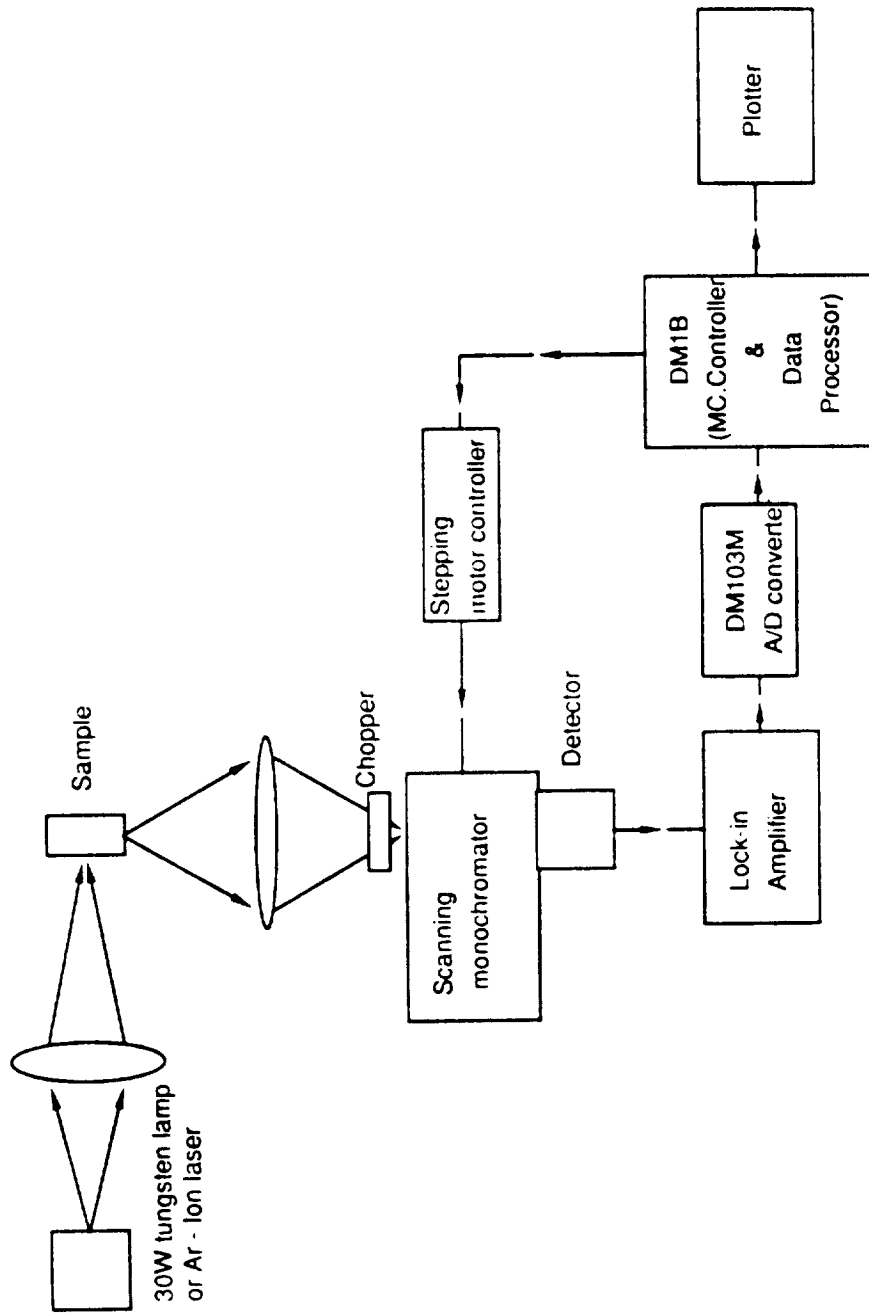


Fig. 3.1 Block diagram of the continuous luminescence apparatus

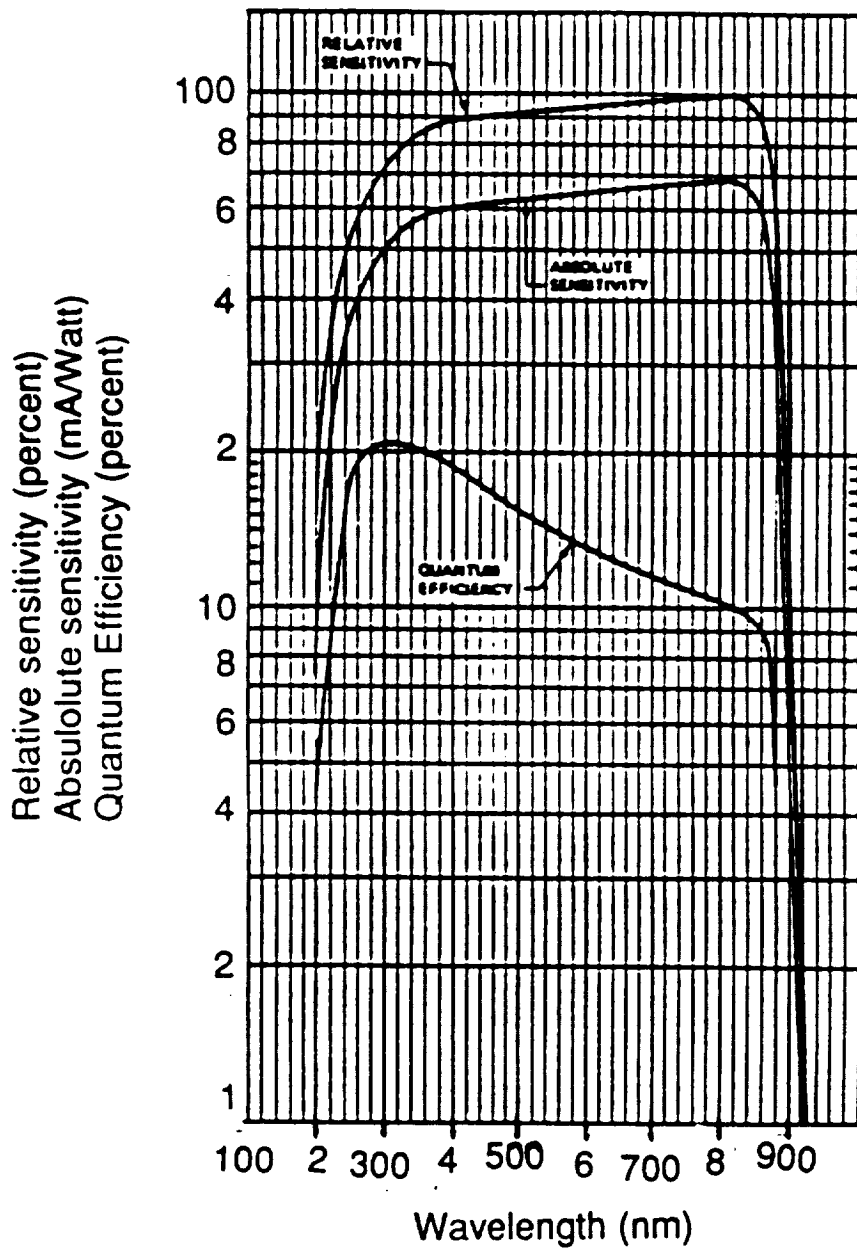


Fig. 3.2 Photocathode spectral response characteristics of the RCA Model C31034 photo-tube.

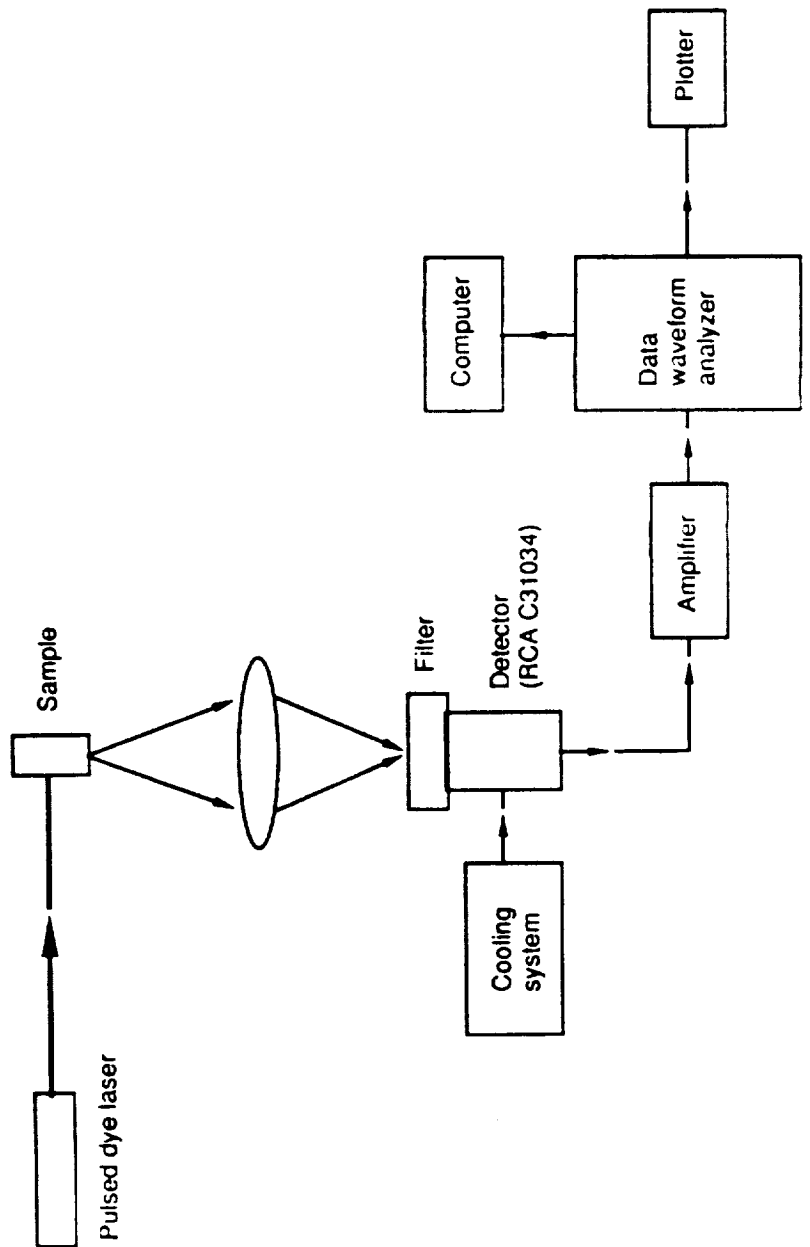


Fig. 3.4 (a) Block diagram of the pulsed luminescence apparatus for optical region.

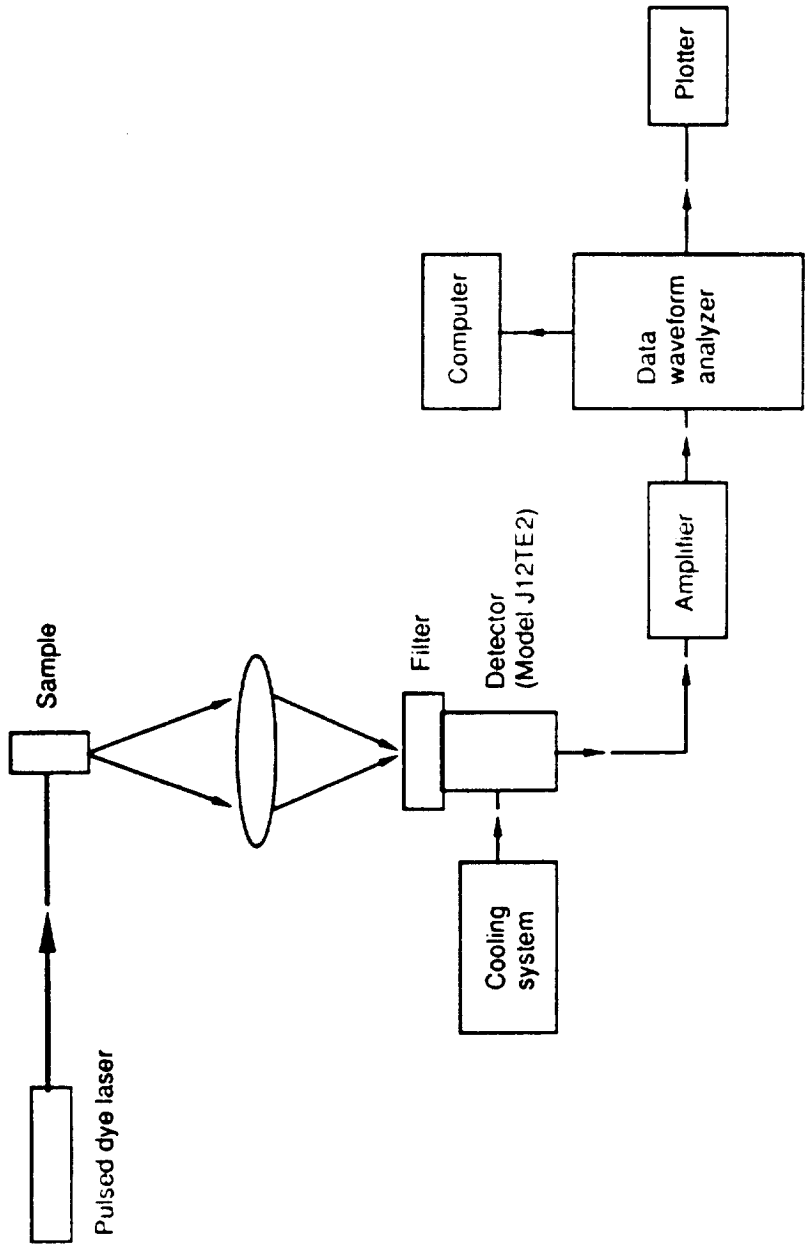


Fig. 3.4 (b) Block diagram of the pulsed luminescence apparatus for infrared region.

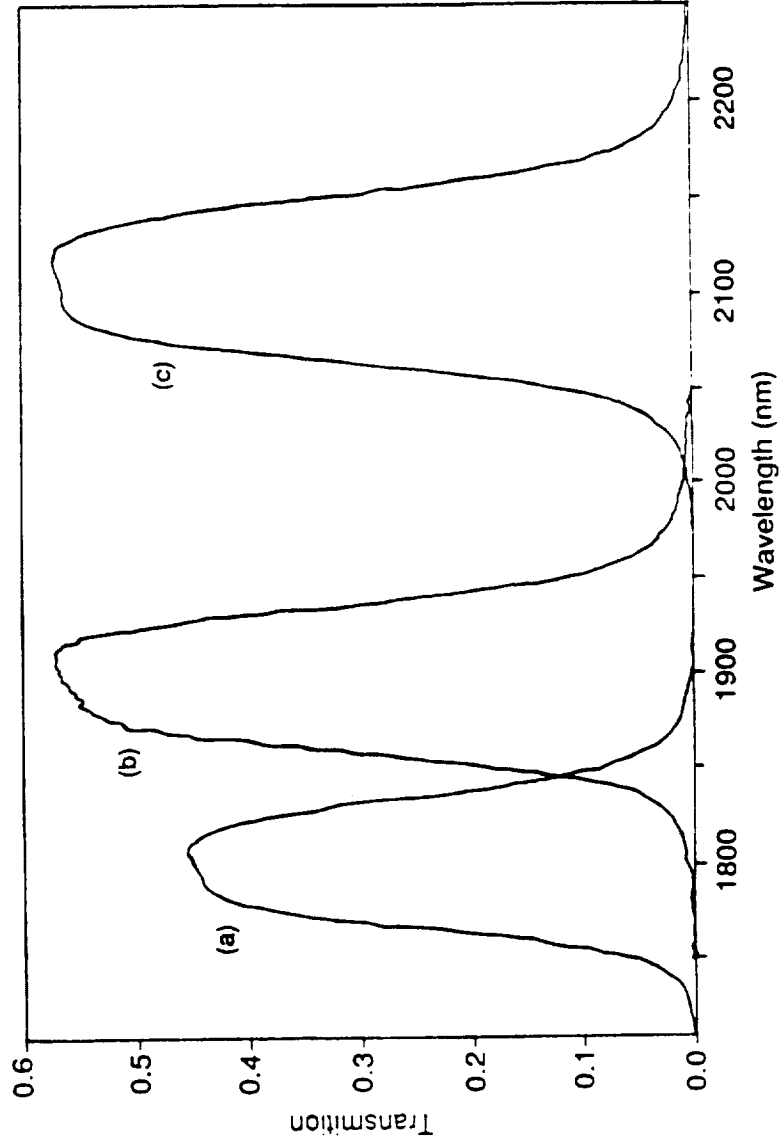


Fig. 3.5 Transmission spectra of the interference filters used for lifetime measurements.

(a) : central wavelength is 1.8 μm .

(b) : central wavelength is 1.9 μm .

(c) : central wavelength is 2.1 μm .

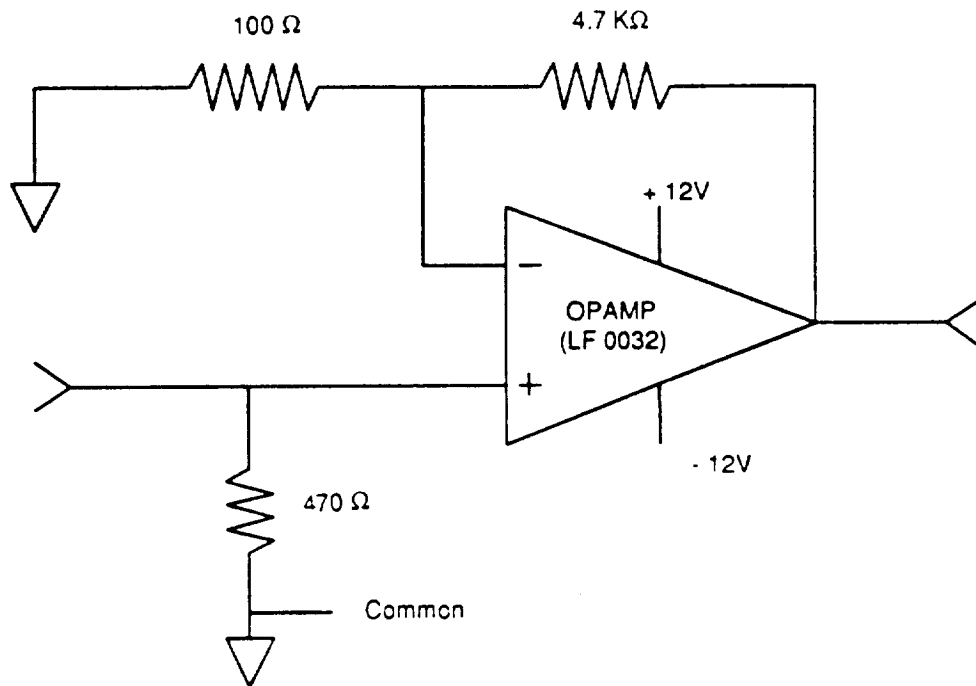


Fig. 3.6 Preamplifier circuit for the InAs infrared detector.

4. SAMPLES EXAMINED

We studied the energy transfer processes between Tm^{3+} and Ho^{3+} ions in LiYF_4 . Here Ho^{3+} acts as an activator and Tm^{3+} as a sensitizer. The energy levels of Tm^{3+} and Ho^{3+} in LiYF_4 are shown in Fig. 4.1. The ${}^3\text{F}_4 \rightarrow {}^3\text{H}_6$ emission of Tm is centered at 1.9 micron and ${}^5\text{I}_7 \rightarrow {}^5\text{I}_8$ emission of Ho at 2.06 micron. Tm^{3+} has an advantage as sensitizer because it can be pumped with a diode laser into its ${}^3\text{H}_4$ level (~ 795 nm).

In order to study energy transfer processes three samples are generally needed; one doped with only sensitizer ions, one doped with only activator ions, and one doped with both sensitizer and activator ions. The samples we studied are the following :

- i) $\text{LiYF}_4: \text{Tm}^{3+}$ (.5% at.)
- ii) $\text{LiYF}_4: \text{Ho}^{3+}$ (1% at.)
- iii) $\text{LiYF}_4: \text{Tm}^{3+}$ (5% at.), Ho^{3+} (.2% at.)

The $\text{LiYF}_4: \text{Ho}^{3+}$ (1% at.) was grown at Oklahoma State University, and the other two crystals at M.I.T. All these crystals were grown by using the Czochralski growth technique.

4.1 Optical Properties of The Host Lattice, LiYF₄

LiYF₄ has the tetragonal crystal structure with lattice parameters 5.167°A (a - axis) and 10.735A (c - axis) [1]. The rare earth ions can be substituted in the Y³⁺ ion sites without charge compensation. The optical, mechanical and thermal properties of the material were reported by Jenssen et al [2] and are reproduced in Table 4.1.

The phase equilibrium diagram of the LiF - YF₃ system was studied by Thoma et al [3]. Data were obtained from thermal analysis of heating and cooling curves and by identifying the phases present in small samples which were quenched after equilibration at high temperatures. The phase diagram obtained by Thoma et al. is shown in Fig. 4.2. Two invariant points occur in the system : an eutectic point at 19 mole % YF₃ and 695 °C and a peritectic point at 49 mole % YF₃ and 819 °C. The same group reported the lattice parameters to be: $a = 5.26 \pm 0.03\text{A}$, and $c = 10.94 \pm 0.03\text{A}$. Calculated density was reported to be 3.77 g/cm³. A few years later, Shand [4] grew the LiYF₄ single crystal by both the Stock-barger and Czochralski techniques. He reported the lattice parameters to be $a=5.16 \pm 0.01\text{A}$, and $c=10.85 \pm 0.01\text{A}$. He also calculated for the density a value $3.995 \pm 0.005 \text{ g/cm}^3$. Fig 4.3 shows the refractive indices of the crystal for wavelengths between 400A and 6500 A.

The transmission limits of LiYF₄ for a 4 mm thick sample is shown in Fig. 4.4. The sample is transparent in the region of 300 to 6000 nm. This makes the material convenient for matching the optical properties of the rare earths.

4.2 The Rare earth ions in a Crystalline Solid

The rare earths are characterized by successive filling of the 4f and 5f shells of their electronic configurations. They are divided into two groups: the lanthanides and the actinides. Each group contains fourteen elements. The lanthanide atoms have the electronic configuration: $1s^2 2s^2 2p^6 3s^2 3p^6 3d^{10} 4s^2 4p^6 4d^{10} 4f^N 5s^2 5p^6$ with two or three outer electrons ($6s^2$ or $5d^6s^2$). The $4f^N$ configuration starts with $N=1$ for Cerium and increases regularly to $N=14$ for Lutecium. These ions are usually found in crystals in their trivalent states.

Intensities of crystal spectra of rare earth ions have been studied by Ofelt [5]. The optical spectra of rare earth ions [6, 7] are described by the electronic transitions between the $4f^N$ levels of their ground state configurations. These transitions are not allowed in a free ion because of the parity rule. They become partially allowed when the free ion is placed in a noncentrosymmetric crystalline solid. The crystal field energy causes the admixture of the $4f^N$ levels with those of the $4f^{N-1} 5d$ state having opposite parity.

The Hamiltonian for an ion in a crystal is given by

$$H = H_{\text{isolated ion}} + H_{\text{electron-static lattice}} + H_{\text{electron-dynamic lattice}} + H_{\text{dynamic lattice}}$$

where

$H_{\text{isolated ion}}$ is the Hamiltonian for the free ion with eigenstates $(2S+1)L_J$,

$H_{\text{electron-static lattice}}$ represents the crystal field energy which describes how the ion is affected by the average static environment,

$H_{\text{electron-dynamic lattice}}$ describes how the ion is affected by the lattice modes; this term modifies the shape and strength of the optical transitions; in addition, it can give rise to nonradiative processes, and

$H_{\text{dynamic lattice}}$ is the vibrational energy of the crystalline lattice; it can be described in terms of lattice phonon modes.

The concentration of the optically active ions is generally so low that we may neglect the interaction among them; this allows us to consider the optical spectroscopy of an individual ion in a crystal field. The effect of the crystal field on the energy levels of the 4f-electrons is weak, because these electrons are well shielded by the electrons of the outer 5s and 5p shells. The energy levels of all the rare earth ions in LaCl_3 have been established experimentally by Dieke [8] and are shown in Fig 4.5.

4.3 Optical Properties of Tm³⁺ in LiYF₄

An analysis of the absorption and luminescence of Tm³⁺ in LiYF₄ was made by Jenssen et al. [9] at temperatures 5 and 77K. The energy levels for the 4f¹² configuration were established by using the experimental data and also obtained by diagonalizing a Hamiltonian that describes the free - ion and crystal field interactions in the basis of states spanning the 4f¹² configuration. The experimental and the calculated energy levels were in agreement.

Brenier et al. [10] studied the dynamics of the relaxation processes for different Tm concentrations in LiYF₄. The decay patterns of different energy levels were obtained by exciting each energy level of Tm³⁺ in the visible and the infrared region selectively. When the ³H₄ level is excited by a pulse, the decay pattern of the luminescence of ³F₄ level shows a rise at early times followed by an exponential decay. The lifetime of the ³F₄ level was reported to be 16 msec at room temperature for a 1 % at. Tm doped single crystal.

4.4 Optical Properties of Ho³⁺ in LiYF₄

LiYF₄ crystals co-doped with Ho³⁺, Er³⁺, and Tm³⁺ are well known laser materials [11-13]. In these crystals, the visible luminescence of Ho is quenched due to the nonradiative transitions between the upper levels, and all the luminescence originates in the first excited level ⁵I₇. The luminescence of LiYF₄ activated with only Ho is found to be strong in both the visible and the infrared regions of the spectrum.

A study of the luminescence and absorption spectra of Ho in LiYF₄ was made by Podzolkina [14] in 1976. The ground state of Ho was found to have two groups of levels separated by a gap ~150 cm⁻¹. The lifetimes of ⁵S₂ and ⁵I₇ levels were reported to be 0.05 and 10 msec at room temperature.

Karayianis et al. [15] experimentally established an energy level scheme for the lowest ten multiplets of Ho in LiYF₄. They also obtained these energy levels by diagonalizing a Hamiltonian which describes the free ion and crystal field interaction in a basis of states spanning the 4f^N configuration. The data were recorded with a 2 % at. Ho doped single crystal. The longest wavelengths transition observed in absorption was those due to the ⁵I₈→⁵I₇ transition. The Stark-split energy levels in the lowest ten multiplets of Ho were tabulated.

The luminescence dynamics of Ho in LiYF₄ was reported by Rubin et al [16]. The Ho ions were excited in their ⁵S₂ levels by using a pulse dye laser. The decay channels and the decay times measured are shown in Fig. 4.6. Rate equations were used to fit the experimental data. These workers studied the different excitation channels responsible for the population of ⁵I₇ level; the

lifetime of this level was reported to be 16 msec at room temperature for 1 % at. Ho concentration, and to increase with increasing Ho concentration due to the radiative transfer of energy among the Ho ions.

REFERENCES (Chapter 4)

- 1) D. Gabbe and A. L. Harmer, J. Cryst. Growth, Vol. 3, 544 (1968).
- 2) H. P. Jenssen, D. R. Gabbe, A. Linz, and C. S. Naiman, IEEE, Quantum Electron. Vol. QE-14, 735 (1978).
- 3) R. E. Thoma, C. F. Weaver, H. A. Friedman, H. Insley, L.A. Harris and H. A. Yakel, Jr., J. Phys. Chem. Vol. 65, 1096 (1961).
- 4) W. A. Shand, J. Crystal Growth, Vol. 5, 143 (1969).
- 5) W. M. Yen and P. M. Selzer, in Laser Spectroscopy, edited by W. M. Yen and P. M. Selzer, Vol. 49, (Springer Verlag Publishing Company), p.141.
- 6) G. S. Ofelt, J. Chem. Phys. Vol. 37, 511 (1962).
- 7) G. F. Imbusch and R. Kopelman, in Laser Spectroscopy, edited by W. M. Yen and P. M. Selzer, Vol. 49, (Springer Verlag Publishing Company), p.1.
- 8) G. H. Dieke, in Spectra and Energy Levels of Rare Earth Ions in Crystals (Wiley Interscience, New York, 1968).
- 9) H. P. Jenssen, A. Linz, R. P. Leavitt, C. A. Morrison, and D. E. Worthman, Phys. Review B, Vol. 11, 92 (1975).
- 10) A. Brenier, J. Rubin, R. Moncorgé and C. Pedrini, J. Physique, Vol. 50, 1463 (1989).
- 11) N. I. Agladze, E. A. Vinogradov, and M. N. Popova, Opt. Spectrosc. (USSR), Vol. 61(1), 1 (1986).

- 12) N. I. Agladze and M. N. Popova, Solid State Commun., Vol. 55, 1097 (1985).
- 13) S. N. Gifeisman, A. M. Tkachuk, and V. V. Prizmak, Opt. Spectrosc. (USSR), Vol. 44 (1), 120 (1978).
- 14) I. G. Podkolzina, A. M. Tkachuk, V. A. Fedoriv and P.P. Feofilov, Opt. Spectrosc. (USSR), Vol. 40 (1), 111 (1976).
- 15) N. Karayianis, D. E. Wortman, and H. P. Jenssen, J. Phys. Chem. Solids, Vol. 37, 675 (1976).
- 16) J. Rubin, A. Brenier, R. Moncorge and C. Pedrini, J. Physique, Vol. 48, 1761 (1987).

TABLE 4.1

Optical, Physical, and Mechanical Properties of LiYF₄

Optical :

Index of refraction at $\lambda = 1.06 \mu\text{m}$	n_o (along a-axis) = 1.4481
.....	n_e (along c-axis) = 1.4704
UV absorption.....	50% at 0.120 nm
Two photon absorption coefficient	
β (cm/Mw) at $\lambda = 266 \text{ nm}$	$< 3.0 \times 10^{-6}$
Damage resistance (Gw/cm ²) at $\lambda = 1.06 \mu\text{m}$	~ 20

Thermal :

Thermal conductivity at 300K (K/cm-°K).....	0.06
Thermal expansion coefficient	
in 0-100°C range (°K-1).....	a axis : 13.8×10^{-6}
	c axis : 9.0×10^{-6}

Mechanical :

Density (g/cm ³).....	3.99
Hardness (Mch).....	4-5
Elastic modulus (N/m ²).....	7.5×10^{10}
Poisson's ratio.....	0.33
Strength (modulus of rupture, in Kg/cm ²).....	335

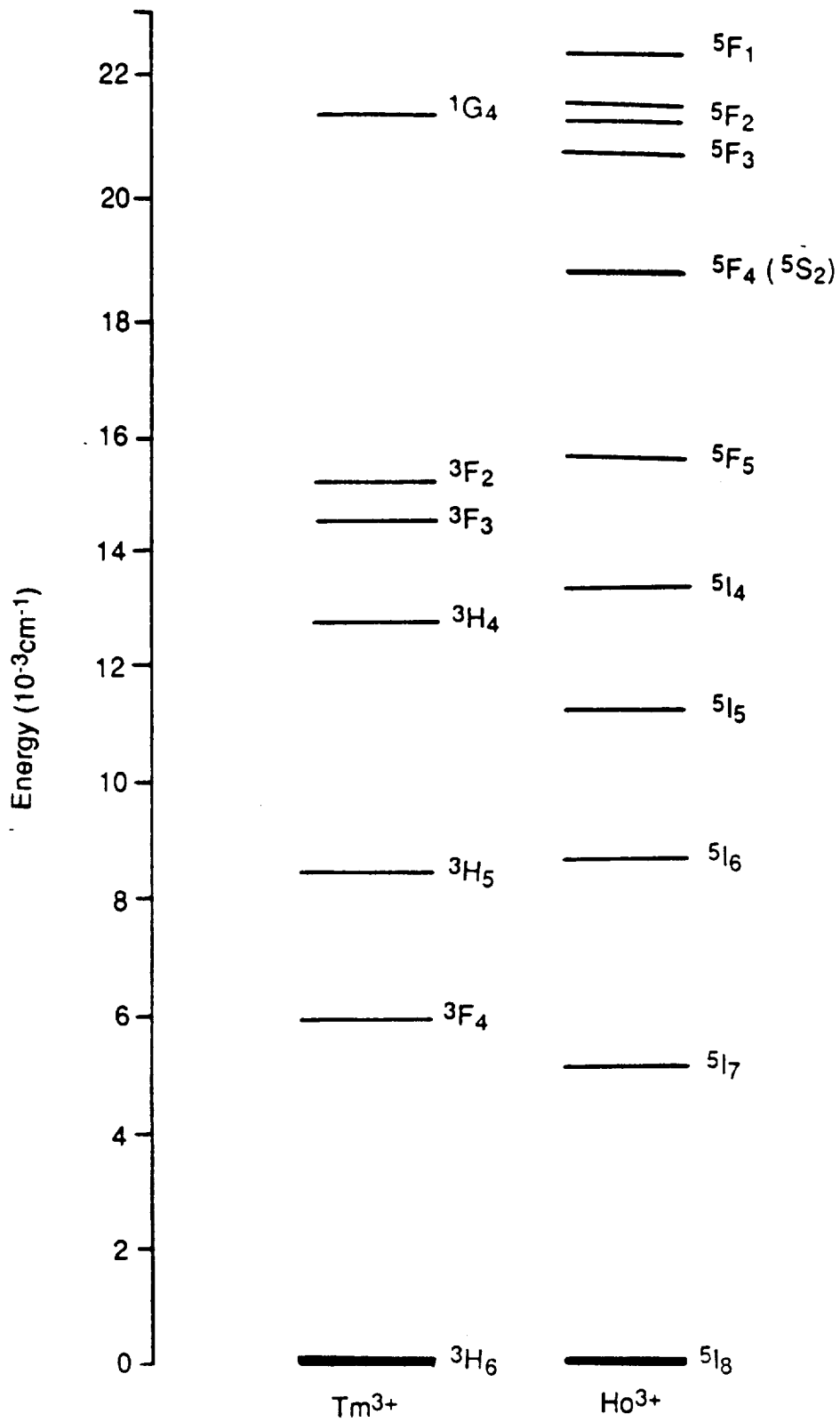


Fig. 4.1 Energy levels of Tm^{3+} and Ho^{3+} in $LiYF_4$.

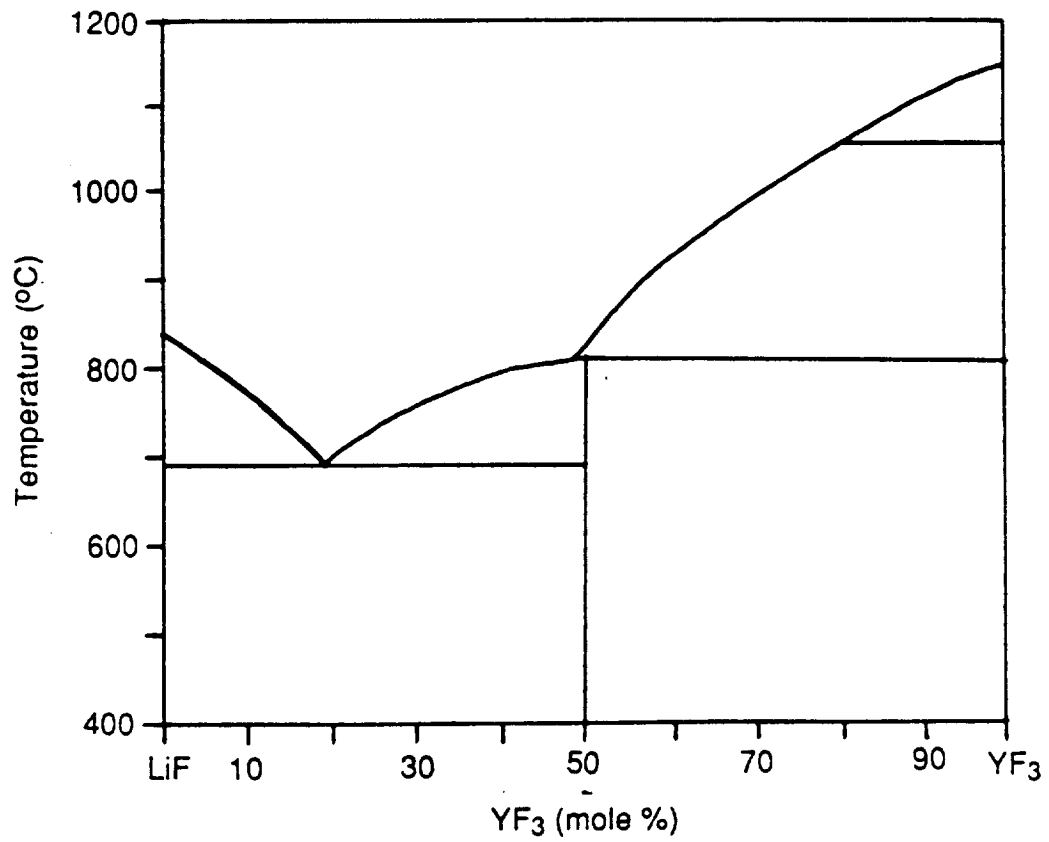


Fig. 4.2 The phase diagram of the LiF - YF₃ [3].

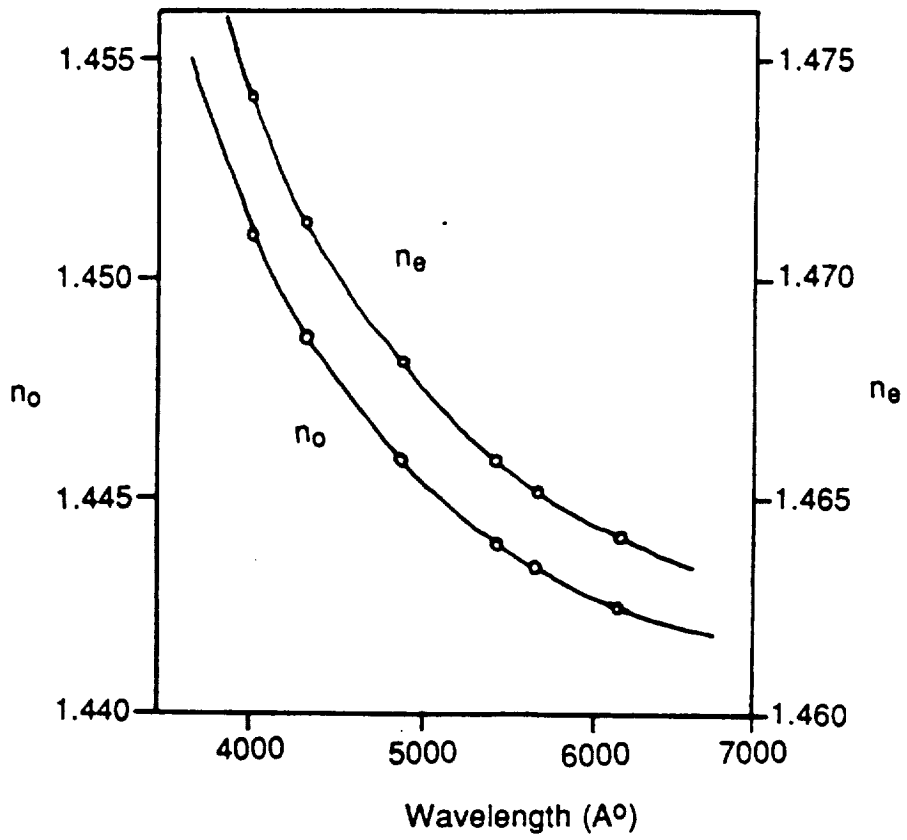


Fig. 4.3 Refractive indices of LiYF₄ crystal [4].

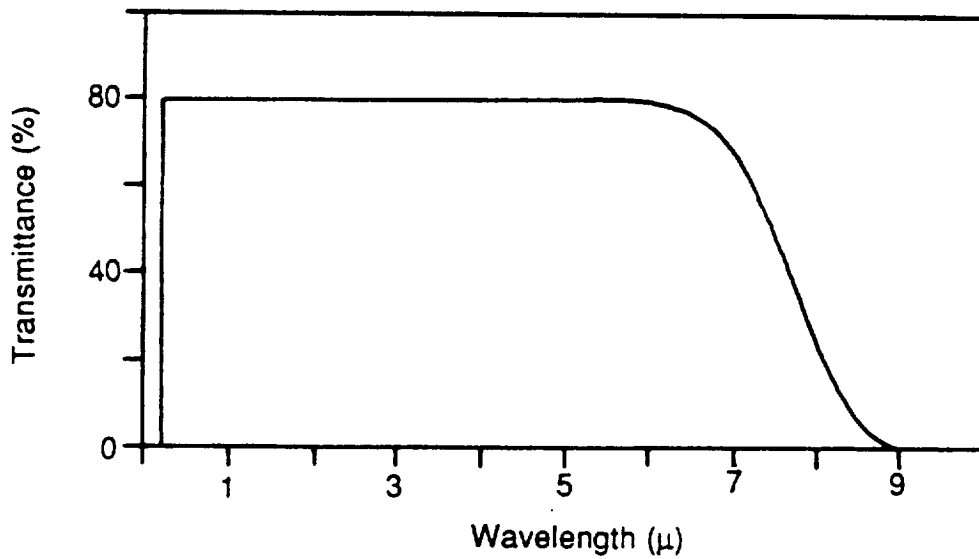


Fig. 4.4 Transmission limits of LiYF₄ [3].

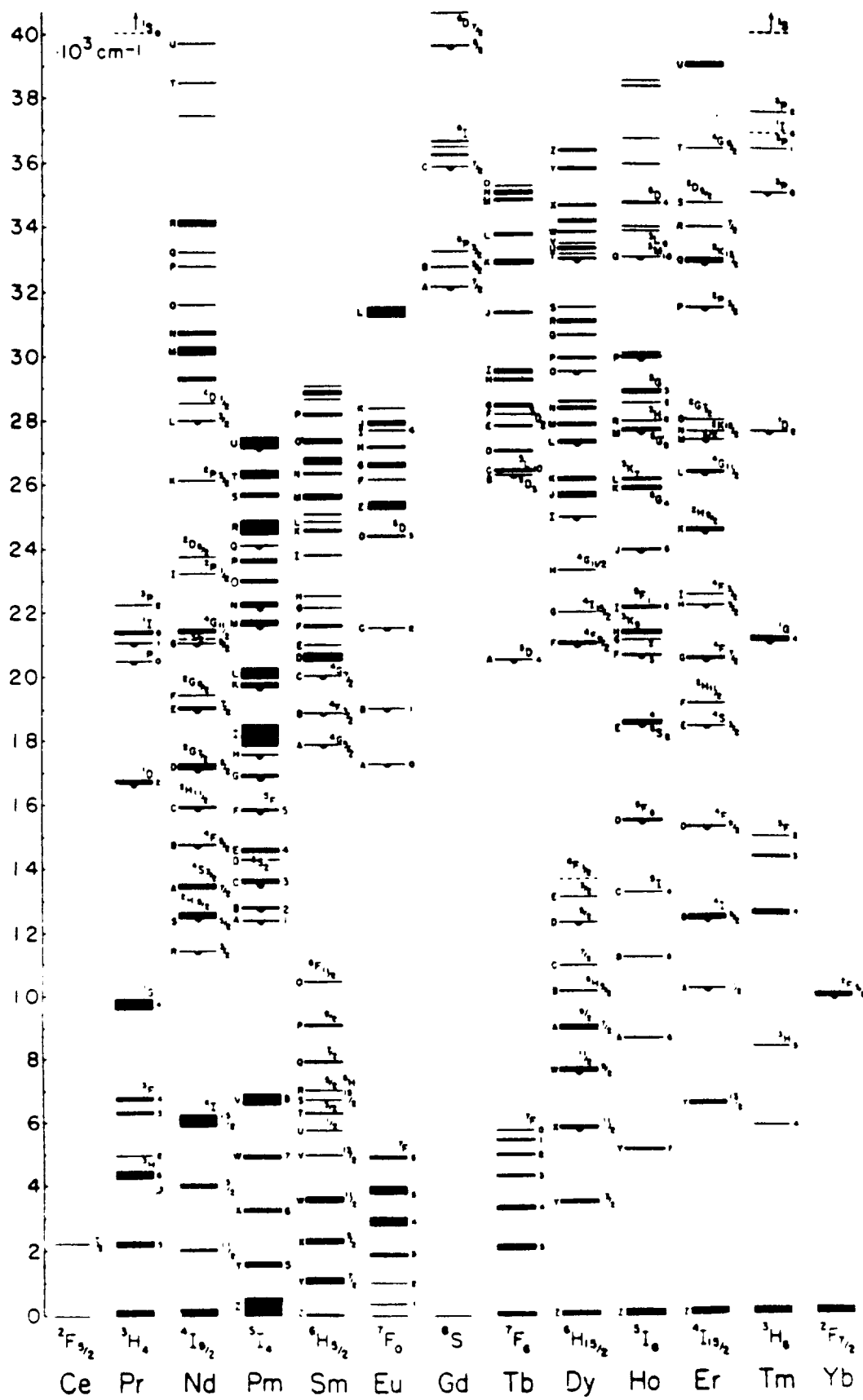


Fig. 4.5 Energy levels of the rare earths in LaCl₃ [8].

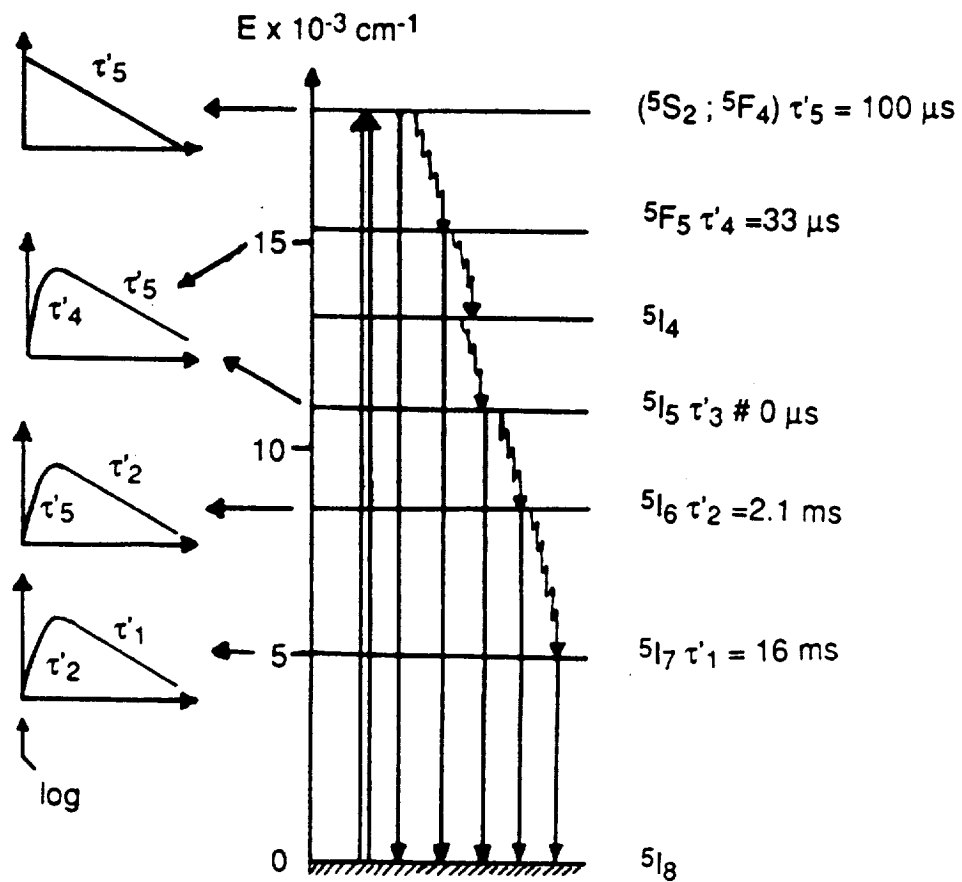


Fig. 4.6 The decay channels and the lifetimes of Ho^{3+} [16] (Ho concentration is 1% at.; 5S_2 level is excited).

5. EXPERIMENTAL RESULTS I. ABSORPTION AND LUMINESCENCE MEASUREMENTS

5.1 LiYF₄ : Tm³⁺ (.5%)

The absorption spectra reported in Table 5.1 and Fig. 5.1 were taken with the Perkin Elmer Model Lambda 9 spectrophotometer described in section 3.1. The strong structured bands are centered at :

470, 660, 680, 795, 1240 and 1685 nm.

Most of the lines are seen in excitation when the luminescence is monitored at 1.7 and 1.8 μm . The strong lines in absorption also tend to be strong lines in excitation.

The luminescence measurements were made for two different directions of the exciting source with respect to the c-axis of the sample:

1) The direction of the exciting source was parallel, and the luminescence from the sample detected was perpendicular to the c-axis.

2) The direction of the exciting source was perpendicular, and the luminescence from the sample detected was parallel to the c-axis.

In both cases the integrated intensities have the same temperature dependence in the 78 to 550K region.

The optical luminescence of Tm^{3+} in LiYF_4 at room temperature is reported in Table 5.2 and Fig. 5.2. The line intensities do not change very much with the temperature of the sample.

The 1.9 μm luminescence of Tm^{3+} in LiYF_4 at temperatures 78 and 300K is given in Table 5.3 and Fig. 5.3. The spectra present much sharper lines at low temperatures.

The integrated intensities of the luminescence designated in Fig. 5.2 with the transition ${}^3\text{H}_4 \rightarrow {}^3\text{H}_6$ and in Fig. 5.3 with the transition ${}^3\text{F}_4 \rightarrow {}^3\text{H}_6$ slightly decrease with increasing temperature (see Tables 5.4 and 5.5 and Figs. 5.4 and 5.5.).

5.2 LiYF₄ : Ho³⁺(1%)

The absorption and the luminescence spectra of LiYF₄ : Ho³⁺ at 300K were measured in the direction of the c-axis.

The absorption spectrum is reported in Table 5.6 and Fig. 5.6. The spectrum consists of nine structured bands corresponding to the transitions from the ground state to various excited states.

The optical luminescence of Ho³⁺ in LiYF₄ is reported in Table 5.7 and Fig.5.7. The spectrum consists of three structured bands centered at :

540, 650 and 750 nm.

The infrared luminescence at 78 and 300K is reported in Table 5.8 and Fig. 5.8. The only emission observed was in the 1.9 - 2.2 μm region. The lines of the band are sharper at 78K than at 300K. We also observed that more luminescence lines appear at low wavelengths with increasing temperature.

The integrated intensity of the luminescence due to the ⁵I₇→⁵I₈ transition first increases and then decreases with increasing temperature (See Table 5.9 and Fig. 5.9).

5.3 LiYF₄ : Tm³⁺ (5%), Ho³⁺ (.2%)

The absorption spectrum of LiYF₄ : Tm³⁺(5%), Ho³⁺(.2%) at 300K is reported in Table 5.10 and Fig. 5.10. This spectrum is simply the superposition of the absorption spectra of LiYF₄ : Tm³⁺ and LiYF₄ : Ho³⁺. Therefore effects due to ion-pairing such as shifting of lines or appearance of additional lines do not exist. In the present spectrum, the lines contributed by Ho³⁺ are considerably weaker due to the lower Ho³⁺ concentration.

The optical luminescence lines of LiYF₄ : Tm(5%), Ho(.2%) at 300K are reported in Table 5.11 and Fig. 5.11. The luminescence lines of both Tm³⁺ and Ho³⁺ were seen from 300 to 900 nm. The most intense lines were those of Tm³⁺ in the 800 nm region.

The infrared luminescence of LiYF₄ : Tm(5%), Ho(.2%) at 300K is reported in Table 5.12 and Fig. 5.12. The spectrum is the superposition of the luminescence spectra of LiYF₄ : Tm³⁺ and LiYF₄ : Ho³⁺.

TABLE 5.1
 ABSORPTION SPECTRUM OF LiYF₄: Tm³⁺ (.5%) AT 300K

$\lambda(\text{nm})$	$\lambda(\text{cm}^{-1})$	Intensity	Energy Level Assignment
464.0	21552	56	1G ₄
466.0	21459	47	
469.8	21286	18	
472.2	21178	14	
476.2	20999	11	
483.6	20678	11	
658.0	15198	32	3F ₂ , 3F ₃
664.4	15051	21	
684.6	14607	378	
686.2	14573	427	
698.2	14323	39	
701.6	14253	49	
704.0	14205	32	3H ₄
780.0	12821	126	
792.0	12626	95	
802.0	12469	28	3H ₅
1172.5	8529	75	
1219.5	8200	170	

TABLE 5.1
 ABSORPTION SPECTRUM OF LiYF₄: Tm³⁺ (.5%) AT 300K
 (Continued)

$\lambda(\text{nm})$	$\lambda(\text{cm}^{-1})$	Intensity	Energy Level Assignment
1690.0	5917	200	 3F ₄
1744.0	5734	100	
1830.5	5463	48	
1880.0	5319	31	

Refer to Figure 5.1

Instrument used: Perkin Elmer Model LAMDA-9

Sample thickness: .5 cm

Ground state: ³H₆

TABLE 5.2
OPTICAL LUMINESCENCE SPECTRUM OF LiYF₄: Tm³⁺(.5%) AT 300K

$\lambda(\text{nm})$	$\lambda(\text{cm}^{-1})$	Intensity	Transitions
634.2	15768	5	1G ₄ →3F ₄
643.4	15543	18	
648.0	15432	38	
653.4	15305	10	
657.6	15207	32	
666.4	15006	12	
757.4	13203	5	3H ₄ →3H ₆
771.8	12957	13	
778.0	12853	22	
789.0	12674	118	
794.2	12591	70	
800.0	12500	63	
806.0	12407	42	
814.0	12285	38	

Refer to Figure 5.2

Source: Coherent Lixel Model 526 Ar-Ion Laser tuned at 460 nm

GO515 ($\lambda < 515$ nm) cut off filter after sample

Detector: RCA C31034 photomultiplier

Spex Model 1269 monochromator; slits (both) : 300 μm

Stanford Research Systems Model SR510 "lock-in" amplifier

Sensitivity : 500 μV

Time Constant : 0.3 sec.

TABLE 5.3
 INFRARED LUMINESCENCE OF LiYF₄: Tm³⁺(.5%)

78K			300K			Transitions
$\lambda(\text{nm})$	$\lambda(\text{cm}^{-1})$	Intensity	$\lambda(\text{nm})$	$\lambda(\text{cm}^{-1})$	Intensity	
1738.3	5753	8	1686.0	5931	15	$^3F_4 \rightarrow ^3H_6$
1746.7	5725	11	1745.7	5728	39	
1757.3	5691	7				
1797.3	5564	56	1797.3	5564	36	
1851.7	5400	9	1850.0	5405	30	
1911.7	5231	60	1911.6	5231	26	
1930.0	5181	37				

Refer to Figure 5.3

Source: Jarrell Ash 30W tungsten Lamp

RG850 ($\lambda < 850$ nm) cut off filter after sample

Detector : Spex Model 1428 PbS detector

Spex Model 1681 .22m monochromator; slits (both) : 500 μm

Stanford Research Systems Model SR510 "lock-in" amplifier

Sensitivity : 50 μV

Time Constant : .3 sec.

TABLE 5.4

TEMPERATURE DEPENDENCE OF 800 nm LUMINESCENCE OF LiYF₄ :Tm³⁺(.5%)

Temperature (K)	Integrated Intensity (a) (A.U.)	Integrated Intensity (b) (A.U.)
80	1.8	2.9
90	1.8	3.3
100	1.8	3.5
150	2.1	4.3
200	2.3	4.6
250	2.5	4.5
300	2.5	4.6
330	2.6	4.6
350	2.6	4.5

(a) : luminescence detected in the direction of the c-axis of the sample.

(b) : luminescence detected at 90° with respect to the direction of the c-axis of the sample.

Refer to Figure 5.4

Source : Jarrell Ash 30W tungsten lamp

Detector : RCA C31034 photomultiplier

SPEX Model 1269 monochromator; slits (both) :500 μm

Stanford Research Systems Model SR510 " lock-in" amplifier;

Sensitivity : 100 μV

Time constant : 0.3 sec.

Transition : ³H₄→³H₆

TABLE 5.5
TEMPERATURE DEPENDENCE OF 1.9 μm LUMINESCENCE OF $\text{LiYF}_4 : \text{Tm}^{3+} (.5\%)$

Temperature (K)	Integrated Intensity (a) (A.U.)	Integrated Intensity (b) (A.U.)
80	1.8	2.7
90	1.9	----
100	2.1	2.7
150	2.2	2.8
200	2.4	2.9
250	2.4	3.0
300	2.3	3.2
310	2.3	-----
350	2.3	3.3
400	2.3	3.1
450	2.2	3.1
500	2.2	3.3
550	2.1	3.4

(a) : luminescence detected in the direction of the c-axis of the sample.

(b) : luminescence detected at 90° with respect to the direction of the c-axis of the sample.

Refer to Figure 5.5

Source : Jarrell Ash 30W tungsten lamp

Detector : Spex Model 1428 PbS detector

SPEX Model 1681B .22m monochromator; slits (both) :500 μm

Stanford Research Systems Model SR510 " lock-in" amplifier;

Sensitivity : 100 μV

Time constant : 0.3 sec.

Transition : $^3F_4 \rightarrow ^3H_6$

TABLE 5.6
 ABSORPTION SPECTRUM OF LiYF₄: Ho³⁺ (1%) AT 300K

$\lambda(\text{nm})$	$\lambda(\text{cm}^{-1})$	Intensity	Energy Level Assignment
415.5	22067	145	
417.0	23981	180	
418.5	23895	90	5G ₅
420.5	23781	65	
422.0	23697	50	
441.0	22676	385	
446.5	22396	360	
448.5	22297	483	
449.9	22227	700	
451.2	22163	665	5F ₁ (5G ₆)
452.8	22085	125	
454.0	22026	140	
456.1	21925	120	
457.8	21844	275	
465.5	21482	45	
467.4	21395	85	3K ₈
468.2	21358	49	
472.5	21164	134	
473.1	21137	138	5F ₂
474.5	21075	48	

TABLE 5.6
 ABSORPTION SPECTRUM OF LiYF₄ : Ho³⁺ (1%) AT 300K
 (Continued)

$\lambda(\text{nm})$	$\lambda(\text{cm}^{-1})$	Intensity	Energy Level Assignment
477.0	20964	20	5F ₃
478.5	20899	30	
479.0	20877	40	
481.6	20764	90	
482.8	20713	70	
483.9	20665	120	
484.4	20644	235	
485.9	20580	65	
488.0	20492	35	
489.1	20446	35	
491.0	20367	25	
535.5	18674	335	5F ₄ (5S ₂)
537.2	18615	420	
538.8	18560	335	
539.5	18536	145	
541.8	18457	215	
543.5	18399	210	
546.0	18315	53	
548.0	18248	41	
549.0	18215	45	
550.0	18182	28	

TABLE 5.6
 ABSORPTION SPECTRUM OF $\text{LiYF}_4 : \text{Ho}^{3+}$ (1%) AT 300K
 (Continued)

$\lambda(\text{nm})$	$\lambda(\text{cm}^{-1})$	Intensity	Energy Level Assignment
639.5	15637	258	$5F_5$
642.0	15576	210	
645.1	15502	63	
646.8	15461	73	
651.7	15344	60	
654.0	15291	76	
656.0	15244	83	
657.0	15221	100	
658.0	15198	123	
1142.5	8753	75	
1154.0	8666	110	
1160.5	8617	53	
1181.0	8467	18	
1193.0	8382	70	
1894.0	5280	70	$5I_7$
1900.0	5263	65	
1909.6	5237	58	
1917.0	5217	133	
1924.4	5196	70	
1934.0	5171	110	
1942.0	5149	140	

TABLE 5.6
 ABSORPTION SPECTRUM OF LiYF₄ : Ho³⁺ (1%) AT 300K
 (Continued)

$\lambda(\text{nm})$	$\lambda(\text{cm}^{-1})$	Intensity	Energy Level Assignment
1947.0	5136	208	5I ₇
1966.0	5087	95	
1996.0	5010	60	
2008.4	4979	53	
2023.0	4943	60	
2040.0	4902	58	
2052.0	4873	78	
2064.0	4845	95	

Refer to Figure 5.6

Instrument used: Perkin Elmer Model LAMDA-9

Sample thickness: 1.2 cm

Ground state: ⁵I₈

TABLE 5.7
OPTICAL LUMINESCENCE SPECTRUM OF LiYF₄: Ho³⁺(1%) AT 300K

$\lambda(\text{nm})$	$\lambda(\text{cm}^{-1})$	Intensity	Transitions
534.6	18706	19	$5S_2 \rightarrow 5I_8$
537.4	18608	32	
541.1	18481	39	
543.4	18403	50	
545.8	18322	60	
548.7	18225	39	
550.0	18182	59	
637.9	15676	38	$5F_5 \rightarrow 5I_8$
640.5	15613	3	
643.4	15542	4	
646.1	15477	5	
648.4	15423	4	
651.1	15359	4	
653.3	15307	6	
655.5	15256	7	
658.1	15195	13	
659.3	15168	13	
739.1	13530	6	$5S_2 \rightarrow 5I_7$
743.9	13443	7	
748.0	13369	12	

TABLE 5.7
OPTICAL LUMINESCENCE SPECTRUM OF LiYF₄: Ho³⁺(1%) AT 300K
(Continued)

$\lambda(\text{nm})$	$\lambda(\text{cm}^{-1})$	Intensity	Transitions
750.5	13324	51	5S ₂ → 5I ₇
752.4	13291	19	
754.2	13259	7	
757.6	13200	15	
757.9	13194	18	

Refer to Figure 5.7

Source: Coherent Lexel Model 526 Ar-Ion Laser tuned at 460 nm

GO515 ($\lambda < 515$ nm) cut off filter after sample

Detector: RCA C31034 photomultiplier

Spex Model 1269 monochromator; slits (both) : 300 μm

Stanford Research Systems Model SR510 "lock-in" amplifier

Sensitivity : 500 μV

Time Constant : 0.3 sec.

TABLE 5.8
INFRARED LUMINESCENCE OF LiYF₄: Ho³⁺(1%)

78K			300K			Transitions
$\lambda(\text{nm})$	$\lambda(\text{cm}^{-1})$	Intensity	$\lambda(\text{nm})$	$\lambda(\text{cm}^{-1})$	Intensity	
1937.0	5163	7	1888.3	5296	12	5 ₁₇ →5 ₁₈
1946.1	5138	10	1914.3	5224	18	
1961.0	5099	15	1944.2	5144	39	
1993.8	5016	6	1959.7	5103	29	
2019.8	4951	14	1998.1	5005	26	
2038.3	4906	20	2018.2	4955	37	
2050.7	4876	48	2050.7	4876	61	
2063.6	4846	61	2058.8	4857	70	

Refer to Figure 5.8

Source: Jarrell Ash 30W tungsten Lamp

RG850 ($\lambda < 850 \text{ nm}$) cut off filter after sample

Detector : Spex Model 1428 PbS detector

Spex Model 1681 .22m monochromator; slits (both) : 500 μm

Stanford Research Systems Model SR510 "lock-in" amplifier

Sensitivity : 20 μV

Time Constant : 0.3 sec.

TABLE 5.9
TEMPERATURE DEPENDENCE OF 2.1 μm LUMINESCENCE OF $\text{LiYF}_4 : \text{Ho}^{3+}(1\%)$

Temperature (K)	Integrated Intensity (A.U.)
80	3.2
100	3.3
150	3.7
200	4.0
250	4.0
300	4.7
350	4.7
400	5.0
450	5.0
500	5.0
550	5.0

Refer to Figure 5.8

Source : Jarrell Ash 30W tungsten lamp

RG850 ($\lambda < 850 \text{ nm}$) cut off filter after sample

Detector : Spex Model 1428 PbS detector

SPEX Model 1681B .22m monochromator; slits (both) :500 μm

Stanford Research Systems Model SR510 " lock-in" amplifier;

Sensitivity : 20 μV

Time constant : 0.3 sec.

Transition : $^5I_7 \rightarrow ^5I_8$

TABLE 5.10

ABSORPTION SPECTRUM OF LiYF_4 : Tm^{3+} (5%), Ho^{3+} (.2%) AT 300K

$\lambda(\text{nm})$	$\lambda(\text{cm}^{-1})$	Intensity	Energy Level Assignment
415.4	24073	60	5G ₅ (Ho ³⁺)
417.0	23981	70	
422.4	23674	20	
446.2	22412	40	5F ₁ (5G ₆)(Ho ³⁺)
448.4	22302	30	
451.2	22163	40	
453.0	22075	80	
457.8	21844	30	
464.2	21542	190	
466.2	21450	160	
469.6	21295	50	3K ₈ , 5F ₂ , 5F ₃ (Ho ³⁺); 2G ₄ (Tm ³⁺)
472.4	21169	60	
476.0	21008	35	
484.0	20661	75	
486.0	20576	50	
488.0	20492	15	
535.6	18671	150	5F ₄ (5S ₂)(Ho ³⁺)
537.6	18601	90	
538.4	18574	48	
539.8	18525	20	
541.0	18484	25	

TABLE 5.10
 ABSORPTION SPECTRUM OF $\text{LiYF}_4: \text{Tm}^{3+}(5\%), \text{Ho}^{3+}(.2\%)$ AT 300K
 (Continued)

$\lambda(\text{nm})$	$\lambda(\text{cm}^{-1})$	Intensity	Energy Level Assignment
544.0	18382	10	$5F_4(5S_2)(\text{Ho}^{3+})$
637.8	15679	150	
640.0	15625	30	
658.0	15198	120	$5F_5(\text{Ho}^{3+}) ;$
664.2	15056	70	$3F_2, 3F_3(\text{Tm}^{3+})$
682.0	14663	1330	
684.4	14611	1500	
700.4	14278	160	
777.6	12860	410	$5I_5(\text{Ho}^{3+}) ; 3H_4(\text{Tm}^{3+})$
780.0	12821	440	
790.0	12658	340	
802.4	12463	100	
812.0	12315	40	
1159.0	8628	20	$5I_6(\text{Ho}^{3+}) ;$
1182.5	8457	68	
1215.5	8227	145	$3H_5(\text{Tm}^{3+})$
1259.0	7943	13	
1680.0	5953	355	$5I_7(\text{Ho}^{3+}) ; 3F_4(\text{Tm}^{3+})$
1742.0	5741	88	
1830.0	5465	35	

TABLE 5.10

ABSORPTION SPECTRUM OF $\text{LiYF}_4: \text{Tm}^{3+}(5\%), \text{Ho}^{3+}(.2\%)$ AT 300K
(Continued)

$\lambda(\text{nm})$	$\lambda(\text{cm}^{-1})$	Intensity	Energy Level Assignment
1855.5	5389	19	$5I_7(\text{Ho}^{3+}) ; 3F_4(\text{Tm}^{3+})$
1877.0	5328	20	
1890.0	5291	8	
1910.5	5234	13	
1940.0	5155	8	

Refer to Figure 5.10

Instrument used: Perkin Elmer Model LAMDA-9

Sample thickness: .2 cm

Ground states: $3H_6$ of Tm^{3+} and $5I_8$ of Ho^{3+}

TABLE 5.11

OPTICAL LUMINESCENCE SPECTRUM OF LiYF₄: Tm³⁺(5%), Ho³⁺(.2%) AT 300K

$\lambda(\text{nm})$	$\lambda(\text{cm}^{-1})$	Intensity	Transitions
534.4	18713	73	$5S_2 \rightarrow 5I_8(\text{Ho}^{3+})$
536.8	18629	75	
539.2	18546	52	
540.8	18491	53	
543.2	18409	59	
545.8	18322	31	
548.7	18225	44	
550.0	18182	27	
638.8	15654	7	$5F_5 \rightarrow 5I_8(\text{Ho}^{3+})$
640.8	15605	5	
643.4	15542	5	
645.4	15494	8	
648.7	15415	27	
652.6	15323	5	
655.3	15260	5	
658.1	15195	13	
667.6	14979	7	
739.5	13523	5	
743.7	13446	4	
748.0	13369	8	
750.0	13333	34	

TABLE 5.11
OPTICAL LUMINESCENCE SPECTRUM OF LiYF₄: Tm³⁺(5%), Ho³⁺(.2%) AT 300K
(Continued)

$\lambda(\text{nm})$	$\lambda(\text{cm}^{-1})$	Intensity	Transitions
751.8	13301	14	$5S_2 \rightarrow 5I_7(\text{Ho}^{3+});$ $3H_4 \rightarrow 3H_6(\text{Tm}^{3+})$
753.9	13264	6	
755.4	13238	11	
757.6	13200	12	
772.2	12950	6	
776.9	12872	8	
789.5	12666	27	
794.2	12591	26	
803.3	12449	22	
803.9	12439	21	
807.9	12378	19	
814.6	12276	20	

Refer to Figure 5.11

Source: Coherent Loxel Model 526 Ar-Ion Laser tuned at 460 nm

GO515 ($\lambda < 515$ nm) cut off filter after sample

Detector: RCA C31034 photomultiplier

Spex Model 1269 monochromator; slits (both) : 100 μm

Stanford Research Systems Model SR510 "lock-in" amplifier

Sensitivity : 1.0mV

Time Constant : 0.3 sec.

TABLE 5.12

INFRARED LUMINESCENCE SPECTRUM OF LiYF_4 : Tm^{3+} (5%), Ho^{3+} (.2%) AT 300K

$\lambda(\text{nm})$	$\lambda(\text{cm}^{-1})$	Intensity	Transitions
1682.0	5945	23	
1743.3	5736	59	
1794.0	5574	60	
1831.8	5459	61	
1843.0	5426	59	
1859.0	5405	54	
1862.3	5370	44	
1878.0	5325	58	
1892.0	5285	68	
1909.5	5237	66	$5I_7 \rightarrow 5I_8(\text{Ho}^{3+});$
1916.5	5218	70	$3H_4 \rightarrow 3H_6(\text{Tm}^{3+})$
1938.9	5158	76	
1944.5	5143	85	
1963.8	5092	51	
1997.0	5008	39	
2007.2	4982	38	
2018.0	4955	51	
2037.3	4908	57	
2050.2	4878	82	
2063.2	4847	95	

Refer to Figure 5.12

Source : Jarrell Ash 30W tungsten lamp

RG850 ($\lambda < 850$ nm) cut off filter after sample

Detector : Spex Model 1428 PbS detector

Spex Model 1681 .22m monochromator; slits (both) : 500 μ m

Stanford Research Systems Model SR510 "lock-in" amplifier

Sensitivity : 20 μ V

Time Constant : 0.3 sec.

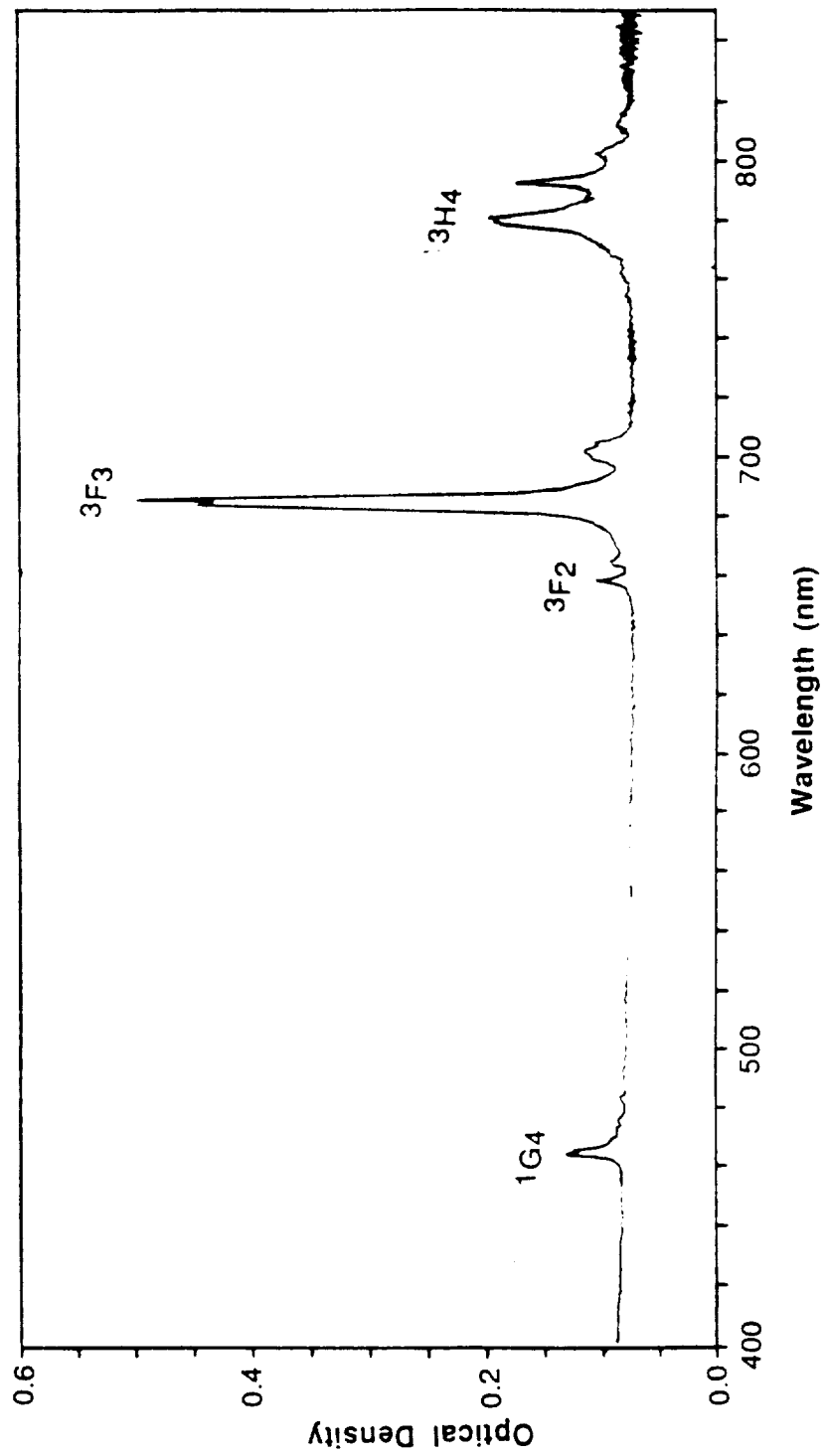


Fig. 5.1 (a) The absorption spectrum of LiYF₄: Tm³⁺ (.5%) in the optical region (T = 300K).

5-26

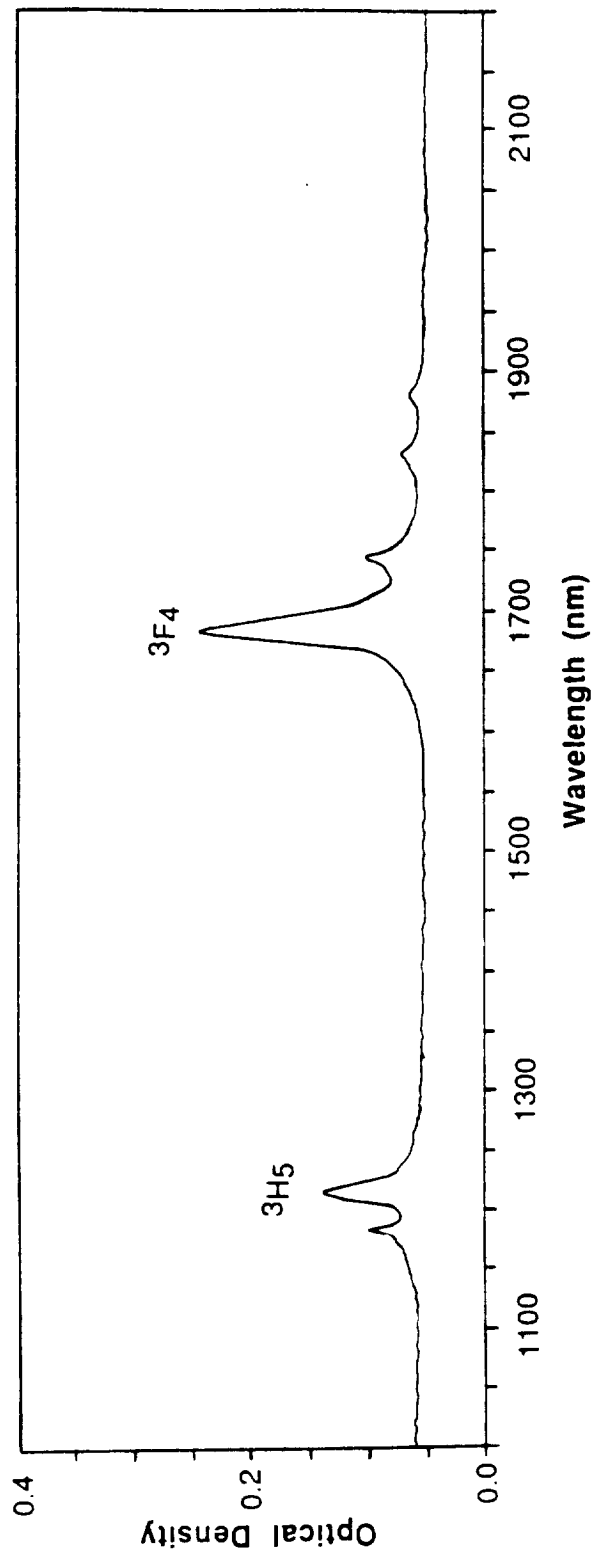


Fig. 5.1 (b) The absorption spectrum of LiYF₄: Tm³⁺ (.5%) in the infrared region (T=300K).

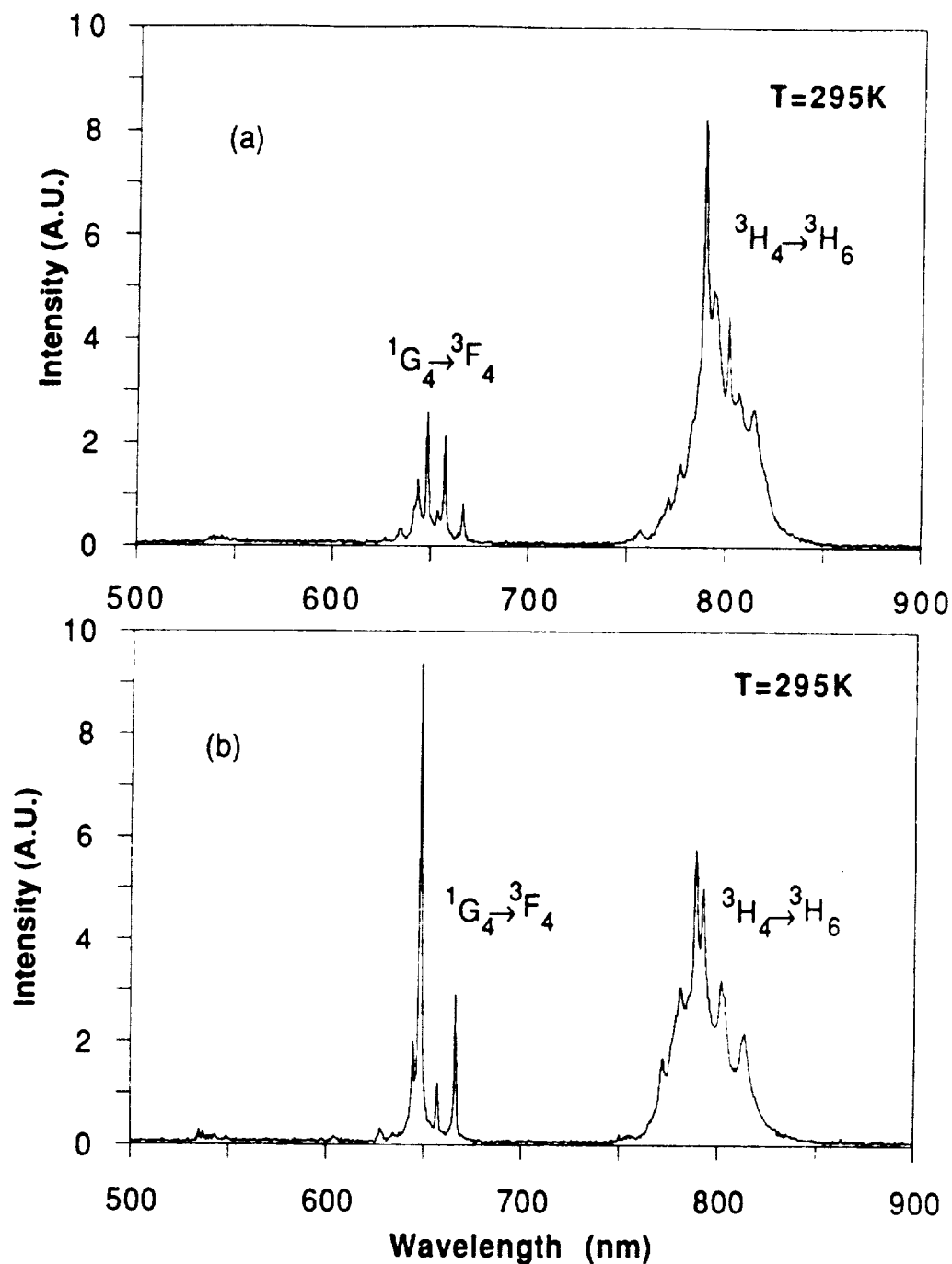


Fig. 5.2 The optical luminescence of Tm^{3+} in $LiYF_4 : Tm^{3+}(.5\%)$
 (a) Luminescence detected in the direction of the c-axis of the sample.
 (b) Luminescence detected at 90° with respect to the c-axis of the sample.

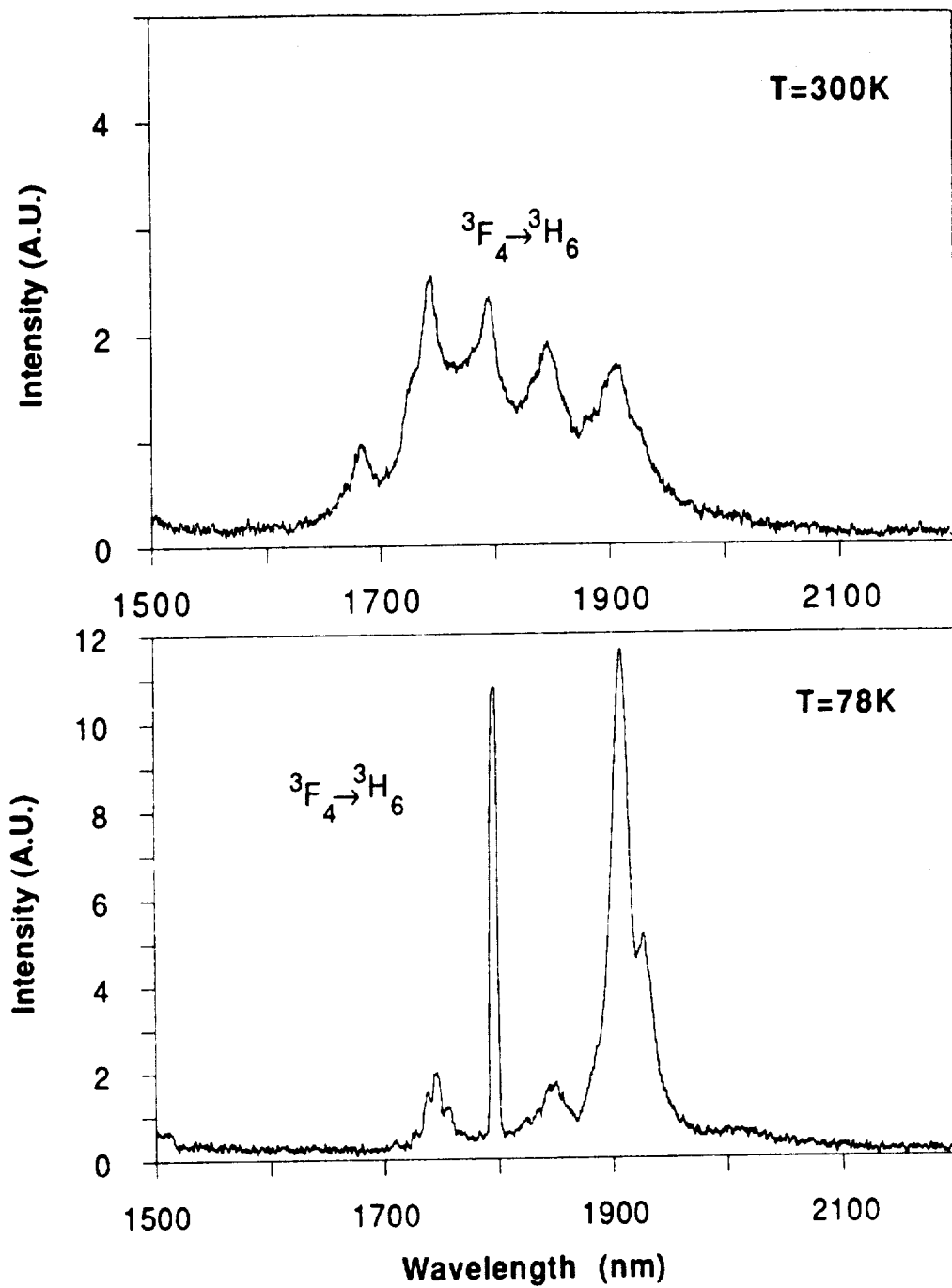


Fig. 5.3 (a) The infrared luminescence of Tm^{3+} in $LiYF_4: Tm^{3+}(.5\%)$ (luminescence detected in the direction of the c-axis of the sample).

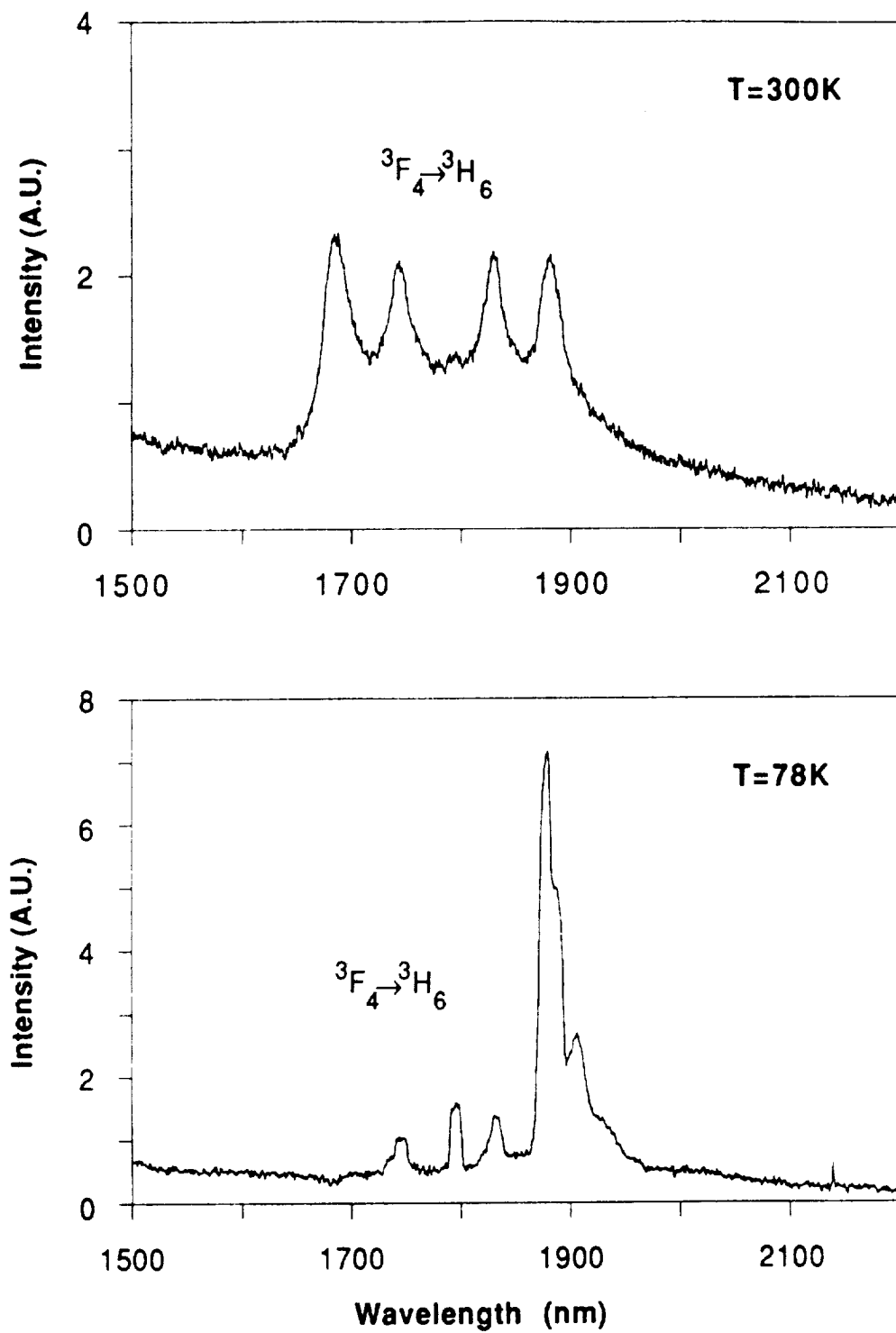


Fig. 5.3 (b) The infrared luminescence of Tm^{3+} in $LiYF_4 : Tm^{3+} (.5\%)$ (luminescence detected at 90° with respect to the c-axis of the sample).

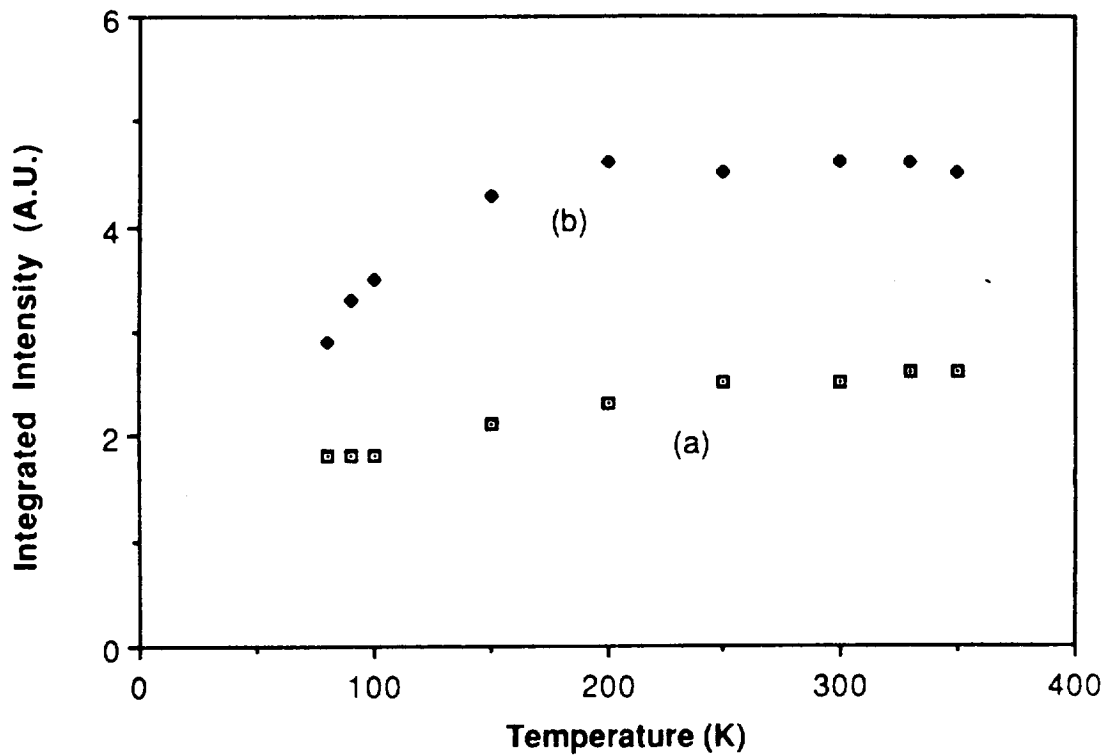


Fig. 5.4 Temperature dependence of 800 nm luminescence of Tm^{3+} in $LiYF_4 : Tm^{3+}$ (.5%).

- (a) : luminescence is detected in the direction of the c-axis of the sample.
- (b) : luminescence is detected at 90° respect to the c-axis of the sample.

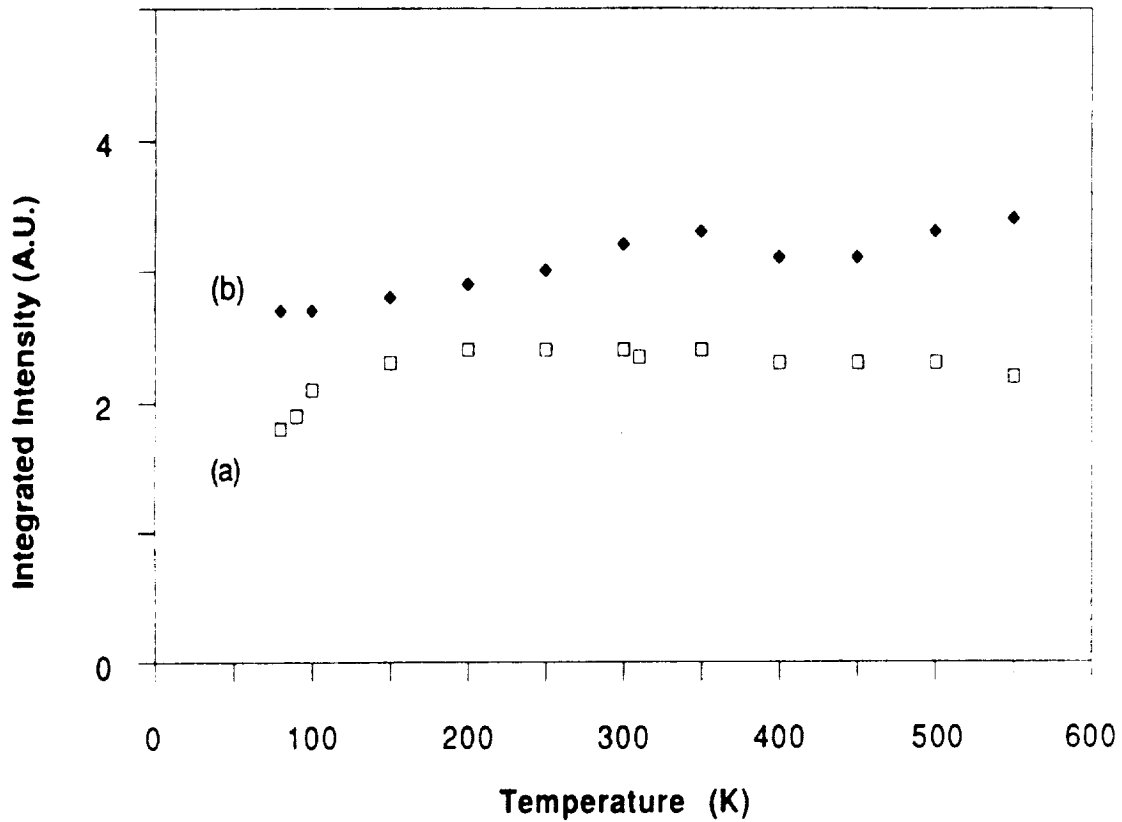


Fig. 5.5 The temperature dependence of 1.9 μm luminescence of Tm^{3+} in $\text{LiYF}_4 : \text{Tm}^{3+}(.5\%)$.

(a) : Luminescence detected in the direction of the c-axis of the sample.

(b) : Luminescence detected at 90° with respect to the c-axis of the sample.

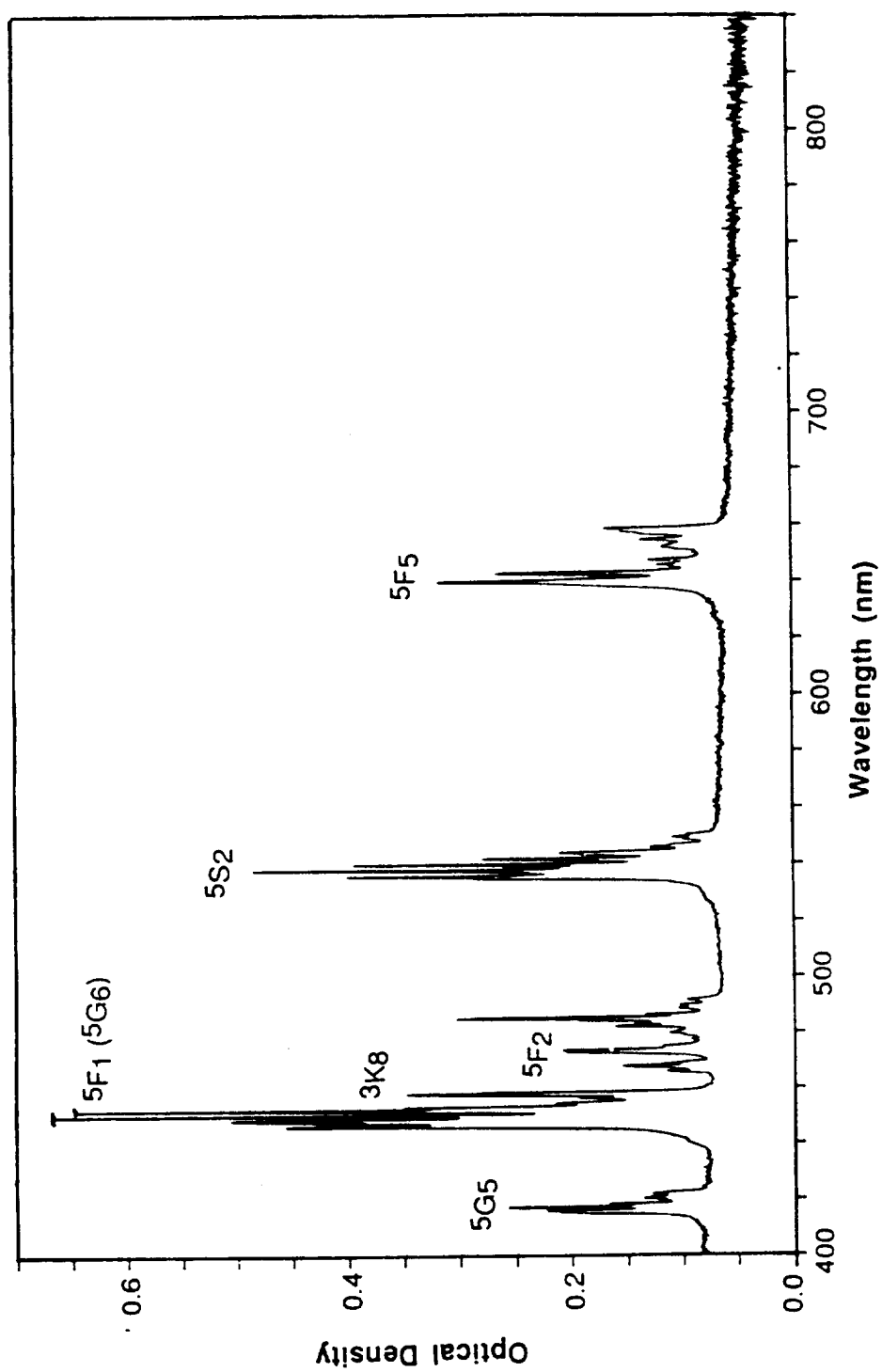


Fig. 5.6 (a) The absorption spectrum of LiYF₄ : Ho³⁺(1%) in the optical region (T=300K).

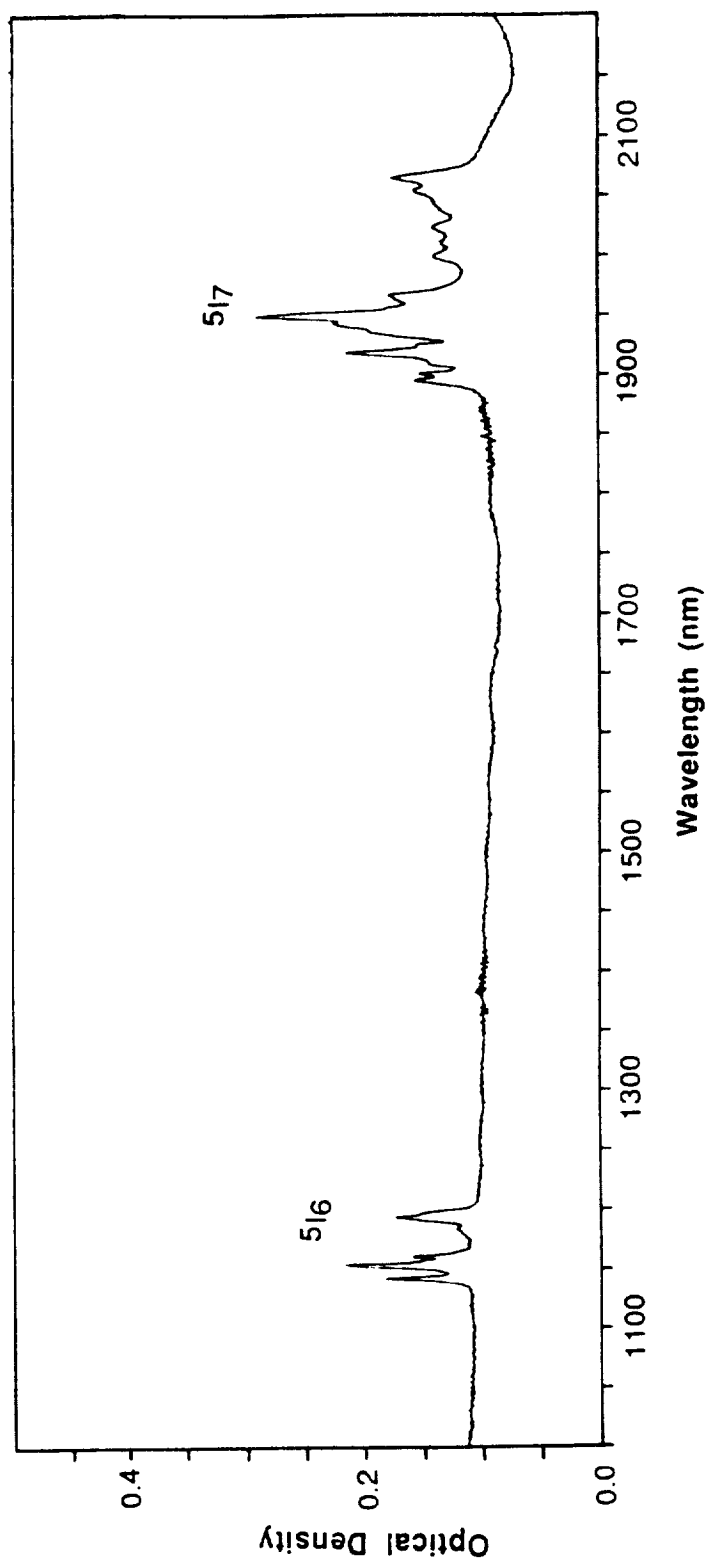


Fig. 5.6 (b) The absorption spectrum of LiYF₄ : Ho³⁺(1%) in the infrared region (T=300K).

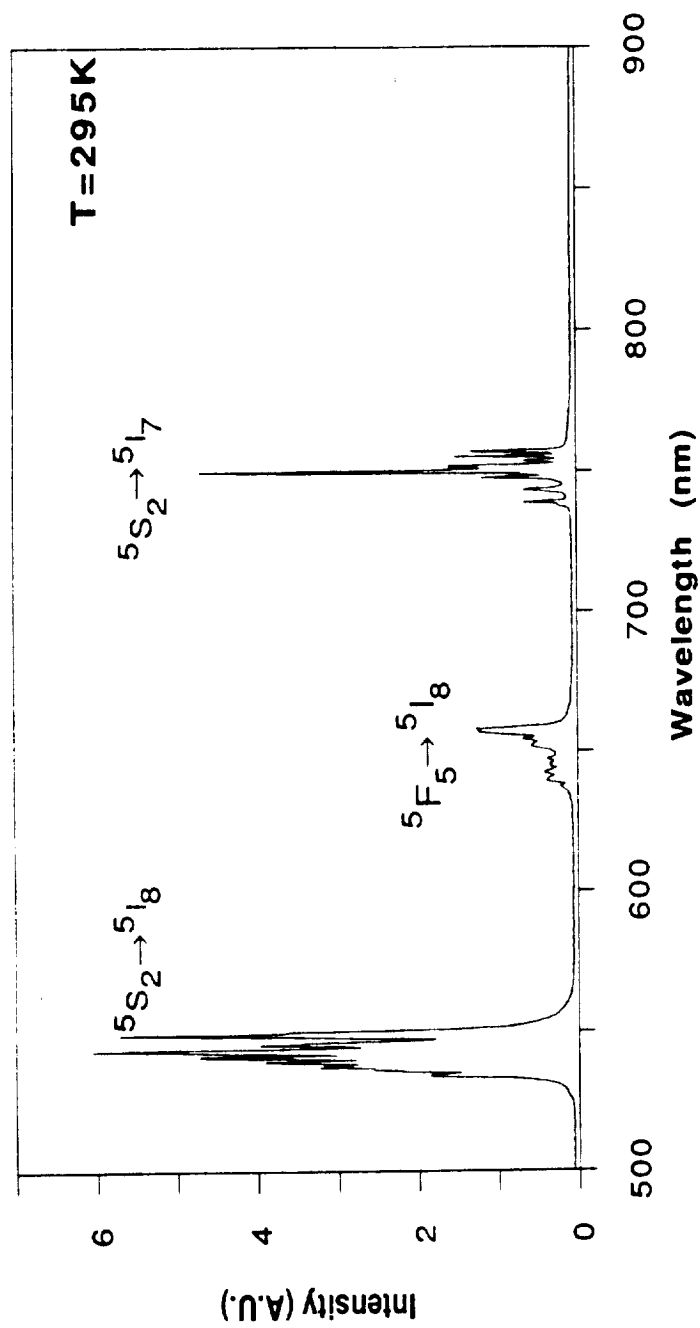


Fig. 5.7 The optical luminescence of Ho³⁺ in LiYF₄ : Ho³⁺(1%).

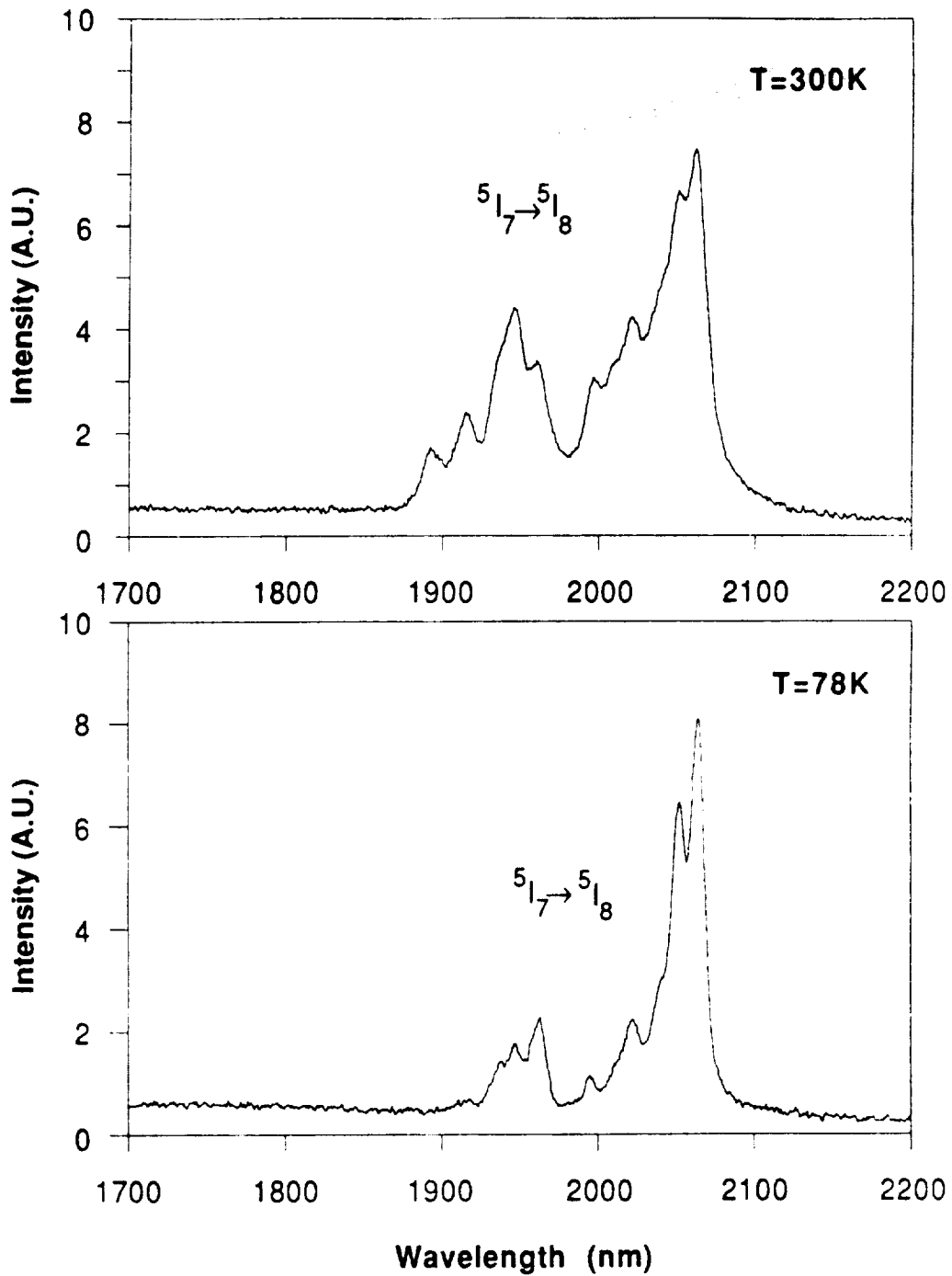


Fig. 5.8 The infrared luminescence of Ho^{3+} in $\text{LiYF}_4 : \text{Ho}^{3+}(1\%)$.

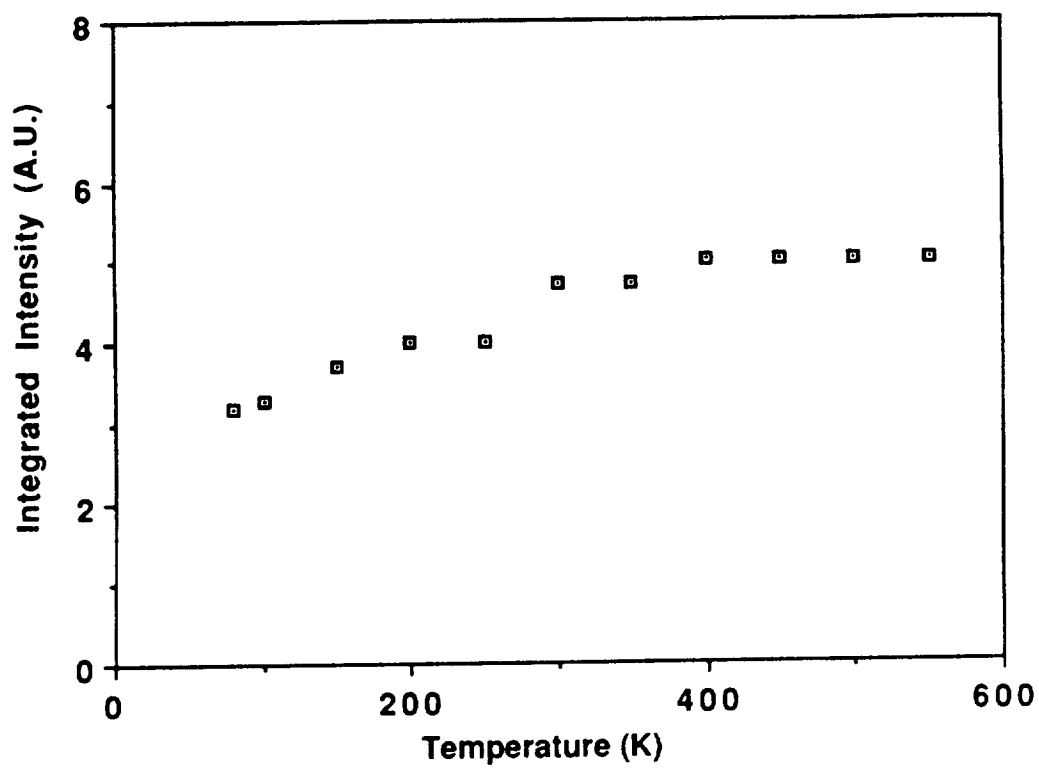


Fig. 5.9 The temperature dependence of 2.1 μm luminescence of Ho^{3+} in $\text{LiYF}_4 : \text{Ho}^{3+}(1\%)$.

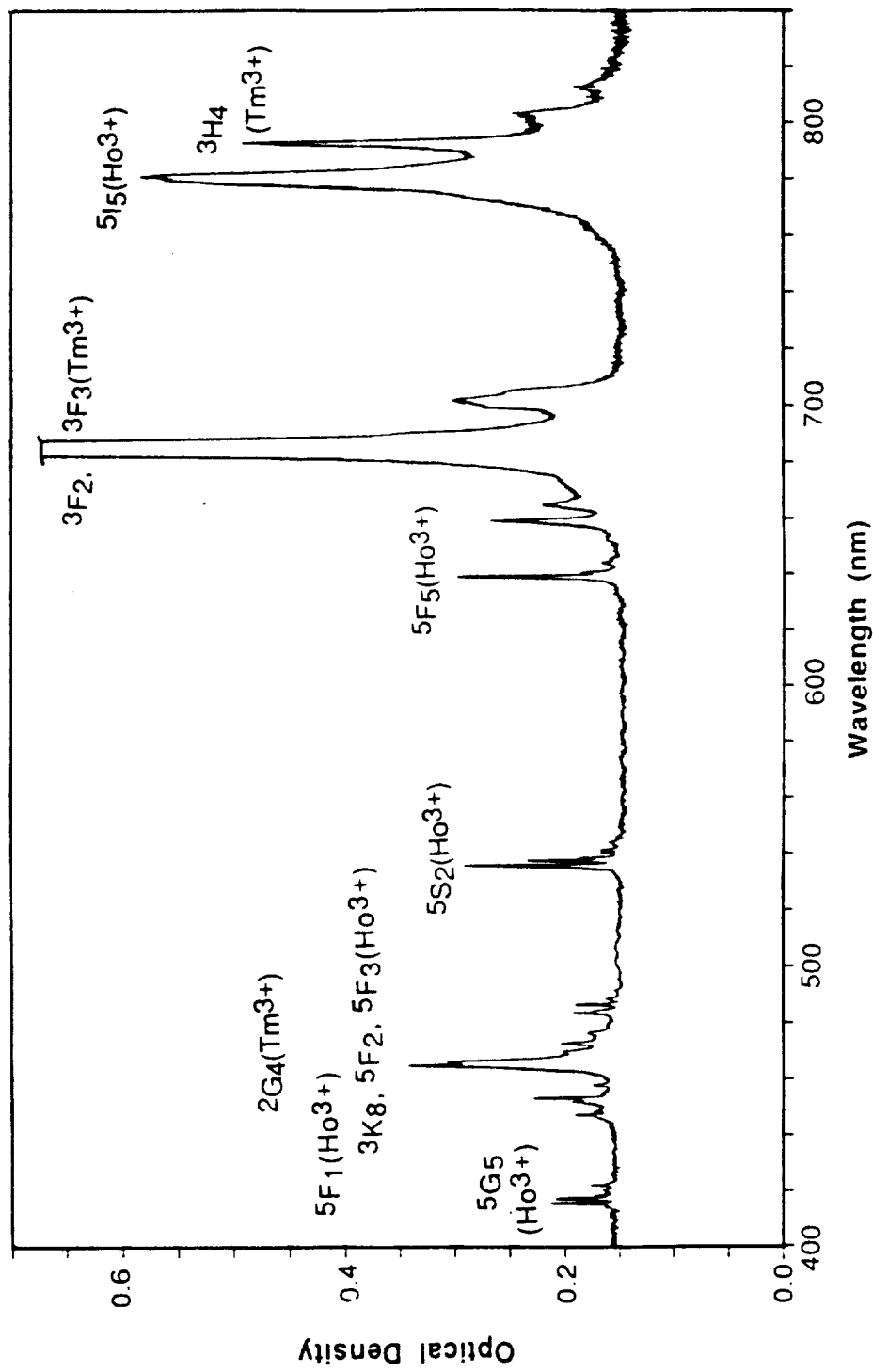


Fig. 5. 10 (a) The absorption spectrum of LiYF₄ : Tm³⁺(5%), Ho³⁺(2%) in the optical region (T = 300K).

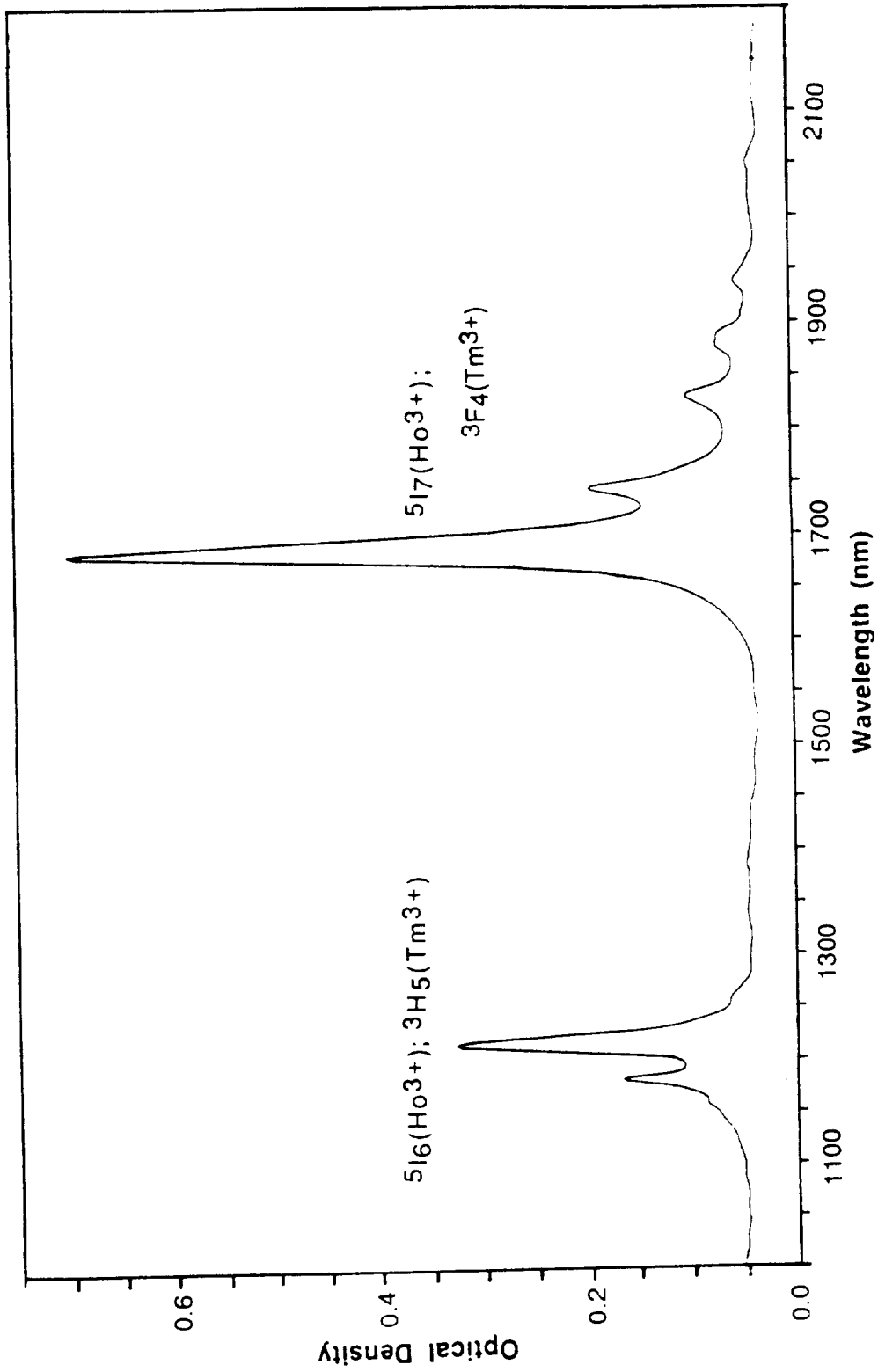


Fig. 5.10 (b) The absorption spectrum of LiYF₄: Tm³⁺(5%), Ho³⁺(.2%) in the infrared region (T=300K).

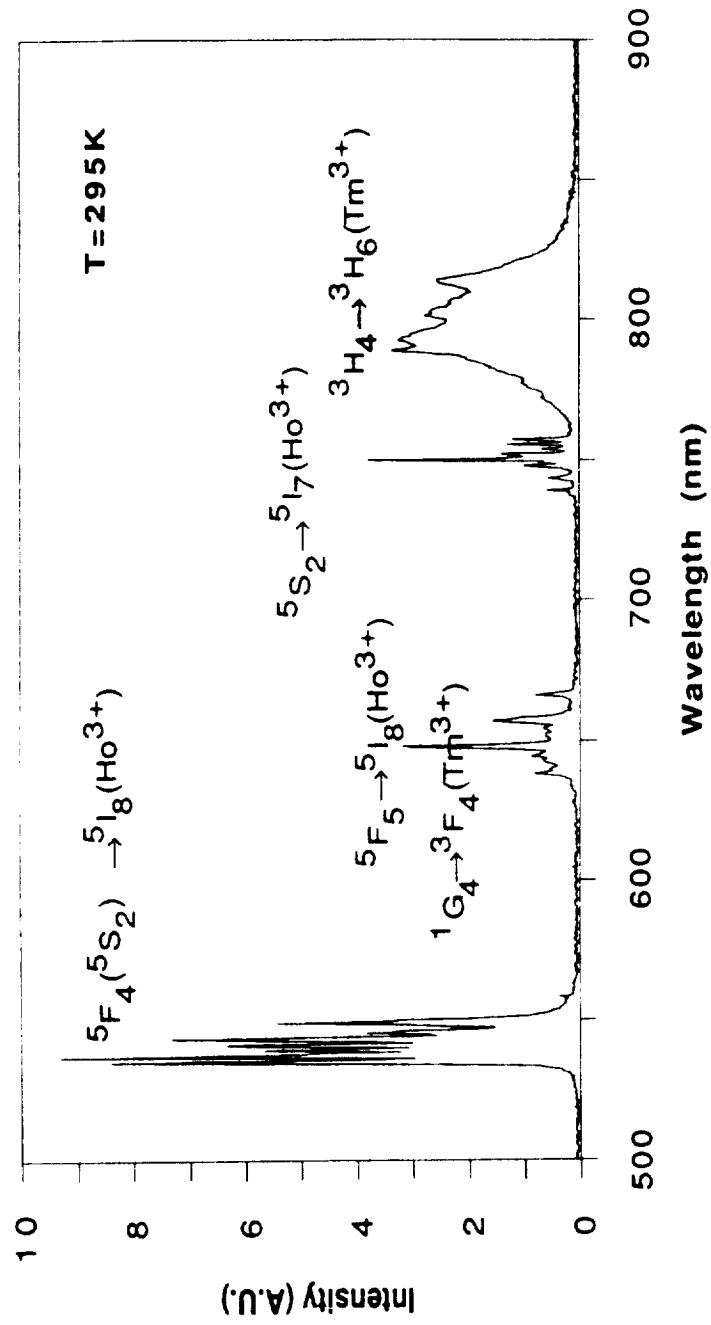


Fig. 5.11 The optical luminescence of LiYF₄: Tm³⁺(5%); Ho³⁺(.2).

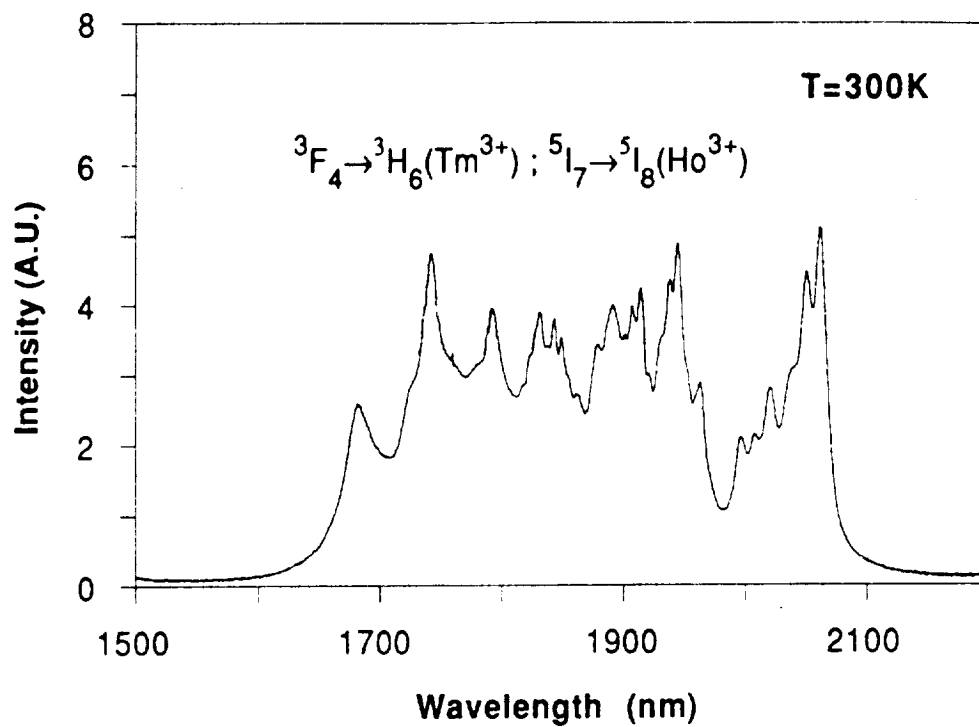


Fig. 5.12 The infrared luminescence spectrum of $LiYF_4 : Tm^{3+}(5\%); Ho^{3+}(.2\%)$ (only 3H_4 level of Tm^{3+} is excited by using a diode laser operated at $T=12.8^\circ C$).

6. EXPERIMENTAL RESULTS II. EXCITATION MEASUREMENTS

6.1 LiYF₄ : Tm³⁺(.5% at.)

The excitation spectra of Tm³⁺ and Ho³⁺ in different samples were measured by monitoring a luminescence line of these ions, while varying the wavelength of the incident radiation by means of the .22 meter SPEX monochromator as described in section 3.2.1. The gratings used were those of 600 grooves/mm blazed at 1.5 μm and 1200 grooves/mm blazed at 500 nm.

The experimental conditions under which the excitation spectra were made are reported in either the figures or the tables.

The excitation spectra of LiYF₄ : Tm(.5%) were measured at 295K by monitoring the luminescence at 1.7, 1.8, and 2.1 μm. No signal was detected when the luminescence was monitored at 2.1 μm, indicating that no emission from Tm³⁺ occurs at this wavelength.

The excitation spectrum of 1.7 μm emission from ³F₄ level of Tm is reported in Table 6.1 and Fig. 6.1. The absorption bands responsible for the 1.7 and 1.8 μm luminescence correlate with the absorption spectrum of LiYF₄ : Tm³⁺(.5% at.).

6.2 LiYF₄ : Ho³⁺(1% at.)

The excitation spectra of LiYF₄ : Ho³⁺(1% at.) were obtained at 295K by monitoring the luminescence at 2.1 μm. No absorption bands were observed when the luminescence was monitored at 1.6, 1.7 and 1.8 μm, indicating that no emission from Ho³⁺ occurs at these wavelengths.

The excitation spectrum of 2.1 μm emission from ⁵I₇ level of Ho is reported in Table 6.2 and Fig. 6.2. The absorption bands responsible for the emission correlate with the absorption spectrum of LiYF₄ : Ho³⁺(1% at.).

6.3 LiYF₄ : Tm³⁺(5%), Ho³⁺(.2%)

The excitation spectra of LiYF₄ : Tm³⁺(5%), Ho³⁺(.2%) were obtained at 295K by monitoring the luminescence at 1.6, 1.7, 1.8 and 2.1 μm. The excitation spectrum of the 1.7 μm emission of LiYF₄ : Tm³⁺(5% at.), Ho³⁺(.2% at.) is reported in Table 6.3(a) and Fig. 6.3(a). The absorption bands responsible for the luminescence from ³F₄ level of Tm and ⁵I₇ level of Ho coincide with those of Tm³⁺ and Ho³⁺ in LiYF₄. The bands can be easily assigned to either Tm³⁺ or Ho³⁺.

The excitation spectrum of 2.1 μm luminescence of the sample is reported in Table 6.3(b) and Fig. 6.3(b). It is simply the superposition of the excitation spectra of the 1.7 μm emission of LiYF₄ : Tm³⁺ and the 2.1 μm emission of LiYF₄ : Ho³⁺.

TABLE 6.1
 EXCITATION SPECTRUM OF LiYF₄: Tm³⁺(.5%) AT T=295K
 (1.7 μm Luminescence Monitored)

$\lambda(\text{nm})$	$\lambda(\text{cm}^{-1})$	Intensity	Energy Level Assignment
656.7	15228	7	 $^3F_2, ^3F_3$
681.0	14684	66	
699.0	14306	20	
774.6	12910	42	 3H_4
786.6	12713	37	
1178.8	8483	53	 3H_5
1208.0	8278	115	
1371.2	7293	19	 $^3F_2, ^3F_3$ (second order)
1404.3	7121	4	
1559.0	6414	8	 3H_4 (second order)
1585.0	6309	8	
1682.5	5944	91	 3F_4
1741.0	5744	31	
1793.0	5577	7	
1832	5459	8	
1880.8	5317	4	

Refer to Figure 6.1

Source: Jarrell Ash 30W tungsten Lamp

Detector: Spex Model 1428 PbS detector

Spex Model 1681 .22m monochromator; slits (both) : 800 μm

Stanford Research Systems Model SR510 "lock-in" amplifier

Sensitivity : 100 μV

Time Constant : .3 sec.

TABLE 6.2

EXCITATION SPECTRUM OF $\text{LiYF}_4: \text{Ho}^{3+}(1\%)$ AT $T=295\text{K}$
 (2.1 μm Luminescence Monitored)

$\lambda(\text{nm})$	$\lambda(\text{cm}^{-1})$	Intensity	Energy Level Assignment
413.4	24190	7	5G_5
446.4	22401	29	$5\text{F}_1, 3\text{K}_8,$ $5\text{F}_2, 5\text{F}_3$
468.6	21340	111	
480.6	20807	19	
533.4	18748	94	5F_4
636.0	15723	106	5F_5
651.3	15354	48	
831.0	12034	3	5I_5
888.0	11261	21	
1078.0	9276	16	5S_2
1152.1	8680	112	5I_6
1195.0	8368	91	
1279.5	7816	32	5F_5
1312.0	7622	15	

TABLE 6.2
 EXCITATION SPECTRUM OF LiYF₄: Ho³⁺(1%) AT T=295K
 (2.1 μm Luminescence Monitored)
 (Continued)

λ(nm)	λ(cm ⁻¹)	Intensity	Energy Level Assignment
1351	7402	6	
1371.8	7290	3	
1419.3	7046	2	
1453.1	6882	3	
1608.4	6217	7	
1780.0	5618	6	
1825.5	5478	5	
1891.2	5288	64	5I ₇
1916.5	5218	56	
1939.3	5156	106	
1997.8	5006	26	
2019.2	4952	31	
2053.0	4871	46	

Refer to Figure 6.2

Source: Jarrell Ash 30W tungsten Lamp

Detector : Spex Model 1428 PbS detector

Spex Model 1681 .22m monochromator; slits (both) : 600 μm

Stanford Research Systems Model SR510 "lock-in" amplifier

Sensitivity : 50 μV

Time Constant : .3 sec.

TABLE 6.3(a)

EXCITATION SPECTRUM OF LiYF_4 : Tm^{3+} (5%), Ho^{3+} (.2%) AT $T=295\text{K}$
(1.7 μm Luminescence Monitored)

$\lambda(\text{nm})$	$\lambda(\text{cm}^{-1})$	Intensity	Energy Level Assignment
460.5	21716	4	$5F_1, 5F_2, 5F_3$
468.0	21368	3	(Ho^{3+})
532.8	18769	7	$5F_4(5S_2)$ (Ho^{3+})
636.0	15723	11	$3F_2, 3F_3(\text{Tm}^{3+});$ $5F_5$ (Ho^{3+})
657.0	15221	17	
663.0	15083	15	
678.0	14749	113	
699.0	14306	43	
774.0	12920	84	$3H_4$ (Tm^{3+})
789.0	12674	76	
798.0	12531	30	
808.5	12369	12	
1178.1	8488	54	$3H_5$ (Tm^{3+});
1208.0	8278	101	$5I_6$ (Ho^{3+})
1276.9	7831	5	

TABLE 6.3(a)
 EXCITATION SPECTRUM OF LiYF₄: Tm³⁺(5%), Ho³⁺(.2%) AT T=295K
 (1.7 μm Luminescence Monitored)
 (Continued)

$\lambda(\text{nm})$	$\lambda(\text{cm}^{-1})$	Intensity	Energy level Assignment
1312.0	7622	6	$3F_2, 3F_3, 3H_4$ (Tm ³⁺); $5F_5$ (Ho ³⁺) (second order)
1328.9	7525	4	
1370.5	7297	37	
1403.0	7128	13	
1562.3	6401	18	
1583.7	6314	20	
1682.5	5944	46	$3F_4$ (Tm ³⁺)
1728.0	5787	22	
1742.3	5740	28	
1796.3	5567	10	
1832.0	5459	6	

Refer to Figure 6.3(a)

Source: Jarrell Ash 30W tungsten Lamp

Detector : Spex Model 1428 PbS detector

Spex Model 1681 .22m monochromator; slits (both) : 550 μm

Stanford Research Systems Model SR510 "lock-in" amplifier

Sensitivity : 100 μV

Time Constant : .3 sec.

TABLE 6.3(b)

EXCITATION SPECTRUM OF LiYF_4 : Tm^{3+} (5%), Ho^{3+} (.2%) AT $T=295\text{K}$
(2.1 μm Luminescence Monitored)

$\lambda(\text{nm})$	$\lambda(\text{cm}^{-1})$	Intensity	Energy Level Assignment
463.5	21575	5	$^5\text{G}_5$ (Ho^{3+})
533.4	18748	7	$^3\text{F}_2, ^3\text{F}_3(\text{Tm}^{3+});$ $^5\text{F}_5$ (Ho^{3+})
636.0	15723	10	
655.8	15249	17	
684.0	14620	128	
697.5	14337	46	
774.3	12915	96	$^3\text{H}_4$ (Tm^{3+})
787.5	12698	81	
807.0	12392	14	
1178.8	8483	62	$^3\text{H}_5$ (Tm^{3+}); $^5\text{I}_6$ (Ho^{3+})
1214.5	8234	118	
1276.3	7835	7	
1318.5	7584	8	$^3\text{F}_2, ^3\text{F}_3, ^3\text{H}_4$ (Tm^{3+}); $^5\text{F}_5$ (Ho^{3+}) (second order)
1331.5	7510	7	
1370.5	7297	46	
1403.0	7128	17	
1559.0	6414	25	
1585.0	6309	26	

TABLE 6.3(b)

EXCITATION SPECTRUM OF LiYF₄: Tm³⁺(5%), Ho³⁺(.2%) AT T=295K
 (2.1 μm Luminescence Monitored)
 (Continued)

λ(nm)	λ(cm ⁻¹)	Intensity	Energy Level Assignment
1689.0	5921	70	3F ₄ (Tm ³⁺); 5 ₁₇ (Ho ³⁺)
1747.5	5722	34	
1793.0	5577	10	
1832.0	5459	9	
1890.5	5290	6	
1910.0	5236	3	
1939.9	5155	4	

Refer to Figure 6.3(b)

Source: Jarrell Ash 30W tungsten Lamp

Detector : Spex Model 1428 PbS detector

Spex Model 1681 .22m monochromator; slits (both) : 350 μm

Stanford Research Systems Model SR510 "lock-in" amplifier

Sensitivity : 50 μV

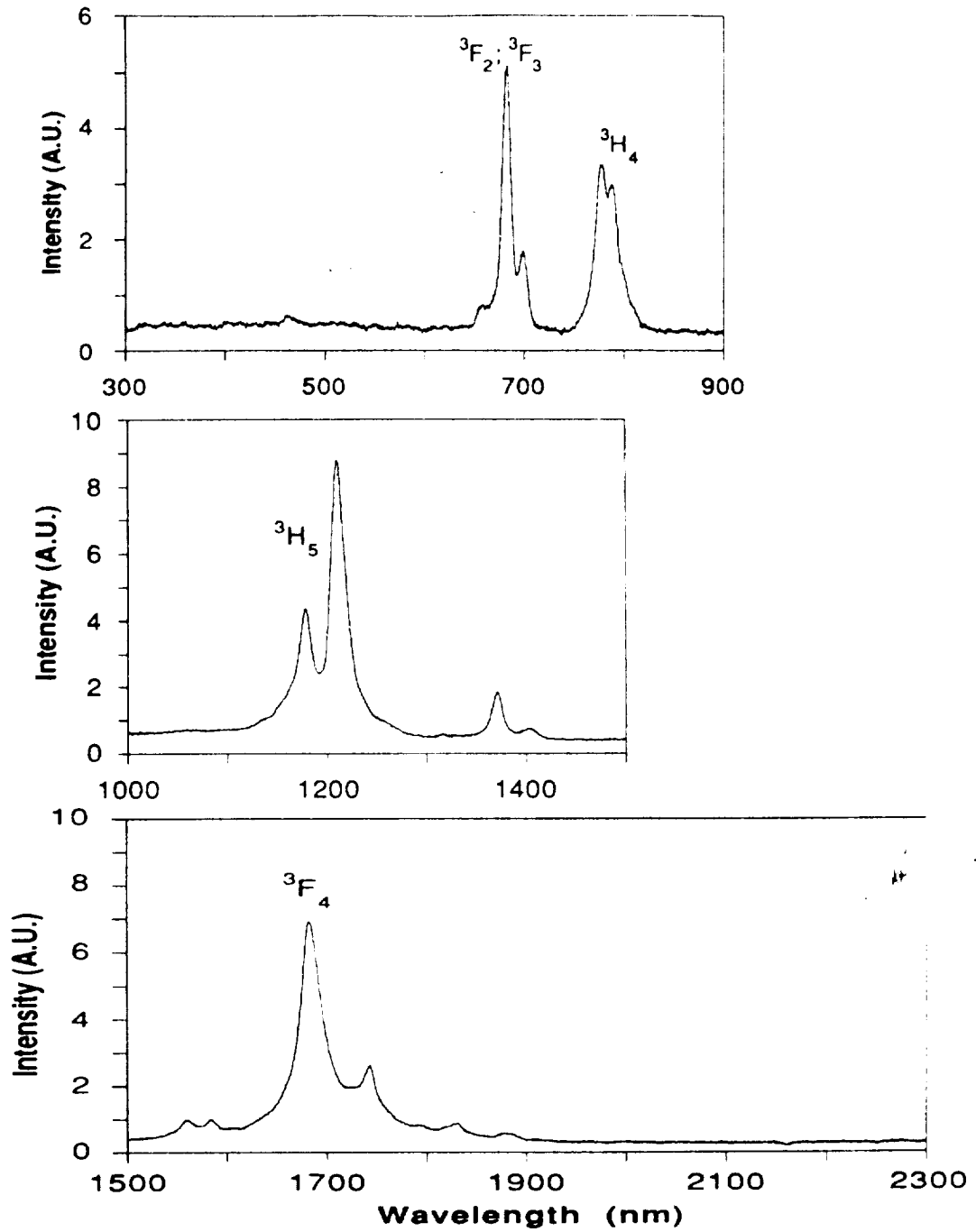


Fig. 6.1 The excitation spectrum of 1.7 μm luminescence of LiYF₄ : Tm³⁺(.5%) at T=295K.

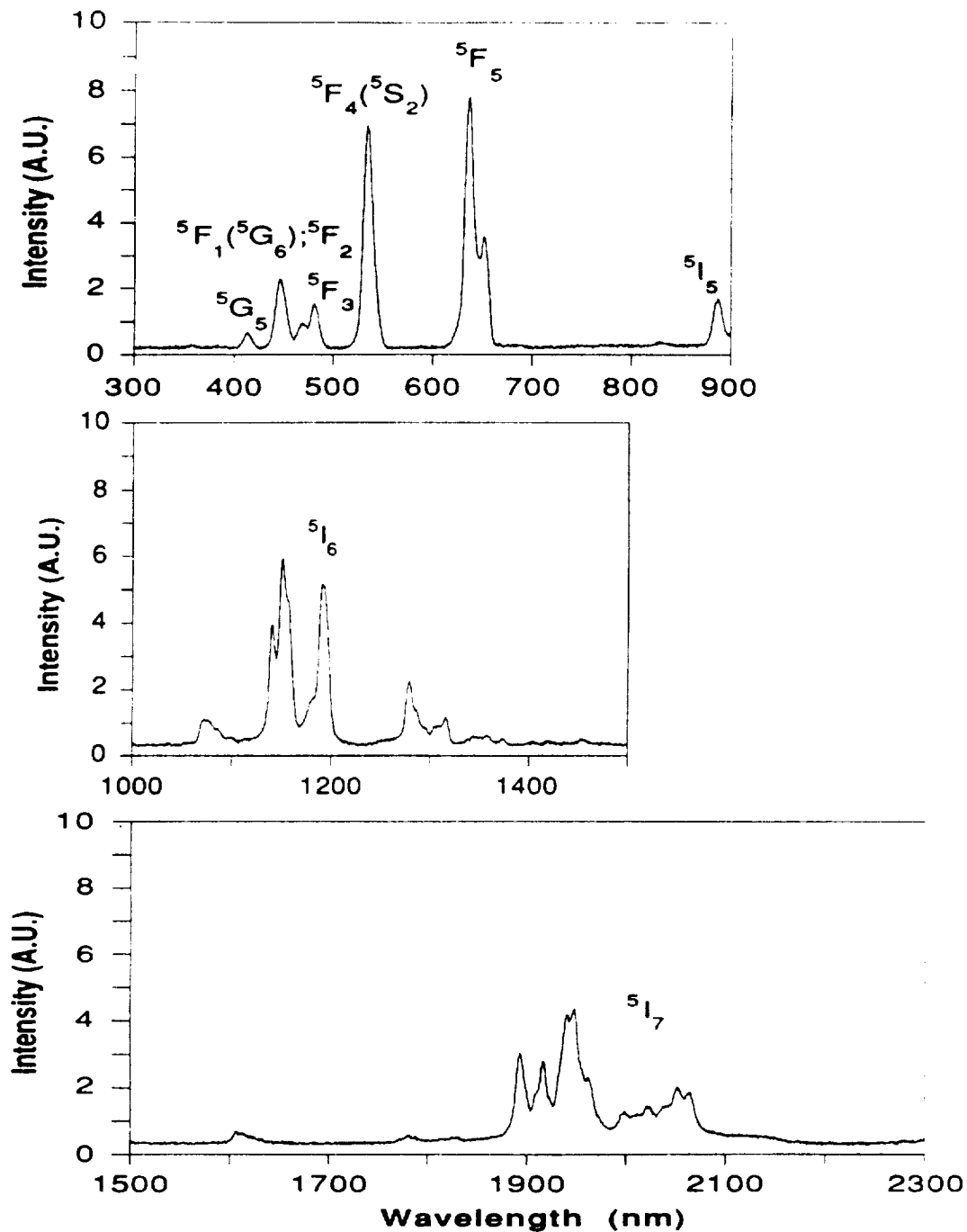


Fig. 6.2 The excitation spectrum of 2.1 μm luminescence of LiYF₄ : Ho³⁺(1%) at T=295K.

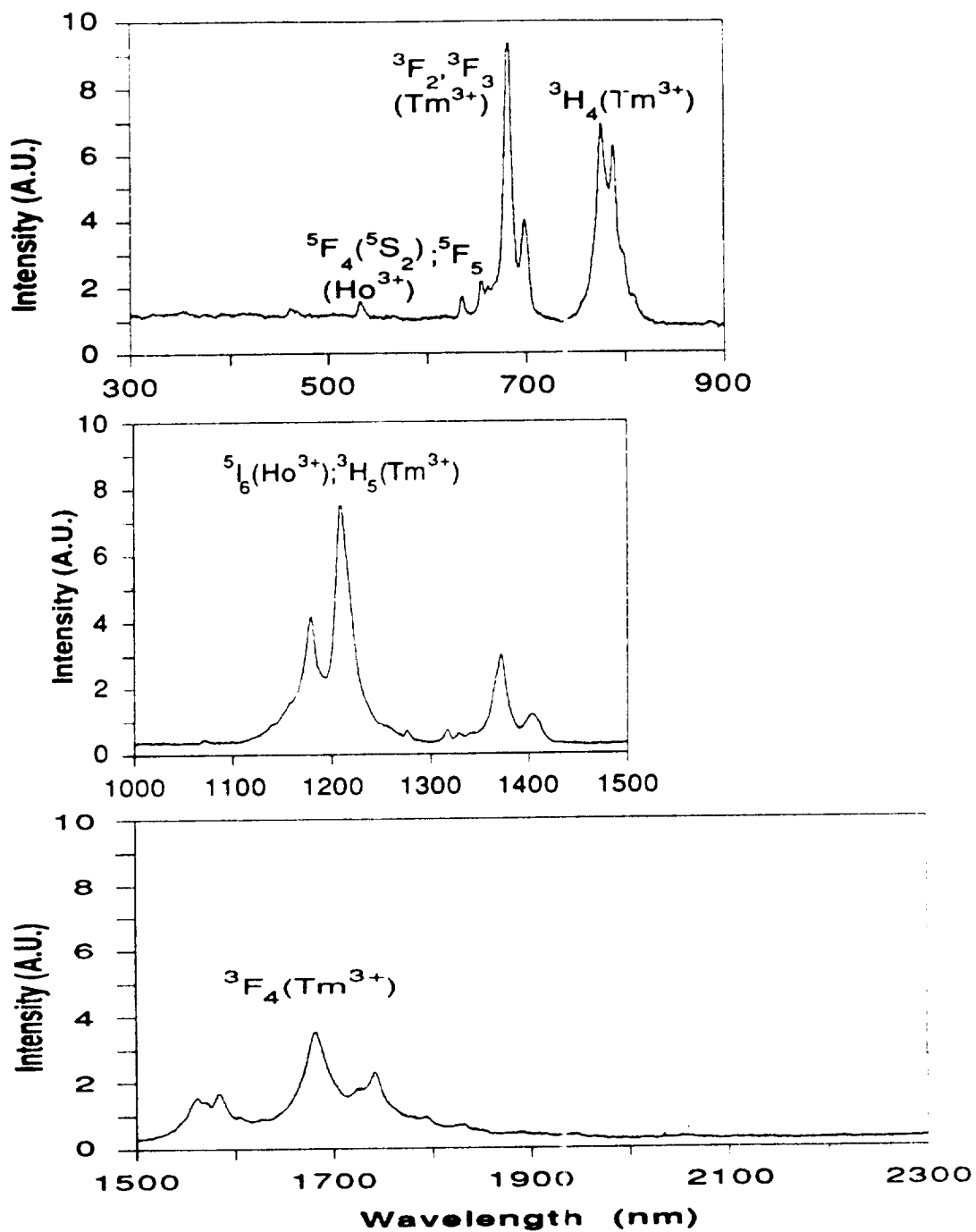


Fig. 6.3 (a) The excitation spectrum of 1.7 μm luminescence of $\text{LiYF}_4 : \text{Tm}^{3+}(5\%), \text{Ho}^{3+}(.2\%)$ at $T=295\text{K}$.

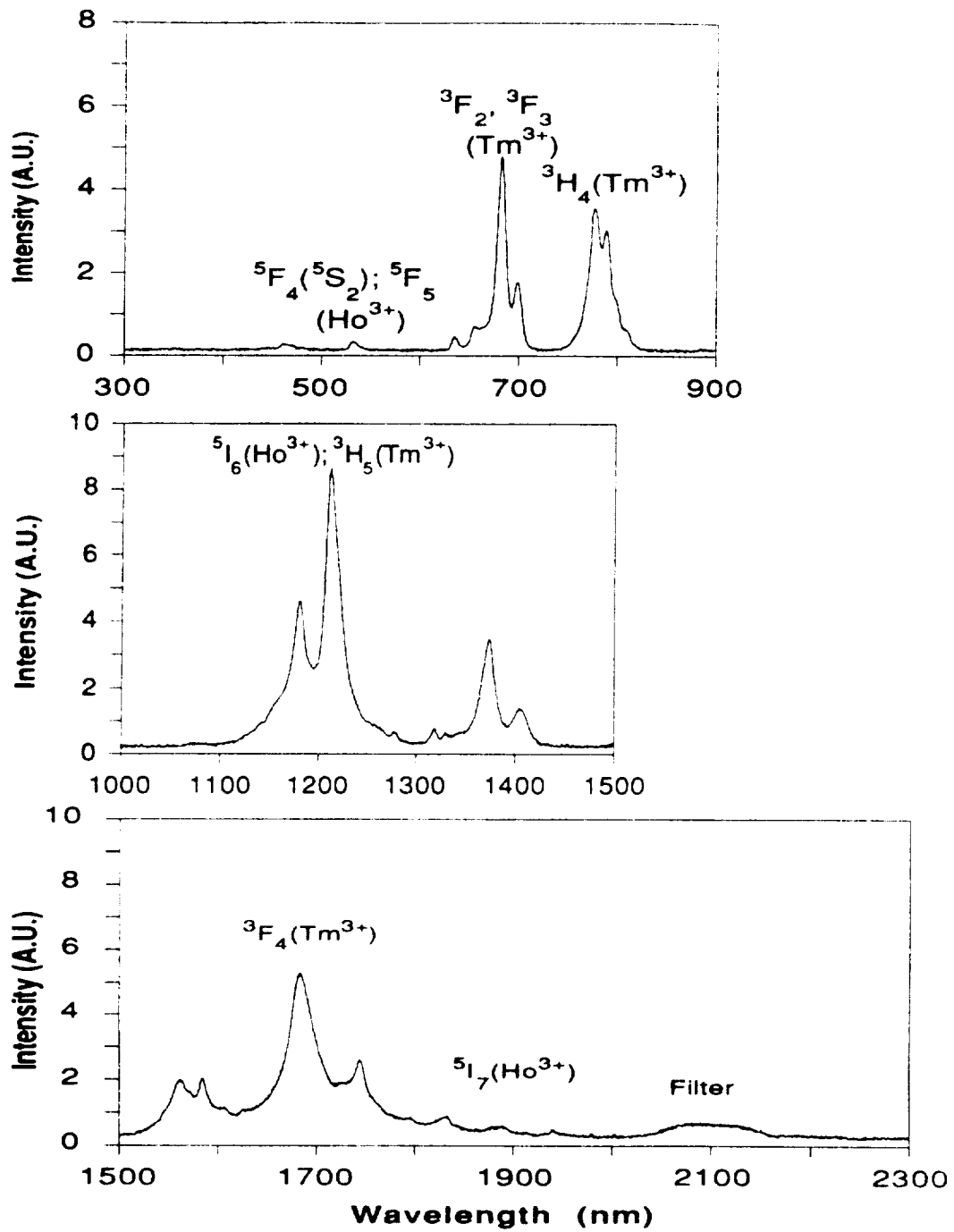


Fig. 6.3 (b) The excitation spectrum of 2.1 μm luminescence of $\text{LiYF}_4 : \text{Tm}^{3+}(5\%), \text{Ho}^{3+}(.2\%)$ at $T=295\text{K}$.

7. EXPERIMENTAL RESULTS III. DECAY PATTERNS

Pulsed luminescence measurements were done by using the apparatus described in section 3.3. An interference filter centered at the wavelength of interest was used to study a decay pattern. The lifetime was measured by using the best exponential fit to the decay curve. The experimental conditions under which the different measurements were done are described either under the figures or at the end of the tables.

Energy transfer rates can be determined by using the measurement of the excited state lifetime of the sensitizer, if the presence of the activator does not introduce structural changes in the crystal. The fluorescence lifetime of the sensitizer is given by

$$1/\tau_F = P_{SA} + 1/\tau_S \quad (7.1)$$

where τ_S is the intrinsic lifetime of the sensitizer. The rate of the energy transfer can then be found experimentally:

$$P_{SA} = 1/\tau_F - 1/\tau_S \quad (7.2)$$

The efficiency of the transfer can be expressed as follows:

$$\eta_\tau = P_{SA} / (1/\tau_S + P_{SA}) = 1 - \tau_F/\tau_S \quad (7.3)$$

7.1 LiYF₄ : Tm³⁺(.5%)

The response to pulsed excitation of the optical luminescence from the ³H₄ level of Tm in LiYF₄ was measured by exciting the sample with 660 nm pulses from the dye laser which pump the system into the ³F₃ level. The measurements were made in the temperature range 77K - 300K. The decay pattern of this emission is found to be pure exponential at all temperatures. The lifetime of the same level, reported in Table 7.1 and Fig. 7.1, decreases with increasing temperature.

The response to pulsed excitation of the infrared luminescence from the ³F₄ level of Tm in this sample was measured by exciting the sample with 795 nm pulses from the dye laser which pump the system into the ³H₄ level. The measurements were made in the temperature range 8 - 550K by monitoring the emission at 1.6, 1.7, 1.8, and 1.9 μm. Table 7.2 and Figs. 7.2, and 7.3 relate to these measurements.

The decay patterns at the various wavelengths present the following features :

- i) At early times of decay, the patterns are different but eventually they become the same. They are reported in Fig. 7.4 for 300, 77 and 8K.
- ii) At high temperatures, all the decay curves are similar. They have a rise at early times followed by an exponential decay.
- iii) At low temperatures, the decay pattern of the 1.6μm emission differs from the others. It shows a double decay at 77K and a rise followed by an exponential decay at 300K.

The temperature dependence of the time constant of the longer component of each decay pattern was obtained by using the best exponential fit to the decay curve, and is reported in Table 7.3 and Fig. 7.5. It was found to decrease with increasing temperature.

7.2 LiYF₄ : Ho³⁺(1%)

The decay pattern of the infrared luminescence from the ⁵I₇ level of Ho in LiYF₄ : Ho³⁺(1%) was obtained at various wavelengths by exciting the sample with 545.7 nm pulses from the dye laser. These measurements were made in the temperature range 77 to 550K by monitoring the luminescence at 1.6, 1.7, 1.8, 1.9 and 2.1 μm.

The pattern at 2.1 μm is given in Fig. 7.6 for 300 and 77K. The following observations can be made:

- i) The decay patterns at 1.9 and 2.1 μm have the same features. They both have a rise followed by an exponential decay (tail).
- ii) The time constants of the rise and the tail at 2.1 μm were found to be 1.4 and 16.6 msec for 300K respectively. In addition to the above a very fast decay was observed at all temperatures.
- iii) The patterns at 1.6 and 1.7 μm show an exponential decay at all temperatures with a time constant 113 μsec at 300K. No luminescence was observed at 1.8 μm.

The time constant of the experimental tail of the 1.9 and 2.1 μm emission was considered to be the lifetime of the ⁵I₇ level. The temperature dependence of this lifetime was obtained by using the best fit to the data, and is reported in Table 7.4 and Fig. 7.7. It increases with increasing temperature until 400K, and then decreases to 17.7 msec at 550K.

7.3 LiYF₄ : Tm³⁺(5%), Ho³⁺(.2%)

The response of the LiYF₄ : Tm³⁺(5%), Ho³⁺(.2%) sample to pulsed excitation was measured in the temperature range 8 - 550K by monitoring the luminescence at 1.6, 1.7, 1.8, 1.9 and 2.1 μm. These measurements were done by exciting either the ³H₄ level of Tm with 795 nm pulses or the ⁵S₂ level of Ho with 545.7 nm pulses from the dye laser. The decay times and decay patterns at the various wavelengths and temperatures are reported in Table 7.5 and Figs. 7.8 and 7.9

The decay curves present the following features :

- i) The patterns at various wavelengths differ only in their initial parts as shown in Fig. 7.10.
- ii) At high temperatures, all the multiple-exponential decays show a rise at early times of the decay (see Table 7.5).
- iii) At low temperatures, all the patterns show three decays; a fast decay, an intermediate decay and a long decay. In addition to the above, the emission from 2.1 μm shows a rise at all temperatures.

The last three figures of this chapter 7.9 to 7.11 and the accompanying Tables 7.6 and 7.7 give the time constants of the tails of the decay curves of the infrared luminescence observed in our experiments.

TABLE 7.1
 TEMPERATURE DEPENDENCE OF LIFETIME OF $Tm^{3+} \ ^3H_4$ ENERGY LEVEL
 IN $LiYF_4 : Tm^{3+}(.5\%at.)$

Temperature (K)	Lifetime (msec)
8	2.40
30	2.38
60	2.36
77	2.38
100	2.36
150	2.25
200	2.21
250	2.11
300	2.04

Refer to Fig. 7.1

Excitation source : EG&G Princeton Applied Research Model 2100
 tunable dye laser pumped by a nitrogen laser

Excitation wavelength : 660 nm

Detector : RCA C13034 photomultiplier tube

Luminescence monitored : $^3H_4 \rightarrow ^3H_6$

Filter used : narrow band interference filter centered at 800 nm

TABLE 7.2

DECAY TIMES OF DECAY PATTERNS AT VARIOUS WAVELENGTHS FOR

T = 300, 77 AND 8K

λ (μm)	<u>T = 300K</u>			<u>T = 77K</u>			<u>T = 8K</u>		
	τ -rise (msec)	τ -fast (msec)	τ -tail (msec)	τ -rise (msec)	τ -fast (msec)	τ -tail (msec)	τ -rise (msec)	τ -fast (msec)	τ -tail (msec)
1.6	0.4	----	12.7	----	2.1	25.7	----	2.3	45.2
1.7	1.1	----	13.7	1.4	----	16.9	----	----	----
1.8	0.9	----	14.2	1.4	----	16.5	1.2	----	18.9
1.9	0.5	2.1	14.3	1.4	----	16.2	1.9	----	16.6

The conditions under which the experiment was done are given under Table 7.3

TABLE 7.3
 TEMPERATURE DEPENDENCE OF LIFETIME OF $Tm^{3+} \ ^3F_4$ ENERGY LEVEL
 IN $LiYF_4 : Tm^{3+}(.5\% \text{ at.})$

Temperature (K)	Lifetime ⁽¹⁾ (msec)	Lifetime ⁽²⁾ (msec)	Lifetime ⁽³⁾ (msec)	Lifetime ⁽⁴⁾ (msec)
8	20.8	-----	20.9	19.5
30	19.8	-----	18.8	19.7
60	19.4	-----	-----	19.3
77	18.4	18.9	18.2	18.3
100	17.2	18.1	17.6	17.8
150	16.2	16.7	16.7	16.9
200	16.0	15.6	16.3	16.2
250	15.2	15.4	15.6	15.4
300	14.5	14.6	14.9	14.3
350	14.4	14.4	14.5	14.8
400	14.3	14.6	14.3	14.7
450	13.9	14.3	14.1	14.2
500	13.1	13.6	13.7	-----
550	13.1	13.3	13.3	13.2

(1) : luminescence monitored at 1.6 μm

(2) : luminescence monitored at 1.7 μm

(3) : luminescence monitored at 1.8 μm

(4) : luminescence monitored at 1.9 μm

Refer to Figs. 7.2, 7.3, 7.4 and 7.5

Excitation source : Quantel tunable dye laser Model TDL-51 pumped by a
Quantel Nd³⁺: YAG (Yttrium Aluminum Garnet)
Model 660A-10

Excitation wavelength : 795 nm (³H₄ level of Tm is excited)

Detector : Judson Infrared Inc. Model J12TE2 InAs detector

Luminescence monitored : ³F₄ → ³H₆

Filters used : 1.6, 1.7, 1.8 and 1.9 μm

TABLE 7.4
TEMPERATURE DEPENDENCE OF LIFETIME OF Ho³⁺ ⁵I₇ ENERGY LEVEL
in LiYF₄ : Ho³⁺(1%at.)

Temperature (K)	Lifetime ⁽¹⁾ (msec)	Lifetime ⁽²⁾ (msec)
77	-----	15.5
100	15.0	15.5
150	15.4	16.0
200	16.6	17.2
250	16.7	17.5
300	17.2	17.6
350	18.1	18.6
400	18.3	18.3
450	18.8	18.7
500	18.5	18.0
550	17.7	17.7

(1) : luminescence monitored at 1.9 μm

(2) : luminescence is monitored at 2.1 μm

Refer to Figs. 7.6 and 7.7

Excitation source : Quantel tunable dye laser Model TDL-51 pumped by a
Quantel Nd³⁺: YAG (Yttrium Aluminum Garnet)
Model 660A-10

Excitation wavelength : 545 nm (⁵S₂ level of Ho is excited)

Detector : Judson Infrared Inc. Model J12TE2 InAs detector

Luminescence monitored : ⁵I₇ → ⁵I₈

Filters used : 1.6, 1.7, 1.8, 1.9 and 2.1 μm

TABLE 7.6
 TEMPERATURE DEPENDENCE OF LIFETIME OF $Tm^{3+} \ ^3F_4$ ENERGY LEVEL
 AND $Ho^{3+} \ ^5I_7$ ENERGY LEVEL IN $LiYF_4 : Tm^{3+}(5\% \text{ at.}), Ho^{3+}(.2\% \text{ at.})$

Temperature (K)	Lifetime ⁽¹⁾ (msec)	Lifetime ⁽²⁾ (msec)	Lifetime ⁽³⁾ (msec)	Lifetime ⁽⁴⁾ (msec)	Lifetime ⁽⁵⁾ (msec)
8	11.5	-----	10.8	10.9	11.6
30	11.6	-----	11.4	11.9	11.7
60	11.8	-----	11.7	11.8	11.8
77	12.1	-----	11.7	11.8	12.0
100	12.1	11.7	12.1	12.1	12.2
150	12.3	12.3	12.3	12.1	12.4
200	12.5	12.6	12.8	12.3	12.7
250	12.8	12.6	12.7	12.7	12.8
300	12.6	12.6	12.8	12.5	12.7
350	12.5	12.3	12.6	12.2	12.5
400	11.9	11.9	11.8	11.8	11.9
450	11.4	11.4	11.4	11.2	11.3
500	10.9	11.0	11.2	10.9	11.1
550	10.5	10.8	10.5	10.8	10.4

(1) : luminescence monitored at 1.6 μm

(2) : luminescence monitored at 1.7 μm

(3) : luminescence monitored at 1.8 μm

(4) : luminescence monitored at 1.9 μm

(5) : luminescence monitored at 2.1 μm

Refer to Figs. 7.8, 7.9, 7.10 and 7.11

Excitation source : Quantel tunable dye laser Model TDL-51 pumped

by a Quantel Nd³⁺: YAG (Yttrium Aluminum Garnet) Model 660A-10

Excitation wavelength : 795 nm (only ³H₄ level of Tm is excited)

Detector : Judson Infrared Inc. Model J12TE2 InAs detector

Luminescence monitored : ³F₄ → ³H₆ (Tm³⁺); ⁵I₇ → ⁵I₈ (Ho³⁺)

Filters used : 1.6, 1.7, 1.8, 1.9 and 2.1 μm

TABLE 7.7

TEMPERATURE DEPENDENCE OF LIFETIME OF $Tm^{3+} \ ^3F_4$ ENERGY LEVEL
AND $Ho^{3+} \ ^5I_7$ ENERGY LEVEL IN $LiYF_4 : Tm^{3+}(5\% \text{ at.}), Ho^{3+}(.2\% \text{ at.})$

Temperature (K)	Lifetime ⁽¹⁾ (msec)	Lifetime ⁽²⁾ (msec)	Lifetime ⁽³⁾ (msec)	Lifetime ⁽⁴⁾ (msec)	Lifetime ⁽⁵⁾ (msec)
150	-----	-----	-----	11.7	12.2
200	-----	-----	-----	12.3	12.4
250	20.9	15.7	12.6	12.8	12.7
300	18.1	13.4	12.3	12.4	12.2
350	16.1	12.7	12.2	11.9	11.6
400	12.5	12.6	11.6	11.5	12.4
450	11.7	12.1	11.3	11.3	12.2
500	10.5	11.5	11.1	11.1	11.6
550	11.9	10.9	10.9	10.7	10.5

(1) : luminescence monitored at 1.6 μm

(2) : luminescence monitored at 1.7 μm

(3) : luminescence monitored at 1.8 μm

(4) : luminescence monitored at 1.9 μm

(5) : luminescence monitored at 2.1 μm

Refer to Fig. 7.12

Excitation source : Quantel tunable dye laser Model TDL-51 pumped
by a Quantel Nd³⁺: YAG (Yttrium Aluminum Garnet)
Model 660A-10

Excitation wavelength : 545 nm (only ⁵S₂ level of Ho is excited)

Detector : Judson Infrared Inc. Model J12TE2 InAs detector

Luminescence monitored : ³F₄ → ³H₆ (Tm³⁺); ⁵I₇ → ⁵I₈ (Ho³⁺)

Filters used : 1.6, 1.7, 1.8, 1.9 and 2.1 μm

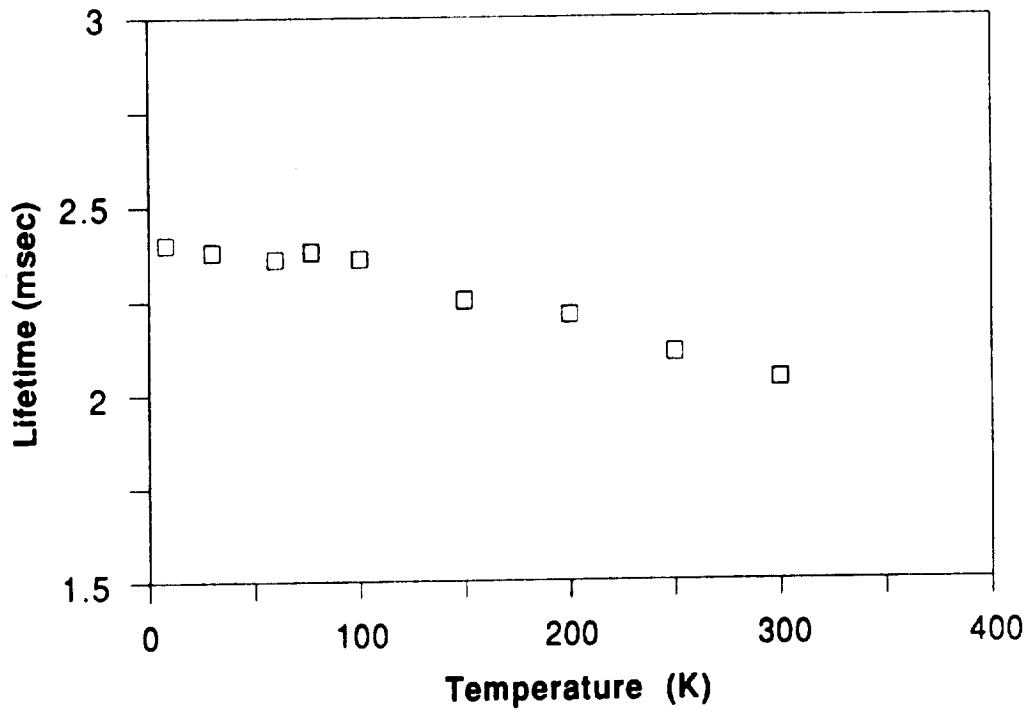


Fig. 7.1 Temperature dependence of lifetime of optical luminescence from 3H_4 level of Tm in $LiYF_4 : Tm^{3+}(.5\%)$ (Excitation into the 3F_3 level).

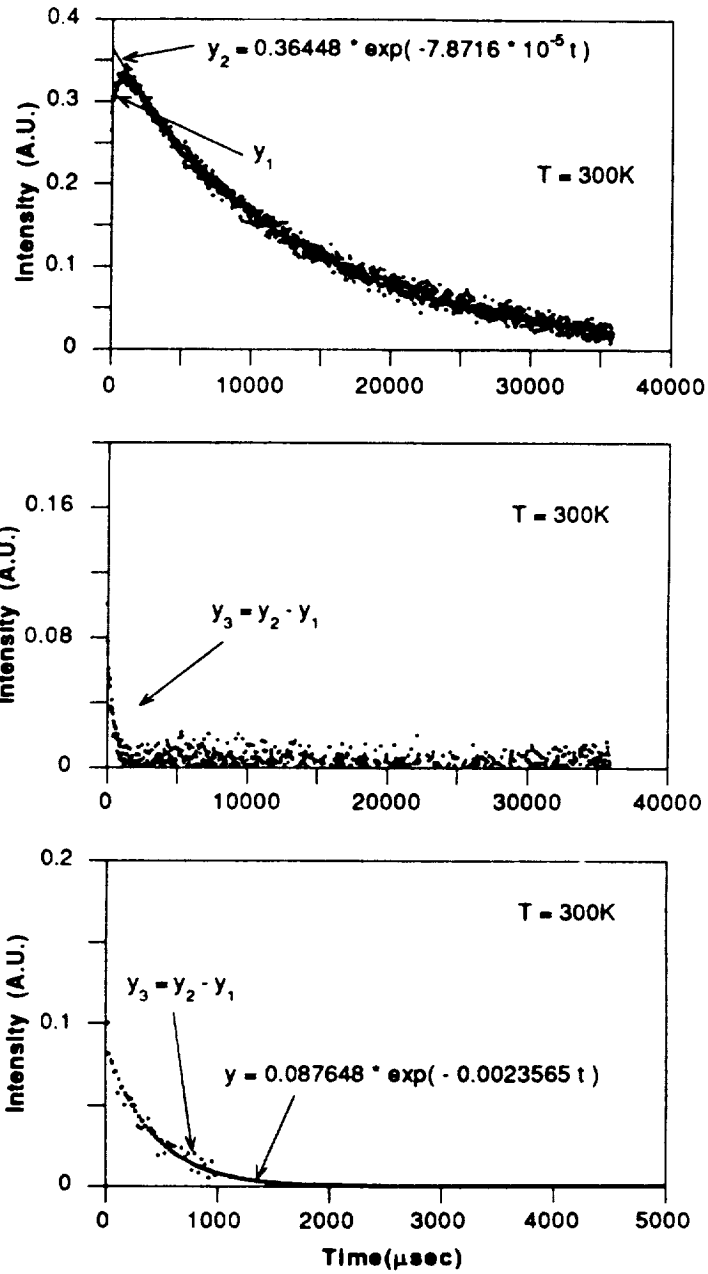


Fig. 7.2 (a) Decay pattern of 1.6 μm emission of LiYF₄ : Tm³⁺(.5%) at 300K.

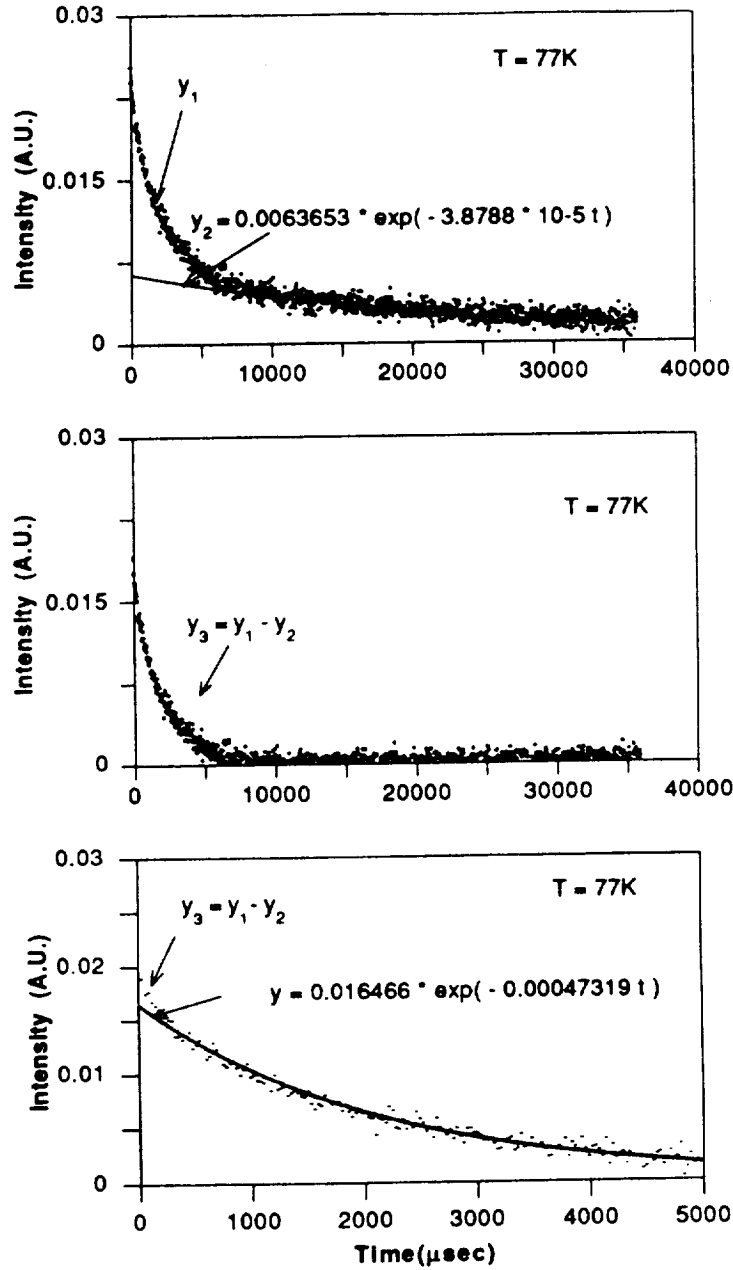


Fig. 7.2 (b) Decay pattern of 1.6 μm emission of LiYF₄ : Tm³⁺ (.5%) at 77K.

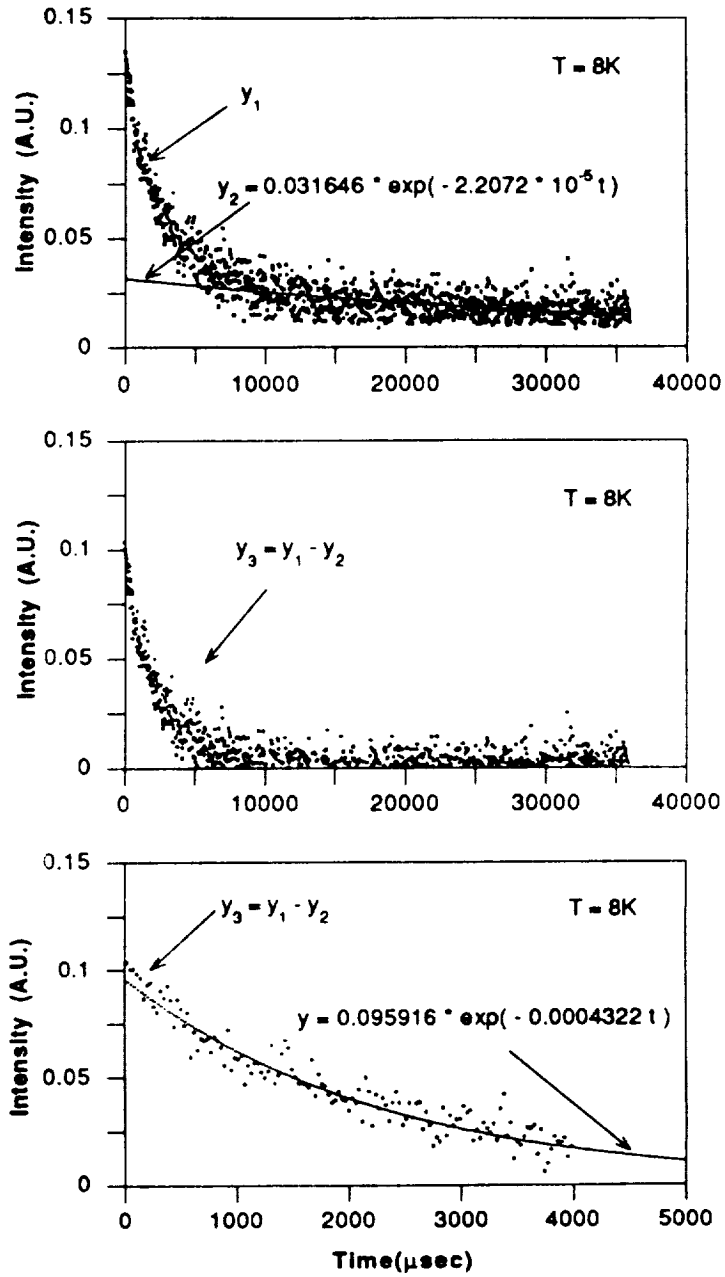


Fig. 7.2 (c) Decay pattern of 1.6 μm emission of LiYF₄ : Tm³⁺ (.5%) at 8K.

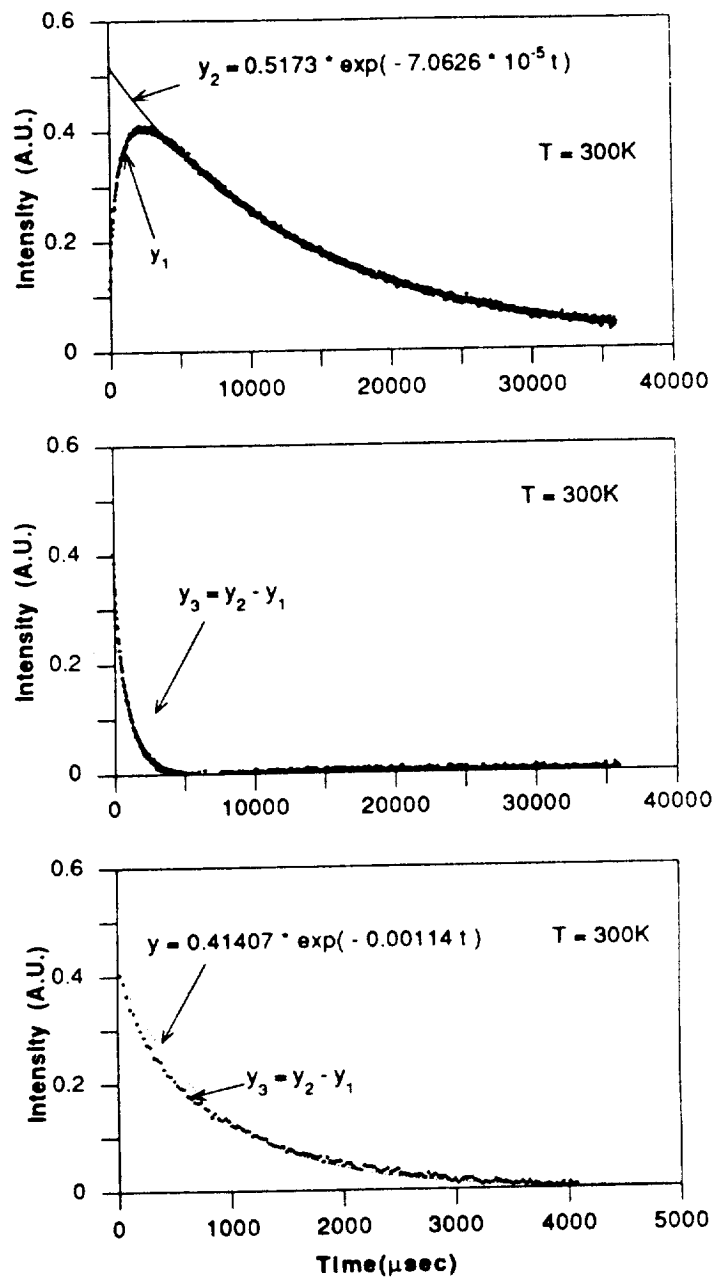


Fig. 7.3 (a) Decay pattern of 1.8 μm emission of LiYF₄ : Tm³⁺(.5%) at 300K.

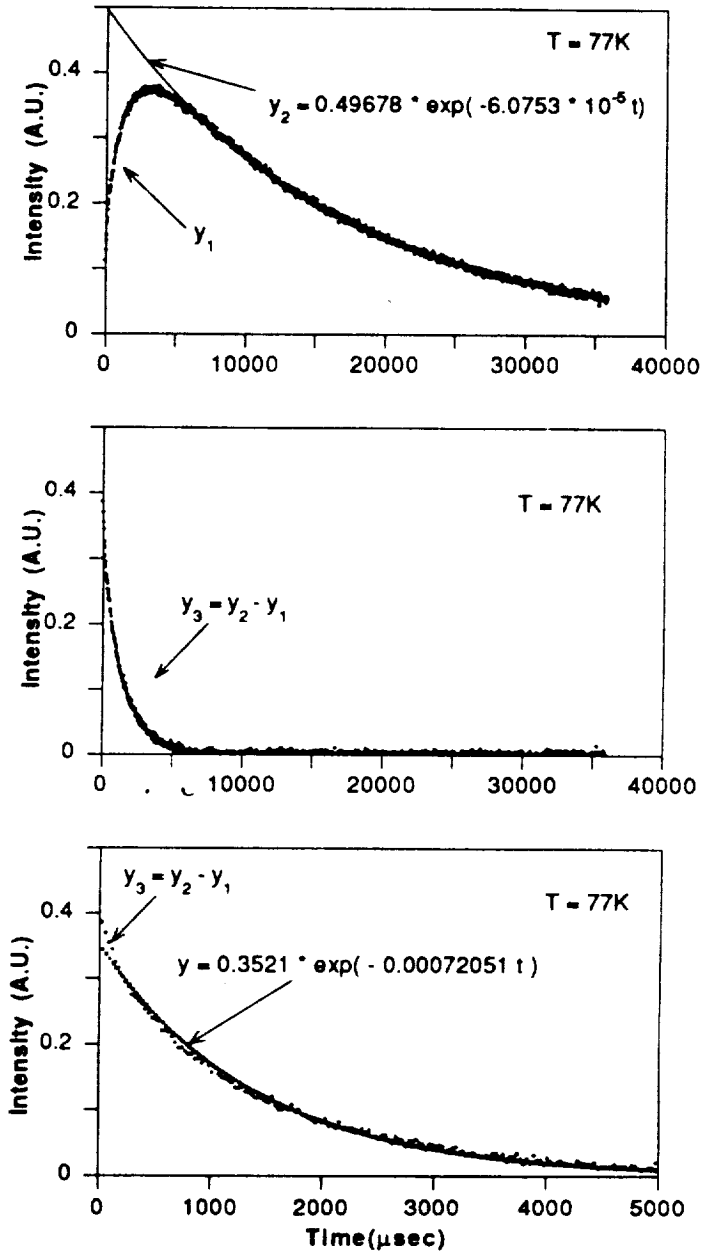


Fig. 7.3 (b) Decay pattern of 1.8 μm emission of $\text{LiYF}_4 : \text{Tm}^{3+} (5\%)$ at 77K.

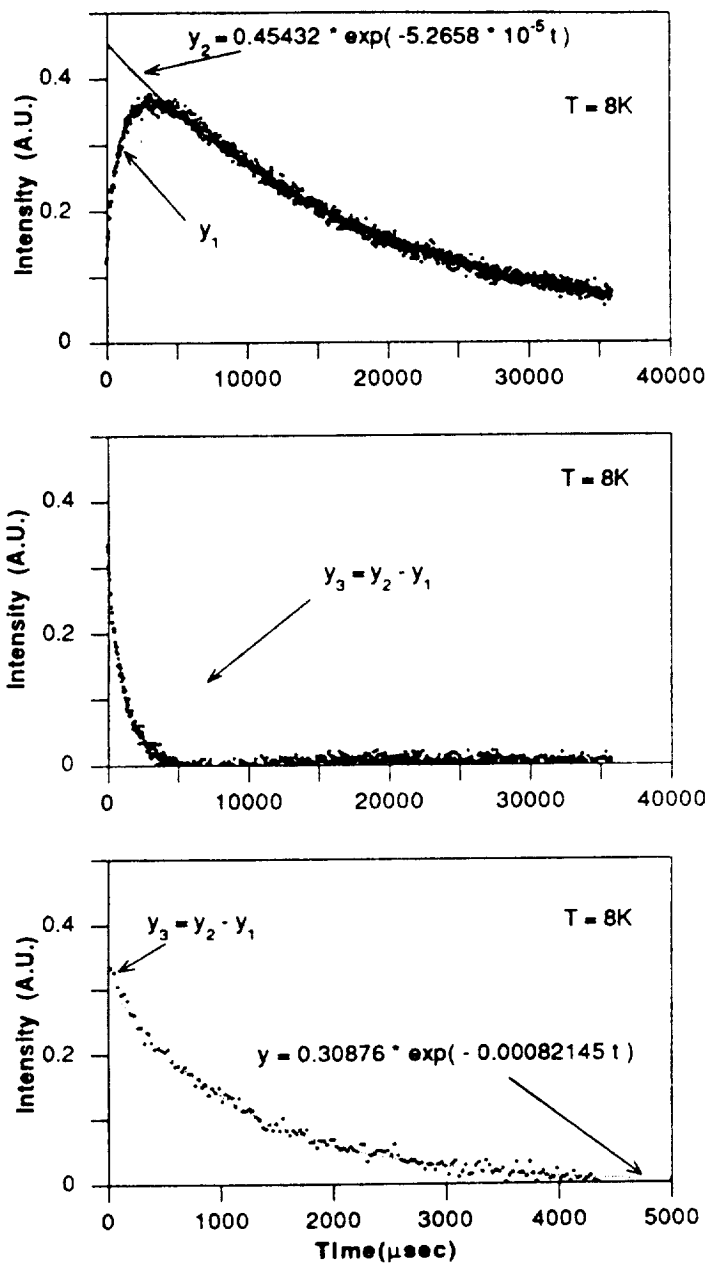


Fig. 7.3 (c) Decay pattern of 1.8 μm emission of LiYF₄ : Tm³⁺(.5%) at 8K.

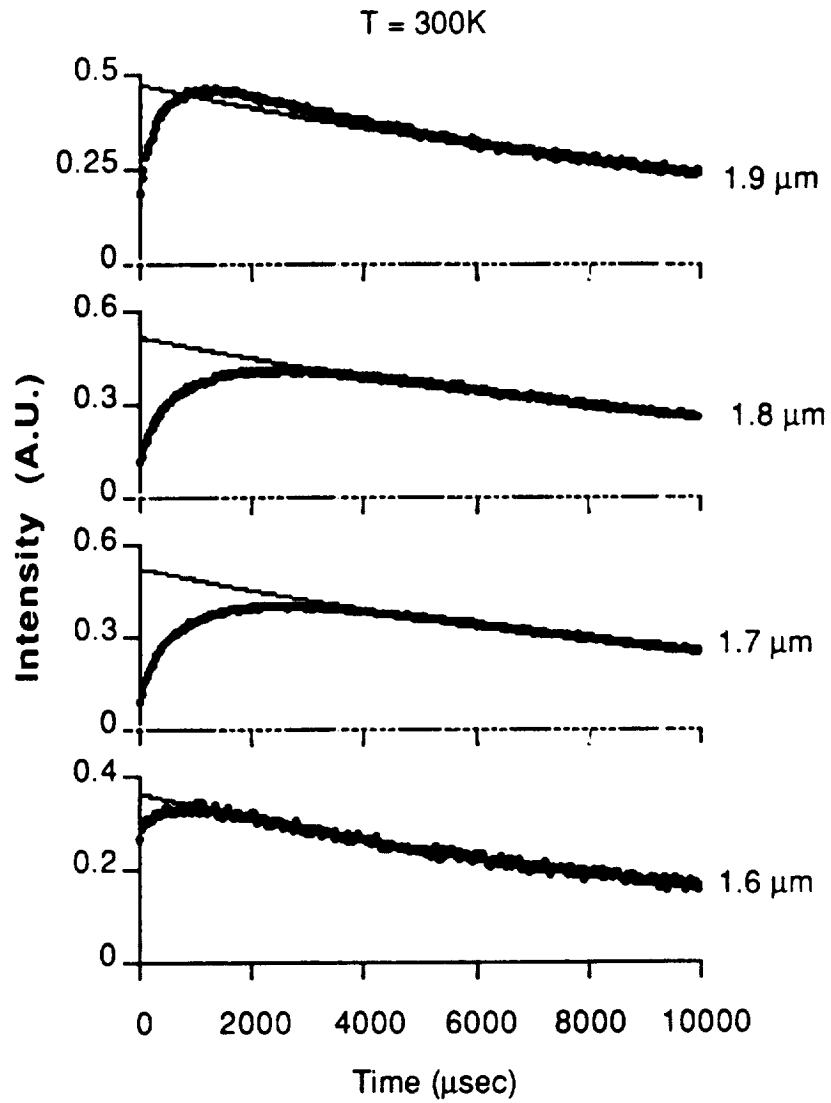


Fig. 7.4 (a) Decay patterns of the emission from different spectral regions of $\text{LiYF}_4 : \text{Tm}^{3+} (.5\%)$ at 300K.

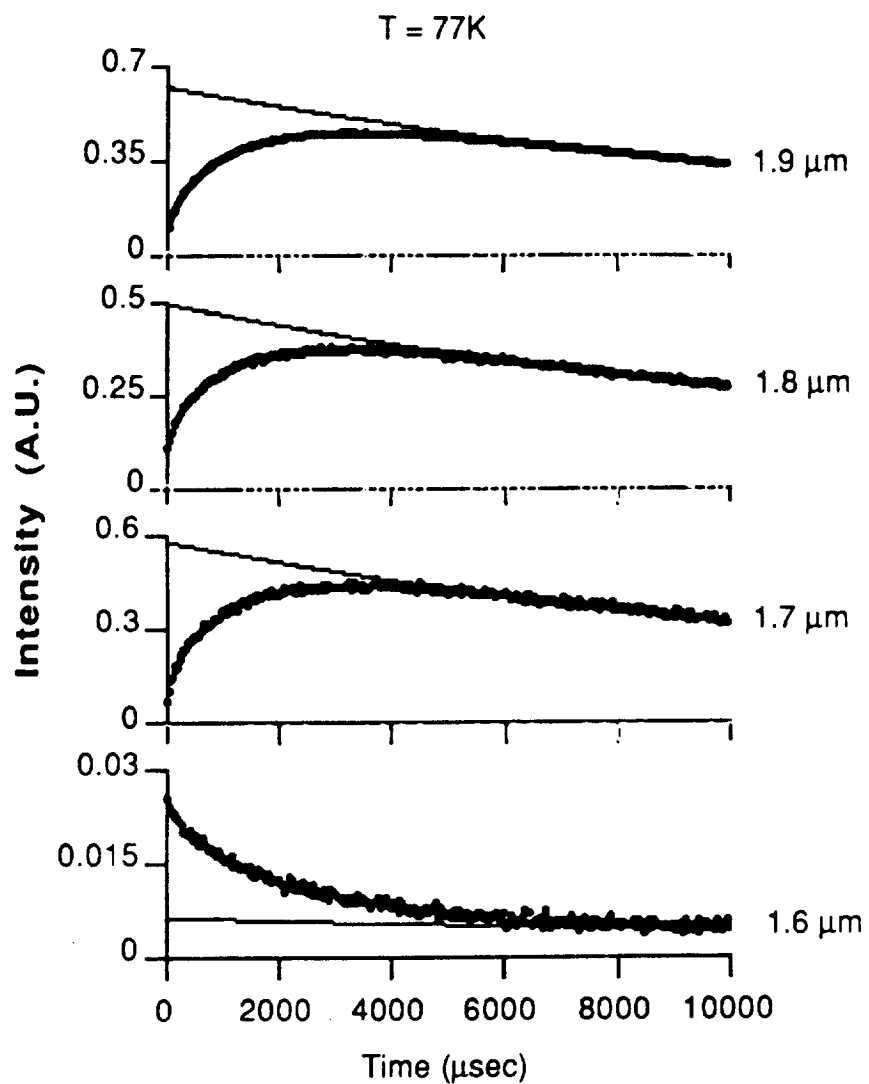


Fig. 7.4 (b) Decay patterns of the emission from different spectral regions of LiYF₄: Tm³⁺(.5%) at 77K.

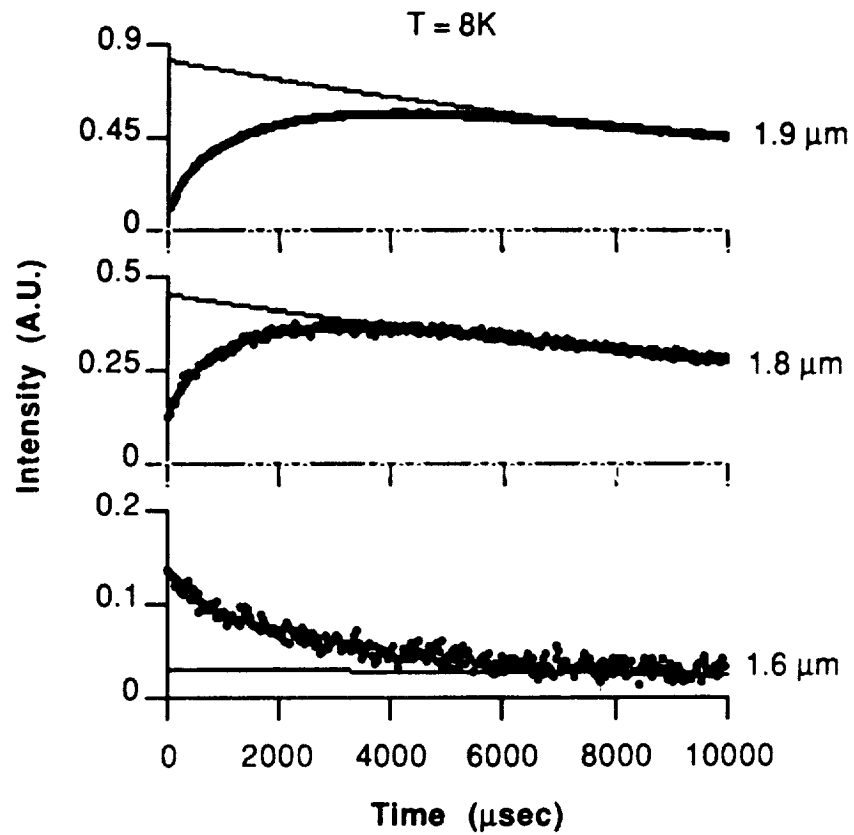


Fig. 7.4 (c) Decay patterns of the emission from different spectral regions of $\text{LiYF}_4 : \text{Tm}^{3+}(.5\%)$ at 8K.

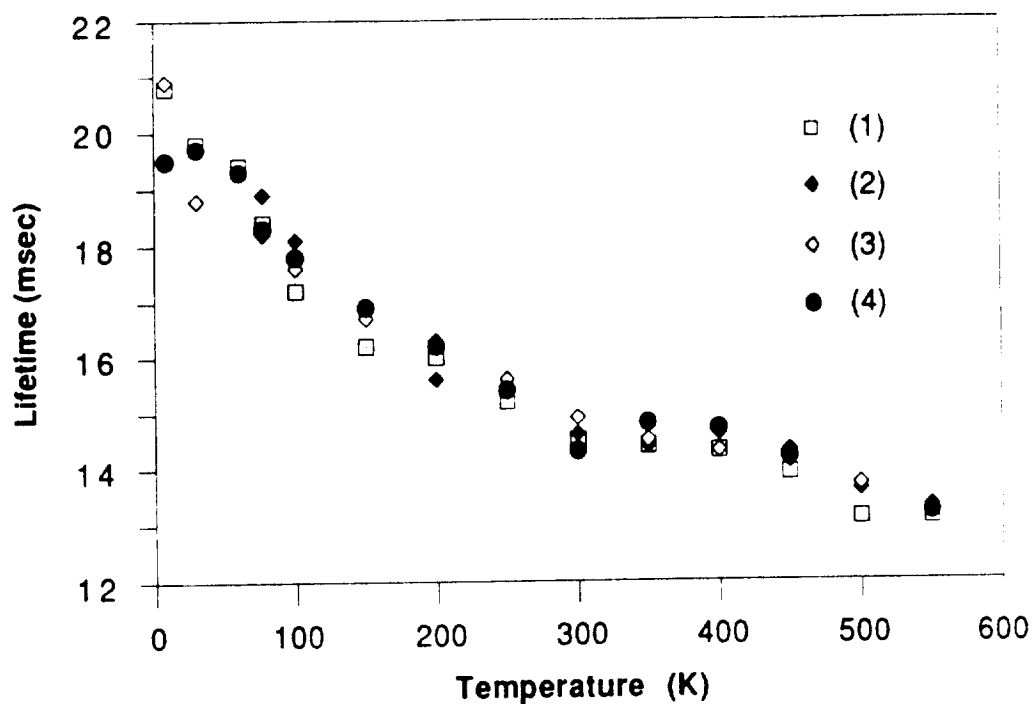


Fig. 7.5 Temperature dependence of lifetime of $Tm^{3+} \ ^3F_4$ energy level in $LiYF_4 : Tm^{3+}(.5\%)$ (3H_4 energy level of Tm is excited).

(1) : luminescence monitored at $1.6 \ \mu m$
 (2) : luminescence monitored at $1.7 \ \mu m$
 (3) : luminescence monitored at $1.8 \ \mu m$
 (4) : luminescence monitored at $1.9 \ \mu m$

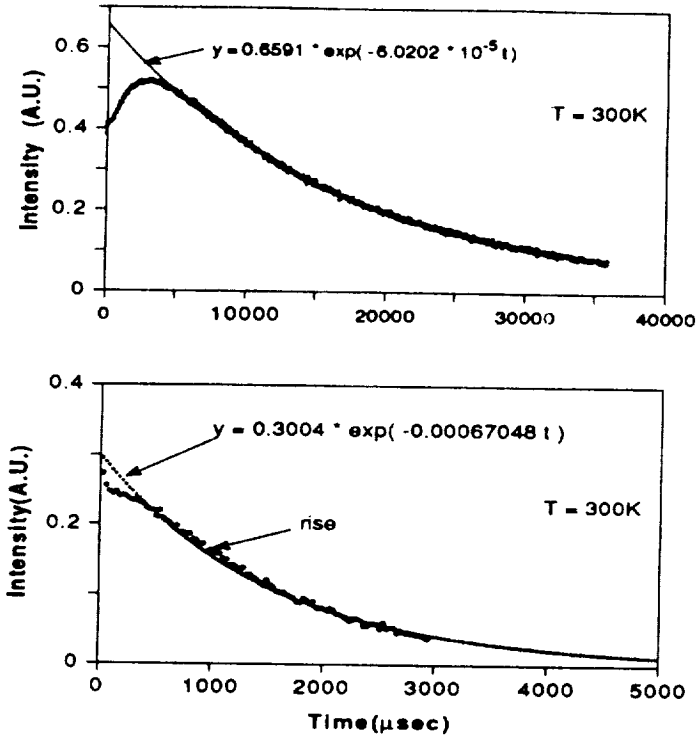


Fig. 7.6 (a) Decay pattern of 2.1 μm emission of $\text{LiYF}_4 : \text{Ho}^{3+}(1\%)$ at 300K.

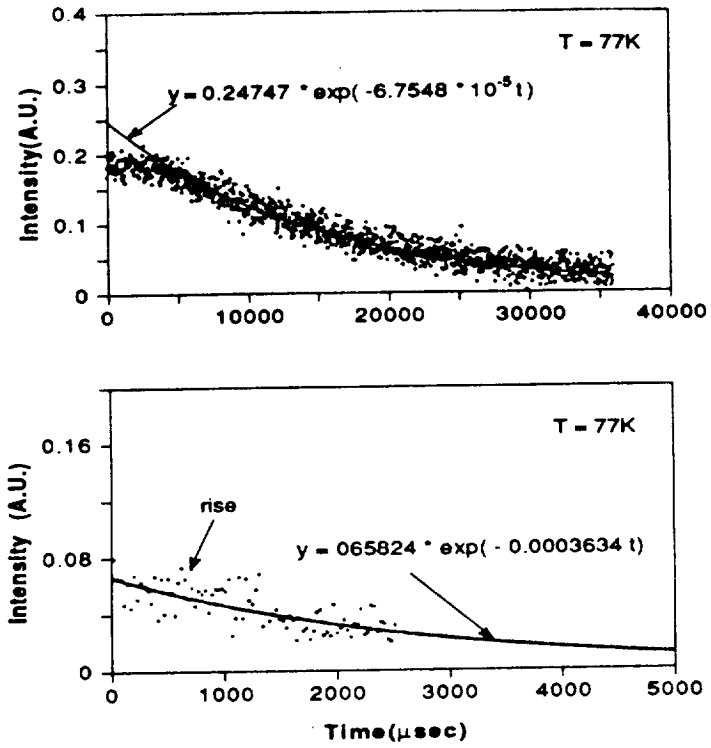


Fig. 7.6(b) Decay pattern of 2.1 μm emission of $\text{LiYF}_4 : \text{Ho}^{3+}(1\%)$ at 77K.

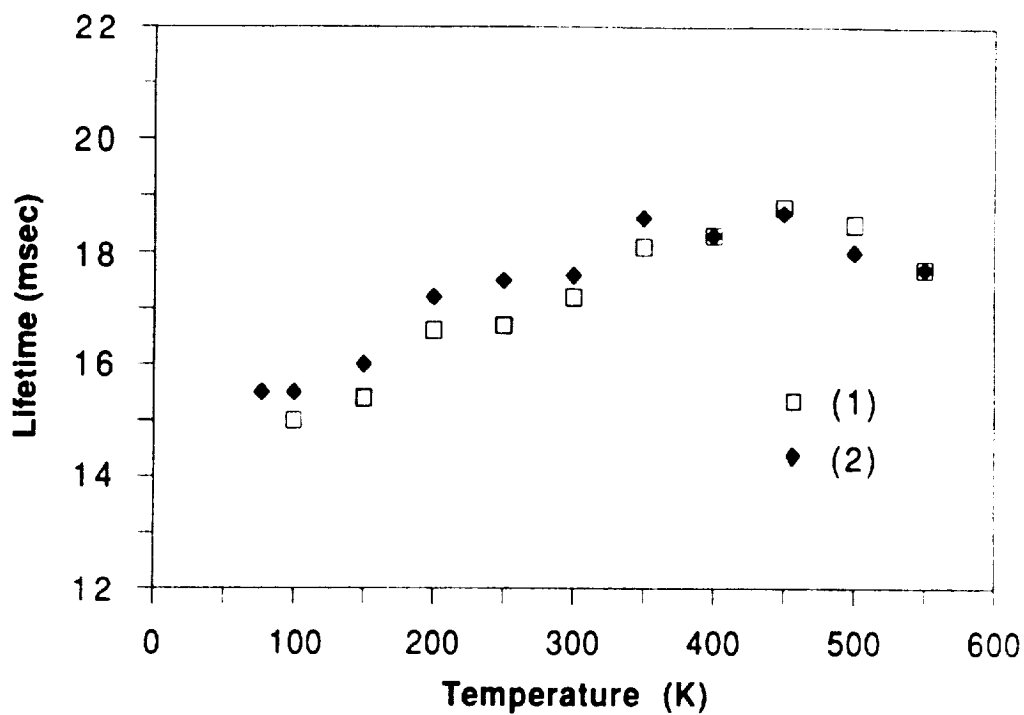


Fig. 7.7 Temperature dependence of lifetime of $\text{Ho}^{3+} 5I_7$ energy level in $\text{LiYF}_4 : \text{Ho}^{3+}(1\%)$ ($5S_2$ energy level of Ho is excited).
 (1) : luminescence monitored at $1.9 \mu\text{m}$
 (2) : luminescence monitored at $2.1 \mu\text{m}$

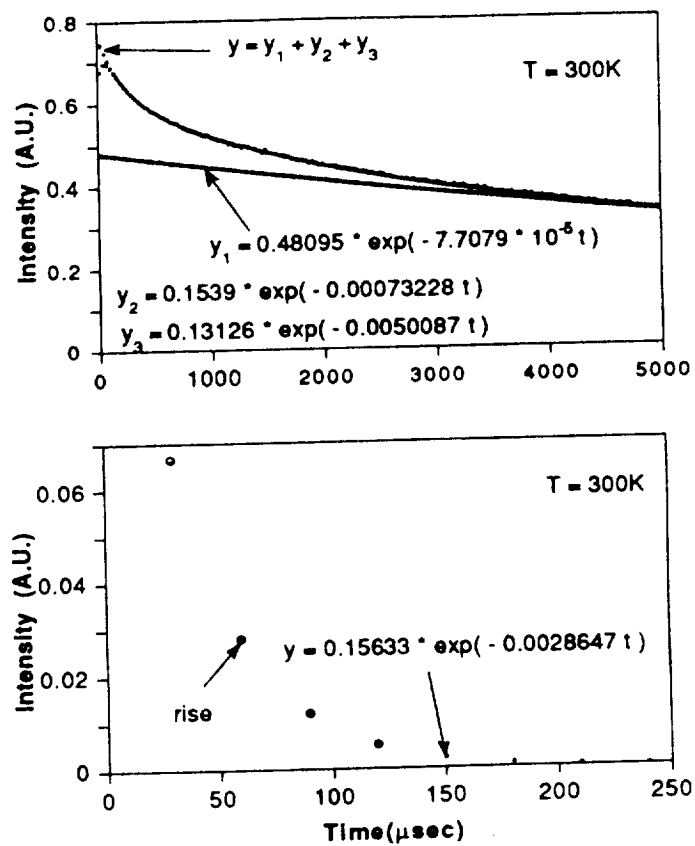


Fig. 7.8 (a) Decay pattern of 1.6 μm emission of $\text{LiYF}_4 : \text{Tm}^{3+}(5\%), \text{Ho}^{3+}(.2\%)$ at 300K ($^3\text{H}_4$ level of Tm is excited with 795 nm pulses from the dye laser).

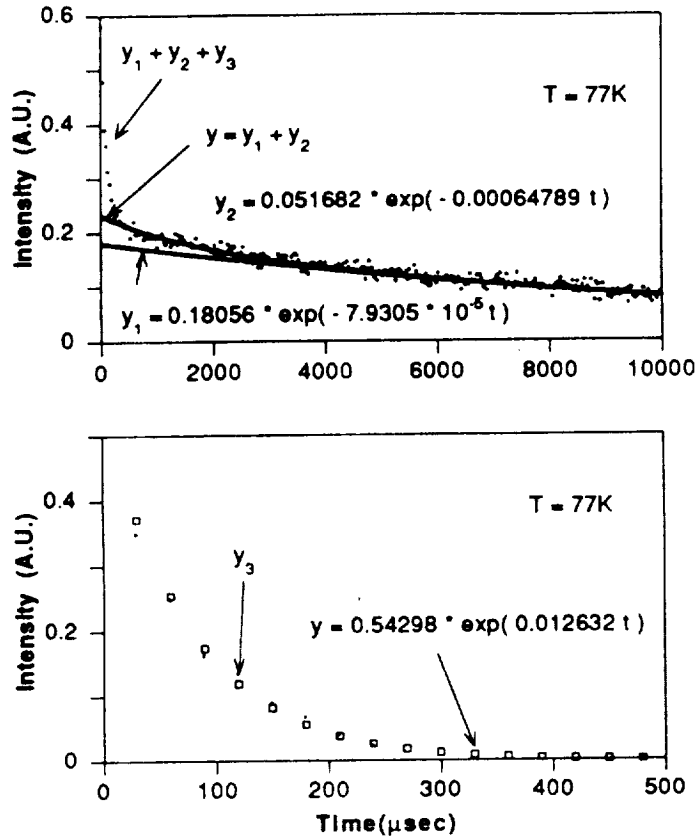


Fig. 7.8 (b) Decay pattern of 1.6 μm emission of $\text{LiYF}_4 : \text{Tm}^{3+}(5\%), \text{Ho}^{3+}(.2\%)$ at 77K ($^3\text{H}_4$ level of Tm is excited with 795 nm pulses from the dye laser).

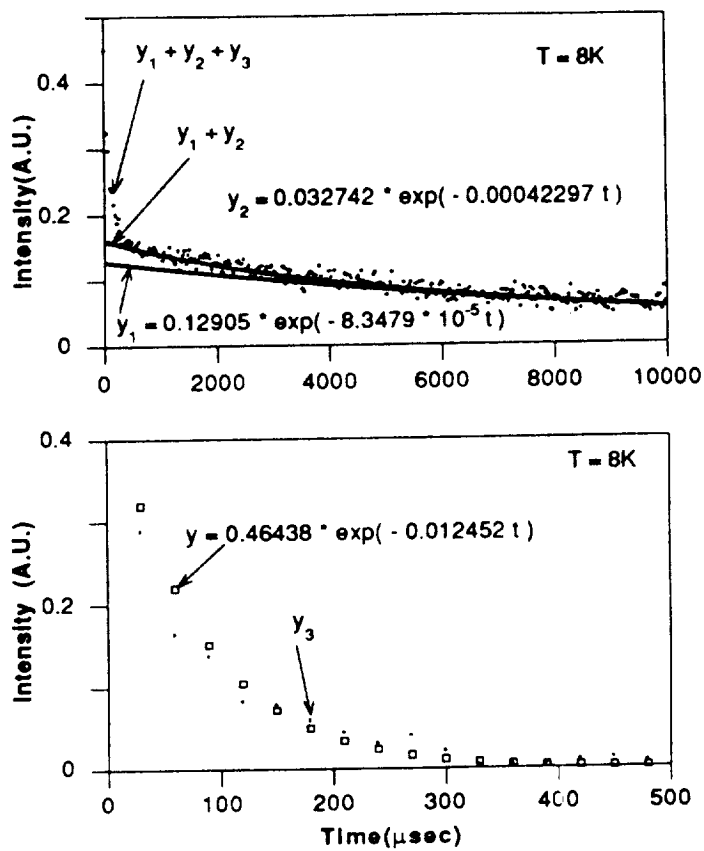


Fig. 7.8 (c) Decay pattern of 1.6 μm emission of $\text{LiYF}_4 : \text{Tm}^{3+}(5\%), \text{Ho}^{3+}(.2\%)$ at 8K ($^3\text{H}_4$ level of Tm is excited with 795 nm pulses from the dye laser).

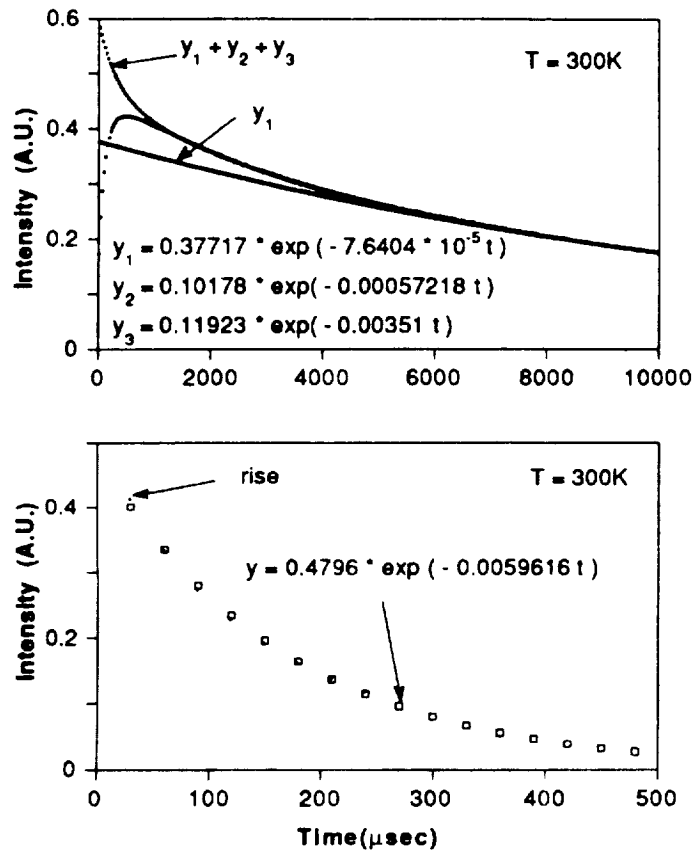


Fig. 7.9 (a) Decay pattern of 2.1 μm emission of $\text{LiYF}_4 : \text{Tm}^{3+}(5\%), \text{Ho}^{3+}(.2\%)$ at 300K ($^3\text{H}_4$ level of Tm is excited with 795 nm pulses from the dye laser).

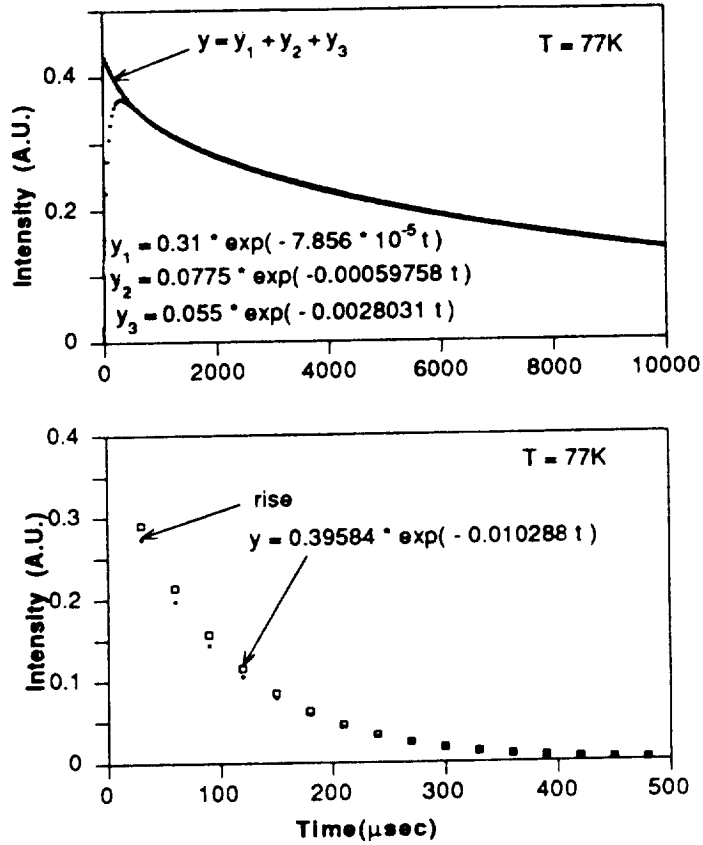


Fig. 7.9 (b) Decay pattern of 2.1 μm emission of LiYF₄ : Tm³⁺(5%), Ho³⁺(.2%) at 77K (³H₄ level of Tm is excited with 795 nm pulses from the dye laser).

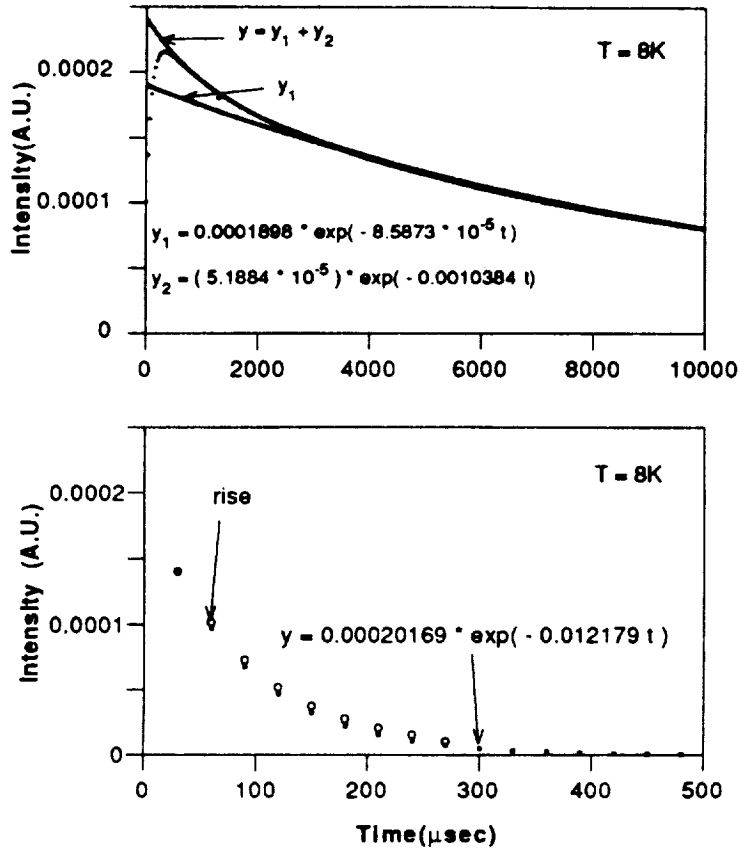


Fig. 7.9 (c) Decay pattern of 2.1 μm emission of $\text{LiYF}_4 : \text{Tm}^{3+}(5\%), \text{Ho}^{3+}(.2\%)$ at 8K ($^3\text{H}_4$ level of Tm is excited with 795 nm pulses from the dye laser).

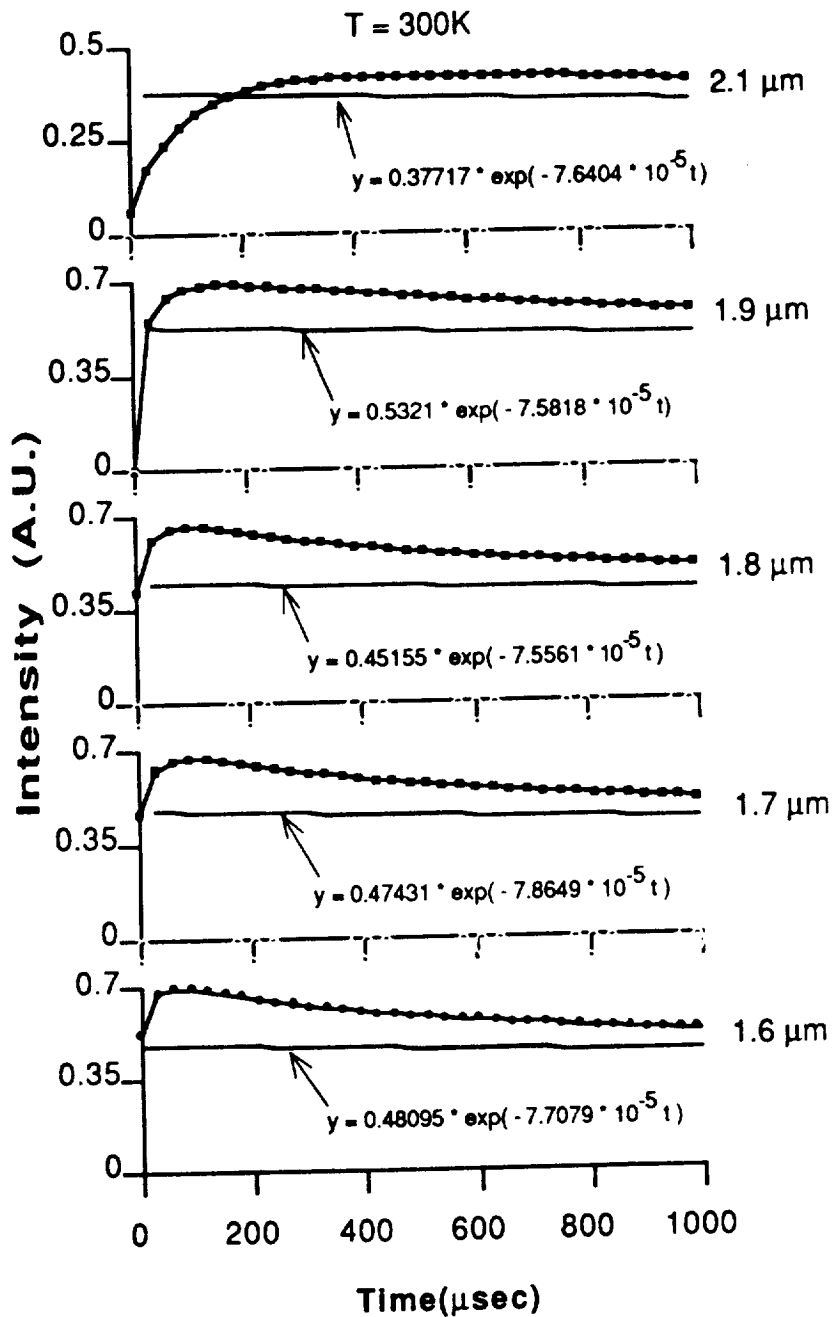


Fig. 7.10 (a) Decay patterns of the emission from different spectral regions of $\text{LiYF}_4 : \text{Tm}^{3+}(5\%), \text{Ho}^{3+}(.2\%)$ at 300K ($^3\text{H}_4$ level of Tm is excited with 795 nm pulses from the dye laser).

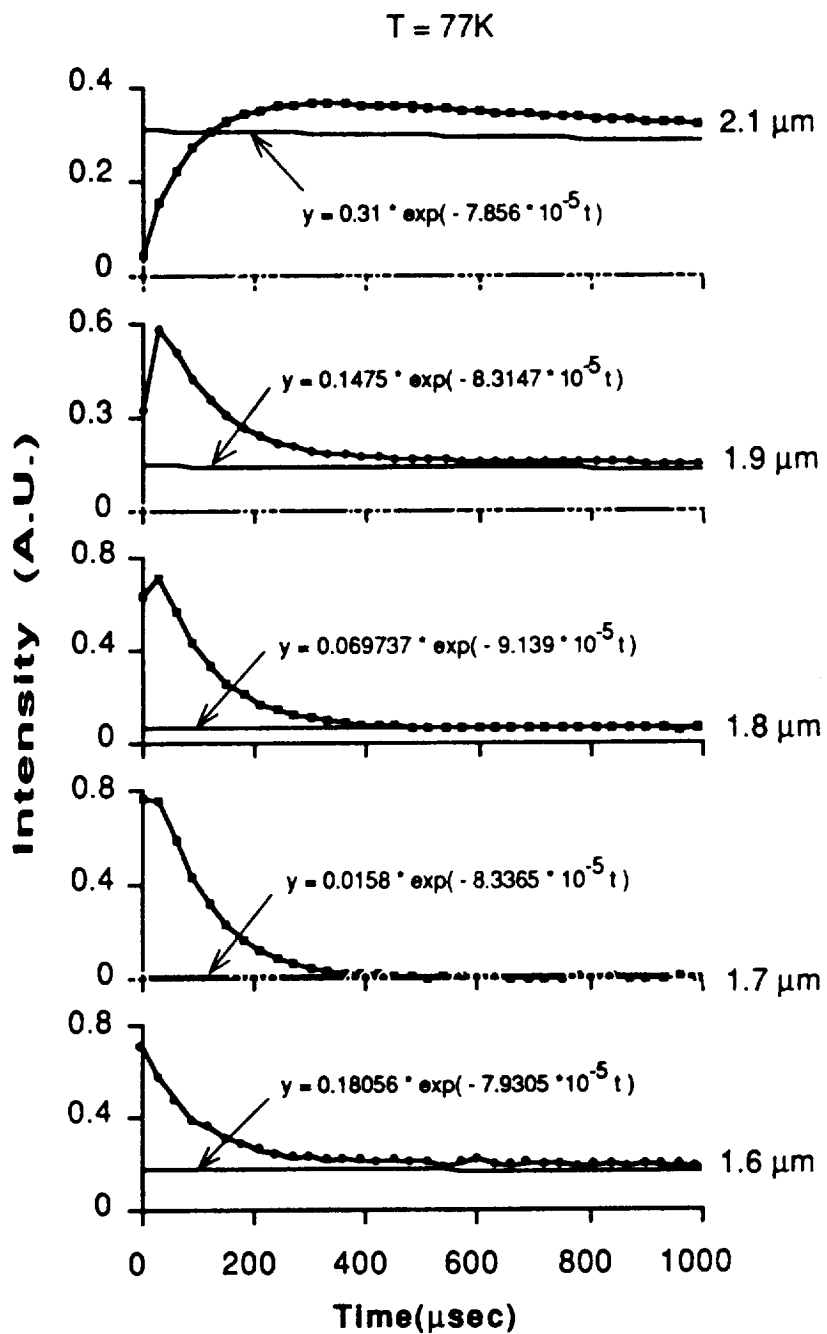


Fig. 7.10 (b) Decay patterns of the emission from different spectral regions of $\text{LiYF}_4 : \text{Tm}^{3+}(5\%), \text{Ho}^{3+}(.2\%)$ at 77K ($^3\text{H}_4$ level of Tm is excited with 795 nm pulses from the dye laser).

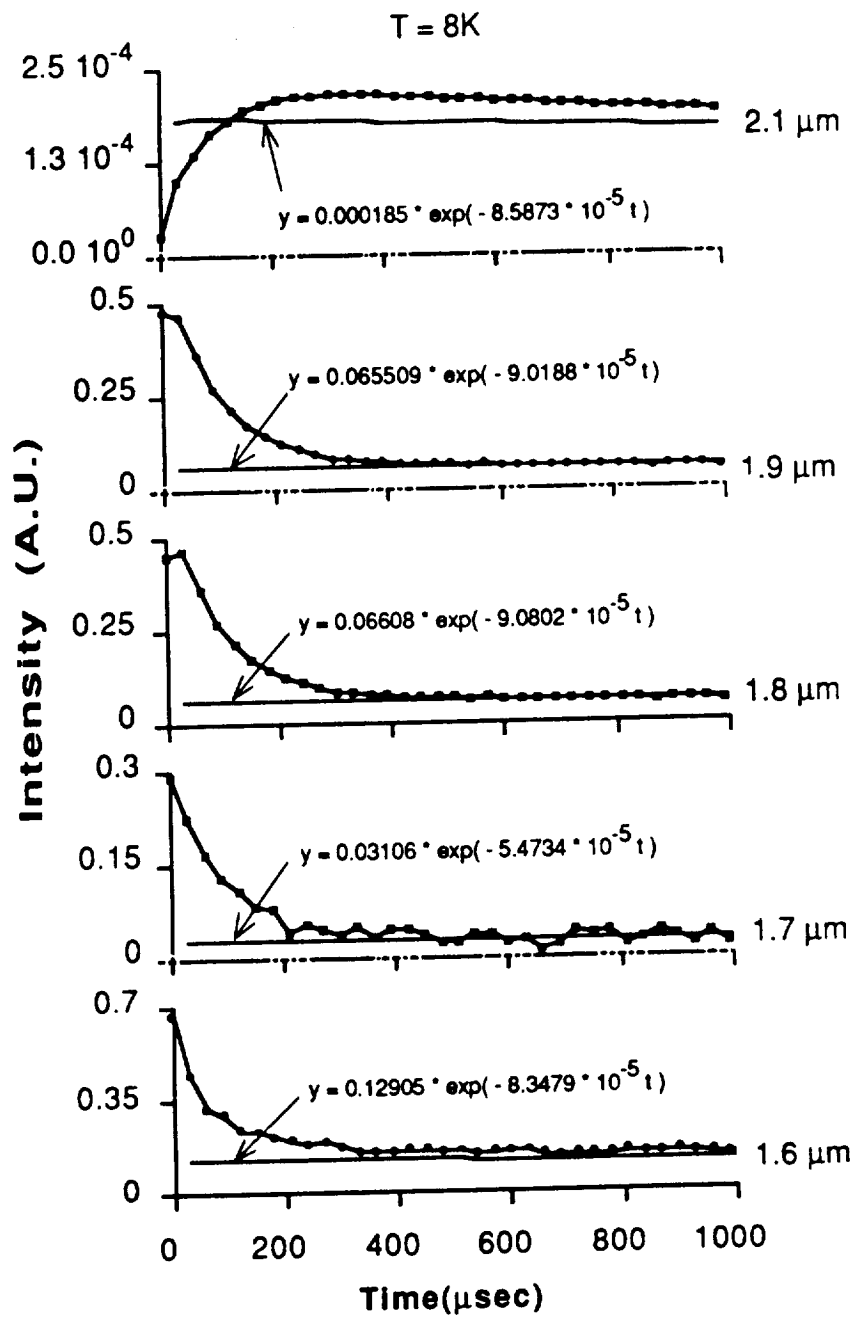


Fig. 7.10 (c) Decay patterns of the emission from different spectral regions of $\text{LiYF}_4 : \text{Tm}^{3+}(5\%), \text{Ho}^{3+}(.2\%)$ at 8K ($^3\text{H}_4$ level of Tm is excited with 795 nm pulses from the dye laser).

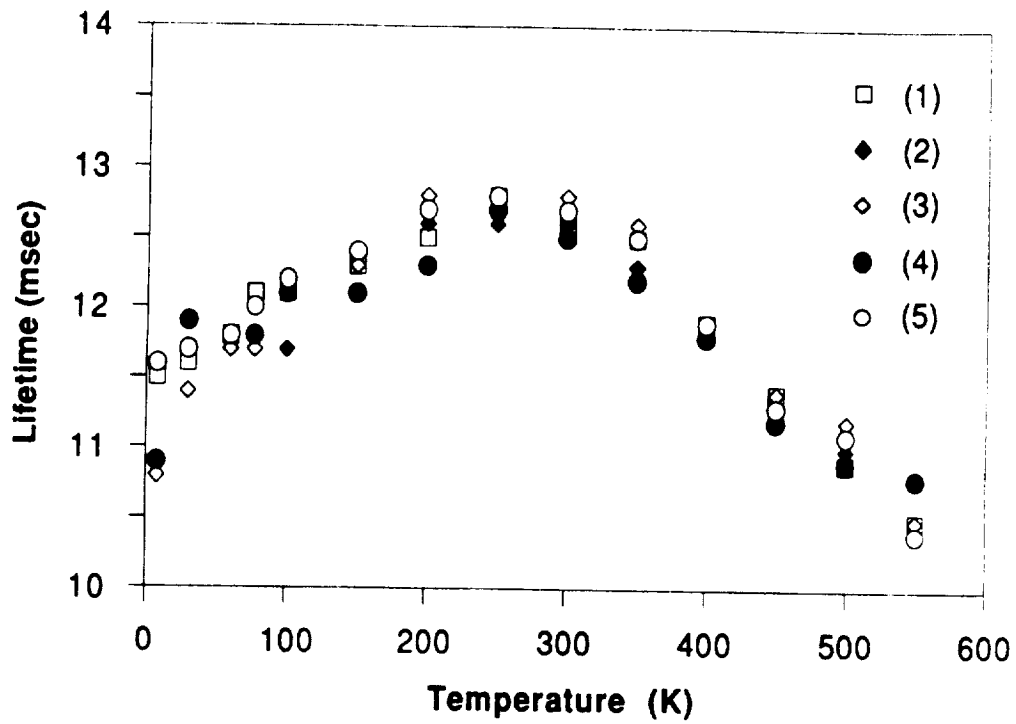


Fig. 7.11 Temperature dependence of the lifetime of $Tm^{3+} \ ^3F_4$ and $Ho^{3+} \ ^5I_7$ energy levels in $LiYF_4 : Tm^{3+}(.5\%), Ho^{3+}(.2\%)$ (3H_4 energy level of Tm is excited).

- (1) : luminescence monitored at 1.6 μm
- (2) : luminescence monitored at 1.7 μm
- (3) : luminescence monitored at 1.8 μm
- (4) : luminescence monitored at 1.9 μm
- (5) : luminescence monitored at 2.1 μm

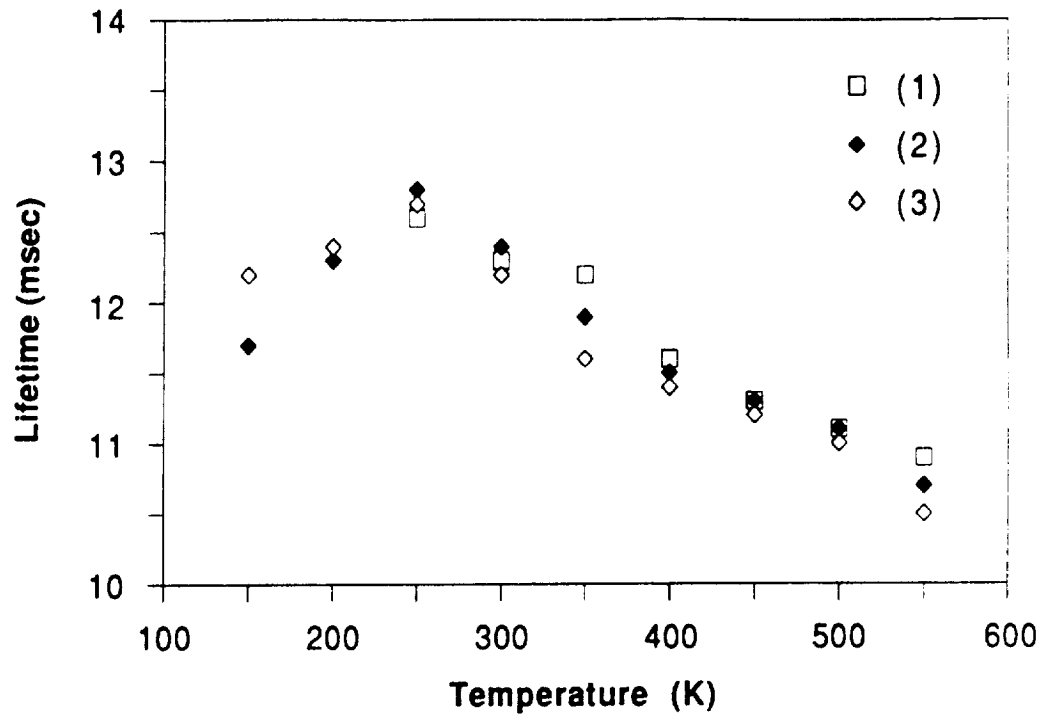


Fig. 7.12 Temperature dependence of the lifetime of $Tm^{3+} \ ^3F_4$ and $Ho^{3+} \ ^5I_7$ energy levels in $LiYF_4 : Tm^{3+}(.5\%), Ho^{3+}(.2\%)$ (5S_2 energy level of Ho is excited).

- (1) : luminescence monitored at $1.8 \ \mu m$
- (2) : luminescence monitored at $1.9 \ \mu m$
- (3) : luminescence monitored at $2.1 \ \mu m$

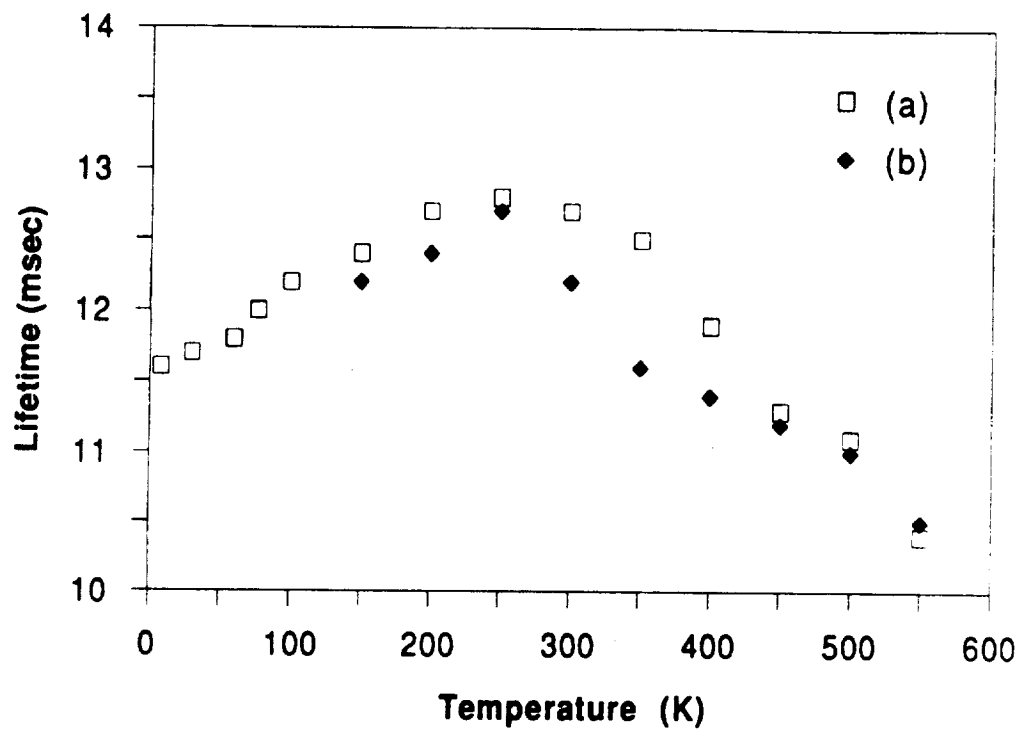


Fig. 7.13 Temperature dependence of the lifetime of $Tm^{3+} \ ^3F_4$ and $Ho^{3+} \ ^5I_7$ energy levels in $LiYF_4 : Tm^{3+}(.5\%), Ho^{3+}(.2\%)$.

(a) : (3H_4 energy level of Tm is excited)

(b) : (5S_2 energy level of Ho is excited)

8. DISCUSSION OF RESULTS I. ABSORPTION, LUMINESCENCE, AND EXCITATION

8.1 LiYF₄ : Tm³⁺(.5%at.)

The absorption spectrum of Tm³⁺ in LiYF₄ at room temperature was shown in Figures 5.1 (a) and 5.1 (b). The various peaks, as indicated in those figures, are consistent with the energy level scheme given by Jønsen et al [Ref. 9 of Ch. 4]. The absorption transitions related to the ³F₄ level are shown in Fig. 8.1 for 300 and 78K. The following observations can be made:

- i) More absorption lines appear at higher temperatures.
- ii) The Stark lines of the absorption band are sharper at low temperatures and become broader at higher temperatures.

The mechanism responsible for these effects is the following:

The absorption or emission of a photon by an ion in a crystal lattice may be accompanied by the absorption or emission of one or more phonons. This process introduces a side band structure for the narrow lines of purely-radiative transitions between the electronic levels of the ion, which is observed as broadening of the absorption or emission lines at higher temperatures.

The luminescence spectrum of the sample in the optical region is stronger when the sample is excited into the Tm ¹G₄ level by an Argon - Ion laser than by a tungsten lamp. We observed that the opposite is true for the emission from the ³F₄ level. This indicates that the energy from the intermediate levels of Tm reaches the ³F₄ level more efficiently than the energy coming from the upper excited levels because of the many jumps necessary to get to this level.

The integrated intensity and the lifetime of the optical emission related to the ${}^3\text{H}_4 \rightarrow {}^3\text{H}_6$ transition have different temperature dependences. This is also true for the emission from the ${}^3\text{F}_4$ level (see Figs. 8.2 and 8.3). This could be due to an increase of the absorption intensity with temperature. We excluded this possibility by verifying that the amount of light from a tungsten lamp passed through the sample did not change with the temperature. The different dependence on the temperature of the intensity and lifetime curves is most likely be due to the fact that the excitation used for the measurements of the intensity was broad band and produced the population of several levels whose decay did not always replenish the luminescent levels.

8.2 LiYF₄ : Ho³⁺(1% at.)

Considering the absorption spectrum of Ho³⁺ in LiYF₄ at room temperature reported in Figs. 5.6 (a) and 5.6 (b), the energy level assignments on these figures agree with the energy level scheme calculated by Karayanis et al [Ref. 15 of Ch. 4].

The absorption spectrum of Ho ⁵I₇ level at 77 and 300K is reported in Fig. 8.4. The Stark lines are sharper at low temperatures and they broaden at higher temperatures. This is due to the temperature dependence of the crystal field acting on the Ho ion.

The Tm ³F₄ → Ho ⁵I₇ energy transfer depends on the absorption coefficient integral of the Ho ⁵I₇ level. The temperature dependence of this integral reported in Table 8.1 and Fig. 8.5 has found to decrease every with increasing temperature.

The integrated intensity of the emission from the Ho ⁵I₇ level and the lifetime of the ⁵I₇ level have different temperature dependence (see Fig. 8.6). The explanation of this fact is similar to the one given in the previous section.

8.3 LiYF₄ : Tm³⁺(5%); Ho³⁺(.2%)

The absorption spectrum of the sample co-doped with Tm³⁺ and Ho³⁺ was shown in Figures 5.10 (a) and 5.10 (b). The spectrum is simply the superposition of the spectra of LiYF₄ : Tm³⁺ and LiYF₄ : Ho³⁺ samples. This means that the interaction between the Tm³⁺ and Ho³⁺ ions does not introduce new energy levels in this system.

The excitation spectrum of the infrared emission of LiYF₄ : Tm³⁺(5%at.); Ho³⁺(.2%at.), reported in Fig. 6.3, was obtained by monitoring the emission at 1.7μm. It contains the Ho absorption bands in addition to the Tm absorption bands. The excitation spectra obtained by monitoring 1.8, 1.9 and 2.1μm were found to be identical to the one obtained for the 1.7μm emission. This is an experimental evidence for the back transfer from ⁵I₇ level of Ho to ³F₄ level of Tm and is consistent with the model in which the transfer is governed by thermalization.

A relevant parameter for the study of the energy transfer between levels ³F₄ of Tm and ⁵I₇ of Ho is the overlap integral between the ³H₆ → ³F₄ Tm absorption and the ⁵I₇ → ⁵I₈ Ho emission. We followed this calculation with the evaluation of the microscopic parameter C⁽⁶⁾ and of the characteristic radius R₀, at which the transfer rate is equal to the lifetime of Tm in absence of Ho. These quantities are reported in Table 8.2 and Fig. 8.9. R₀ is measured to be 2.3 × 10⁻⁷ cm at room temperature.

TABLE 8.1
The Temperature Dependence of The Absorption Coefficient Integral
of 5I_7 level of Ho^{3+} in $LiYF_4$

T(K)	Absorption Coefficient Integral ($\times 10^3 \text{ cm}^{-2}$)
78	0.126
100	0.125
150	0.124
200	0.124
250	0.122
300	0.121
350	0.121

Refer to Figures 8.5 and 8.6

Source: Jarrell Ash 30W tungsten Lamp

Detector : Spex Model 1428 PbS detector

Spex Model 1681 .22m monochromator; slits (both) : 150 μm

Stanford Research Systems Model SR510 "lock-in" amplifier

Sensitivity : 1mV

Time Constant : 0.3 sec.

TABLE 8.2

The Temperature Dependence of R_0^6 , $C^{(6)}$, and reciprocal Lifetime of 3F_4 level of Tm^{3+} in $LiYF_4$

T(K)	R_0^6 ($\times 10^{-40} \text{ cm}^6$)	$C^{(6)}$ ($\times 10^{-38} \text{ cm}^6/\text{sec}$)	Reciprocal Lifetime of Tm^{3+} ($\text{sec})^{-1}$
78	5.74	3.11	0.54
100	4.13	2.33	0.56
150	2.72	1.64	0.60
200	1.92	1.20	0.62
250	1.55	1.01	0.65
300	1.31	0.09	0.686
350	1.24	0.086	0.69

Refer to Figure 8.8, 8.9 and 8.10

See the conditions reported under Tables 5.12 and 8.2

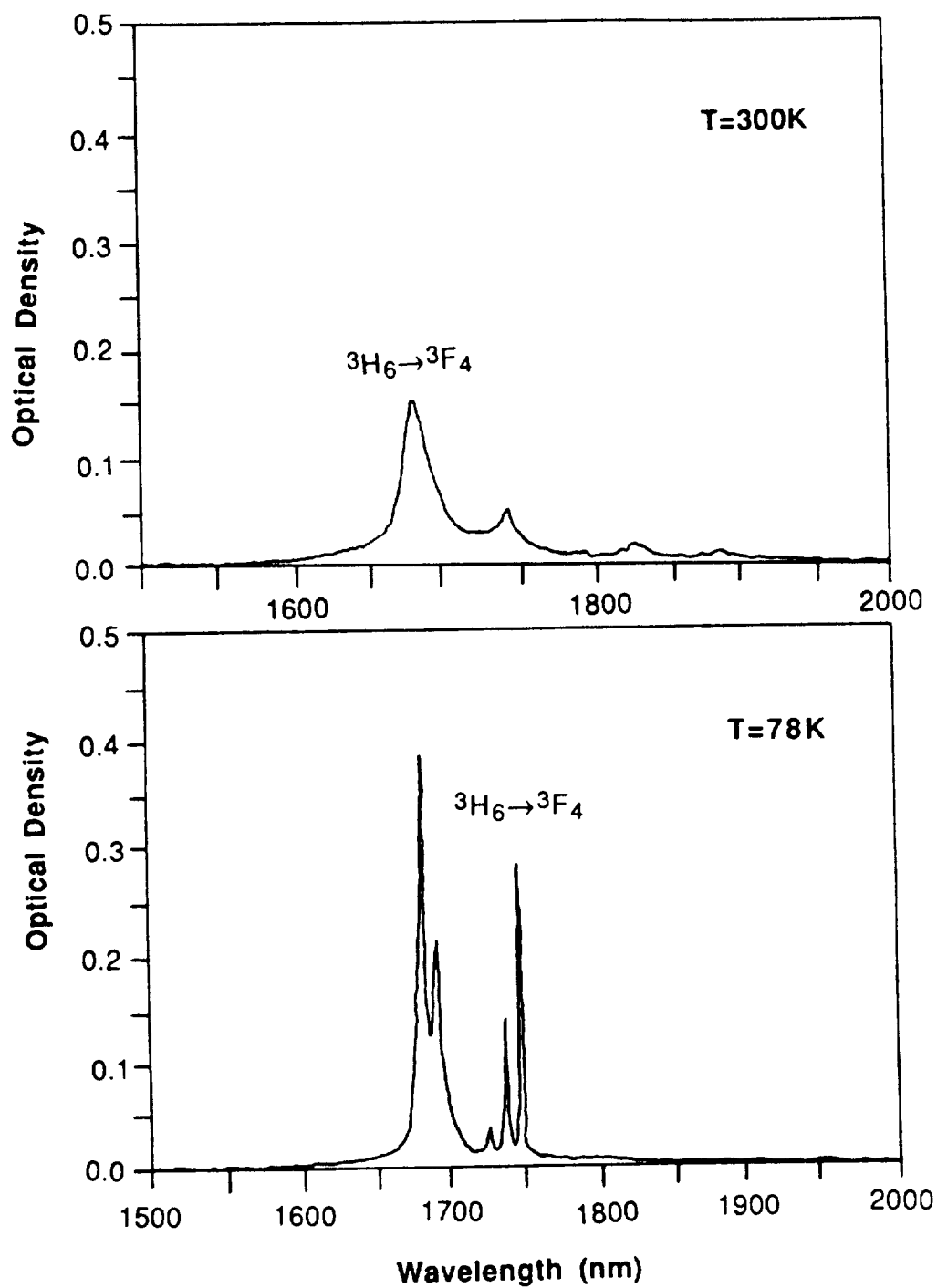


Fig. 8.1 The absorption spectrum of 3F_4 level of Tm^{3+} in $LiYF_4$.

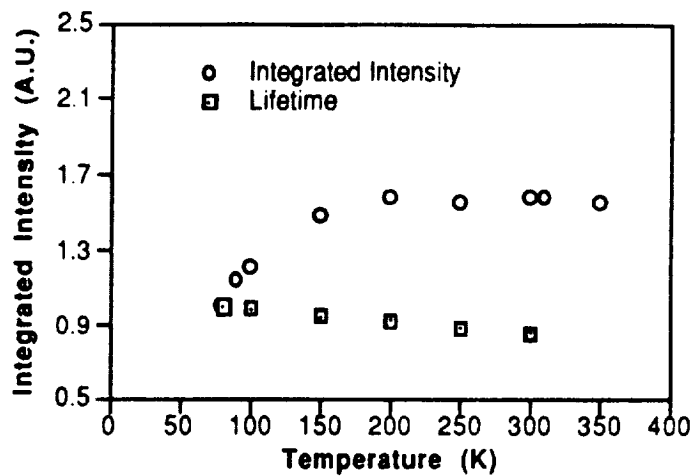


Fig. 8.2 Comparison of the temperature dependence of the integrated intensity and the lifetime of the 3H_4 level of Tm in LiYF₄ (The integrated intensity was obtained by exciting the system by a tungsten lamp, and the lifetime was measured by exciting the system into the 3F_3 level with a laser pulse).

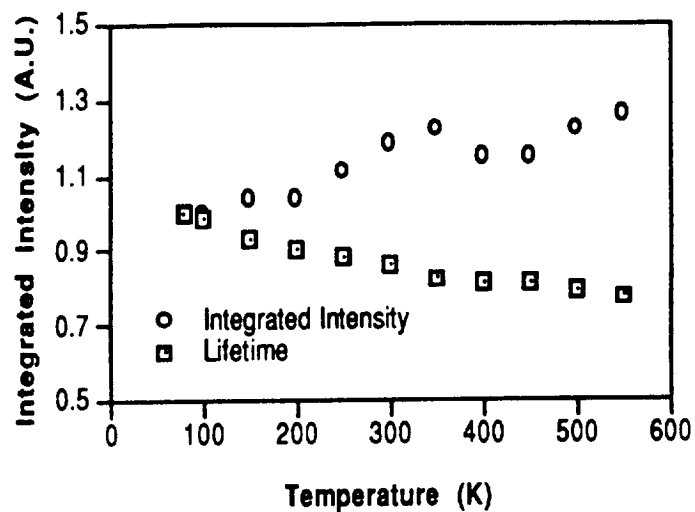


Fig. 8.3 Comparison of the temperature dependence of the integrated intensity and the lifetime of the 3F_4 level of Tm in LiYF₄ (The integrated intensity was obtained by exciting the system by a tungsten lamp, and the lifetime was measured by exciting the system into the 3H_4 level with a laser pulse).

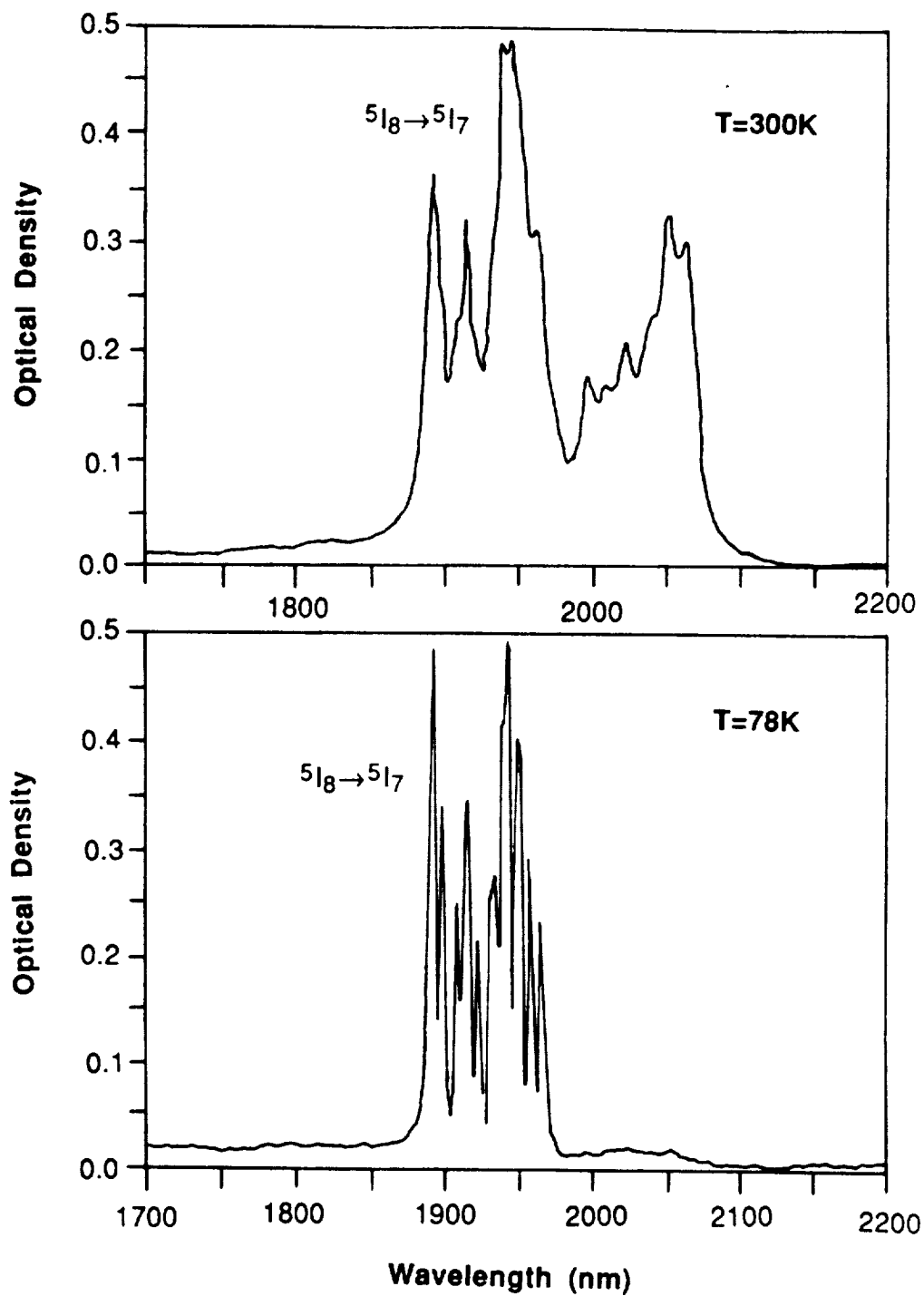


Fig. 8.4 The absorption spectrum of $5I_7$ level of Ho^{3+} in LiYF_4 .

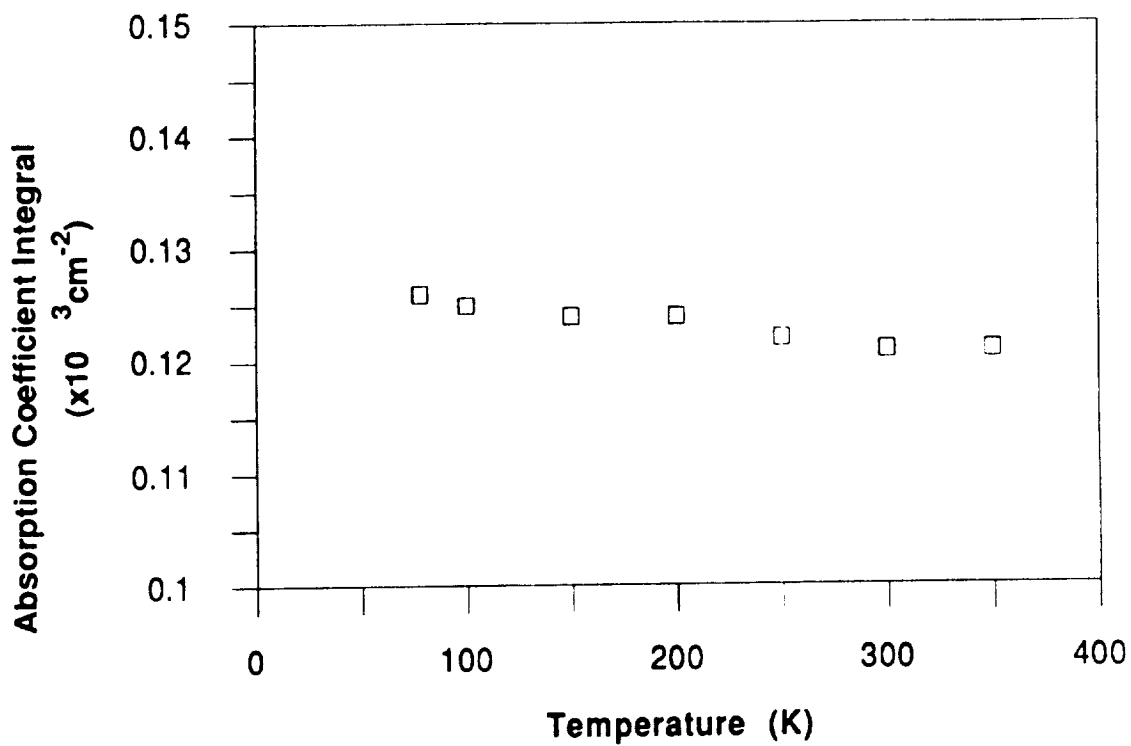


Fig. 8.5. The absorption coefficient integral of $5I_7$ level of Ho^{3+} in LiYF_4 versus temperature.

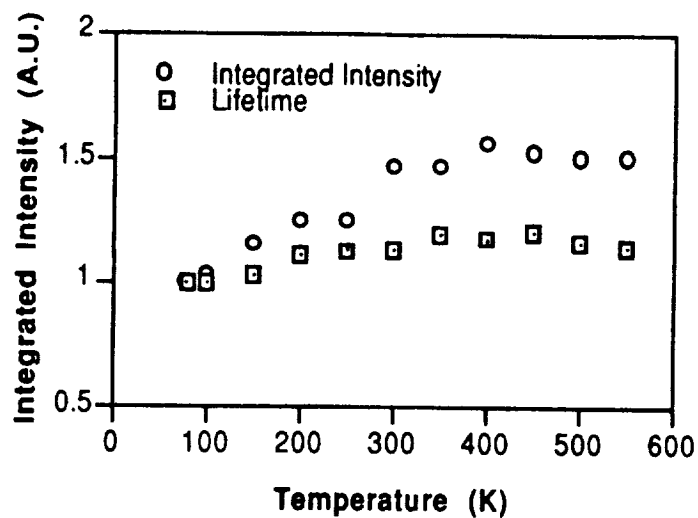


Fig. 8.6 Comparison of the temperature dependence of the integrated intensity and the lifetime of the 5I_7 level of Ho in $LiYF_4$ (The integrated intensity was obtained by exciting the system by a tungsten lamp, and the lifetime was measured by exciting the system into the 5S_2 level with a laser pulse).

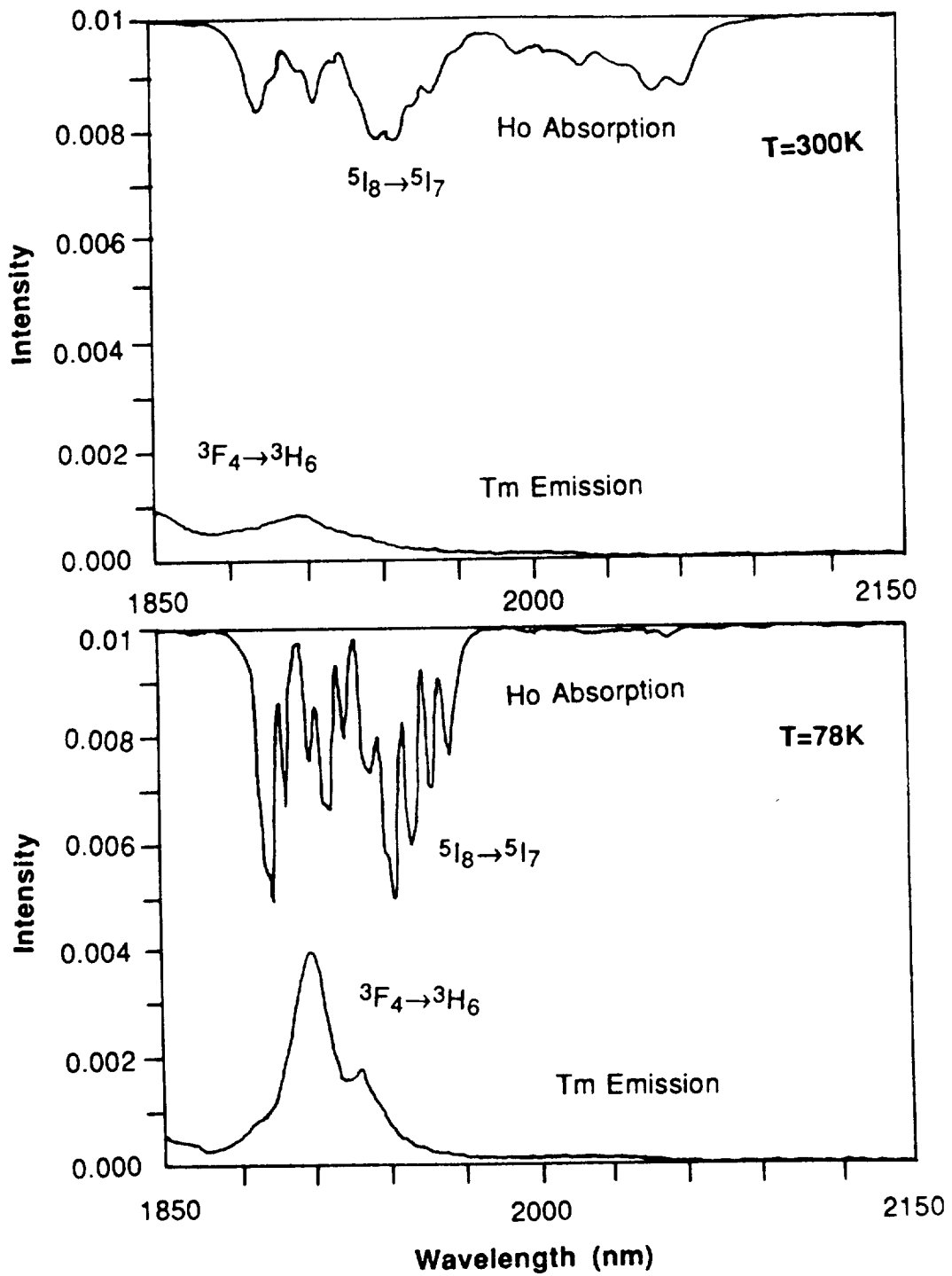


Fig. 8.7 The overlap between the normalized emission and the absorption spectrum of $3F_4$ level of Tm^{3+} and absorption spectrum of $5I_7$ level of Ho^{3+} in LiYF_4 .

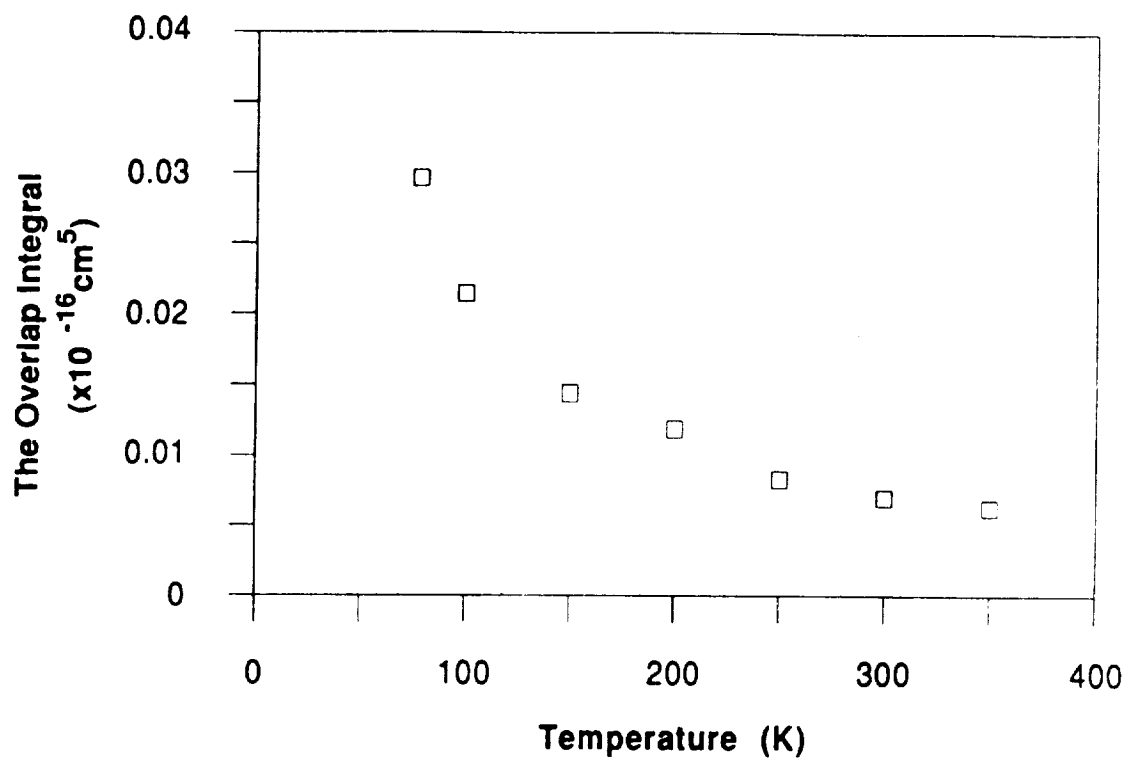


Fig. 8.8. The temperature dependence of the overlap integral between the normalized emission spectrum of 3F_4 level of Tm^{3+} and the absorption spectrum of 5I_7 level of Ho^{3+} in $LiYF_4$.

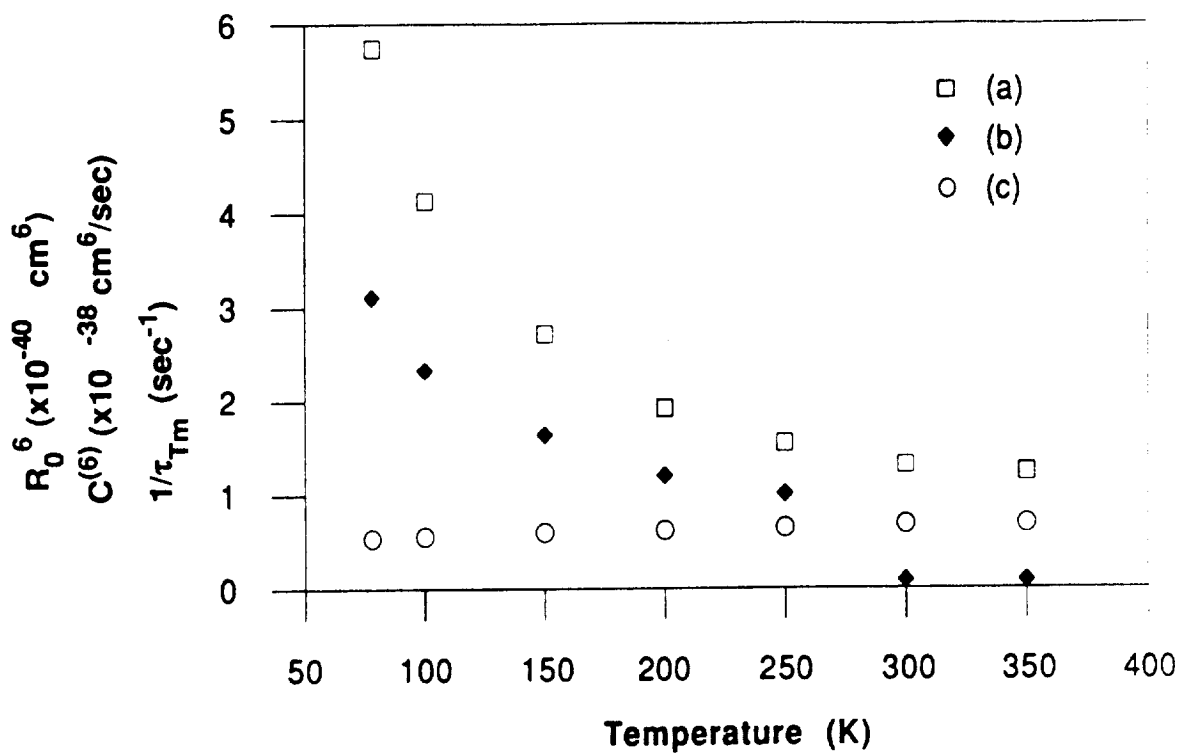


Fig. 8.9. The temperature dependence of

(a) : R_0^6 ,

(b) : The macroscopic interaction parameter, $C^{(6)}$, and

(c) : The reciprocal lifetime of 3F_4 level of Tm^{3+} in $LiYF_4$.

9. DISCUSSION OF RESULTS II. DECAY PATTERNS AND (Tm) $^3F_4 \leftrightarrow$ (Ho) 5I_7 ENERGY TRANSFER

9.1 Considerations on Luminescence Decay Patterns

When one of the levels of a multilevel system is excited by a pulse of energy the system may relax to the ground state directly or via many jumps between the intermediate levels. The process may be studied by considering a three level system with two metastable states indicated by the indices of 3 and 2, and a ground state, 1 (see Fig. 9.1). If levels 3 and 2 are connected by certain probabilities p_{32} and p_{23} which depend on the ground state population, N_0 , the rate equations of the population is given by [1]

$$\dot{N}_3 = - N_3 p_{31} - N_3 p_{32} + N_2 p_{23} \quad (9.1.1)$$

$$\dot{N}_2 = - N_2 p_{21} - N_2 p_{23} + N_3 p_{32}$$

where p_{31} is the decay rate from state 3 to the ground state, and p_{21} is the decay rate from state 2 to the ground state.

Three different cases can be considered.

1) $p_{23} = p_{32} \sim 0$: The equations above become

$$\dot{N}_3 = - N_3 p_{31} \quad (9.1.2)$$

$$\dot{N}_2 = - N_2 p_{21}$$

The solutions are

$$N_3 = N_3(0)\exp(-p_{31}t) \quad (9.1.3)$$

$$N_2 = N_2(0)\exp(-p_{21}t)$$

In this case, each level decays with its characteristic decay time since there is no connection between the levels.

2) $p_{23} \rightarrow 0$: The rate equations become

$$\dot{N}_3 = -N_3p_3$$

$$\dot{N}_2 = -N_2p_2 + N_3p_{32} \quad (9.1.4)$$

where $p_3 = p_{31} + p_{32}$, and $p_2 = p_{21}$

The solutions for these equations are

$$N_3 = N_3(0)\exp(-p_3t) \quad (9.1.5)$$

$$N_2 = \left[N_2(0) + \frac{p_{32}}{p_3 + p_{21}} \right] \exp(-p_{21}t) + \left[\frac{N_2(0) p_{32}}{p_3 - p_{21}} \right] \exp(-p_3t)$$

The decay curve of the emission from level 2 is superposition of two exponential as can be seen in (9.1.5). Three different cases can be observed:

1-1) If $p_3 \gg p_{21}$ the decay pattern of the $N_2(t)$ shows an exponential with the decay time equal to $1/p_{21}$.

1-2) If the exciting pulse is short enough, $N_2(t)$ can show a maximum at a time t_{\max} after the end of the pulse. This time is related to the populations and probabilities as follows:

$$t_{\max} \geq 0 \text{ for } p_{32} \frac{N_3(0)}{N_2(0)} \geq p_{21} \quad (9.1.6)$$

1-3) If $p_{21} > p_3$, and $N_2(0) > \frac{p_{32}N_3(0)}{p_{21} - p_3}$ a double decay is observed. The presence of the double decay in case of three level system shows that level 2 is also excited directly from some absorption band above level 3 or the energy is transferred from some other ion.

3) If $p_{23} \neq 0$, and $p_{32}, p_{23} \gg p_{31}, p_{21}$: the solutions for the rate equations given in (9.1.1) are

$$\begin{aligned} N_3(t) &= \left[\frac{N_3(0)p_{23} + N_2(0)p_{23}}{p_{32} + p_{23}} \right] \exp(-pt) \left[\frac{N_2(0)p_{23} + N_3(0)p_{32}}{p_{32} + p_{23}} \right] \exp(-(p_{32} + p_{23})t) \\ N_2(t) &= \left[\frac{N_2(0)p_{32} + N_3(0)p_{32}}{p_{32} + p_{23}} \right] \exp(-pt) \left[\frac{N_3(0)p_{32} + N_2(0)p_{23}}{p_{32} + p_{23}} \right] \exp(-(p_{32} + p_{23})t) \end{aligned} \quad (9.1.7)$$

where $p = \frac{p_{21}p_{32} + p_{31}p_{23}}{p_{32} + p_{23}}$

If the two metastable levels are thermalized, they decay with the same time constant that depends on intrinsic lifetimes $\tau_2 = 1/p_{21}$ and $\tau_3 = 1/p_{31}$ of the two levels and the energy difference ΔE between the two levels. The ratio of the

initial populations of these levels can be expressed in terms of Boltzman distribution which is

$$\frac{N_3(0)}{N_2(0)} = \frac{p_{23}}{p_{32}} = \exp\left(\frac{\Delta E_{32}}{kT}\right)$$

and

(9.1.8)

$$N_3(t) = N_3(0) \exp(-pt) = N_2(0) \left(\frac{p_{23}}{p_{32}}\right) \exp(-pt)$$

where

$$p = p_{21} \left(\frac{e^{\Delta E_{32}/kT}}{1 + e^{\Delta E_{32}/kT}}\right) + p_{31} \left(\frac{1}{1 + e^{\Delta E_{32}/kT}}\right)$$

or

(9.1.9)

$$p = \frac{1}{\tau} = \frac{\frac{1}{\tau_2} + \frac{1}{\tau_3} e^{-\Delta E_{32}/kT}}{1 + e^{-\Delta E_{32}/kT}}$$

We can make the following observation : if two decays coming from different levels have the same lifetime they originate either from two levels in thermal equilibrium or two different and not normalized levels which accidently have the same lifetime.

9.2 LiYF₄ : Tm³⁺(.5%)

We obtained the response to the pulsed excitation of the ³H₄ level by exciting the system into the ³F₃ level. The decay pattern of this level was found to be an exponential at all temperatures. This shows that the lifetime of the ³F₃ level is much shorter than the lifetime of the ³H₄ level.

When the ³H₄ level of Tm is excited by a pulse from the laser the ion may first relax to the ³F₄ level and then decay to the ground state. The relaxation from ³H₄ level to the ³F₄ level may occur directly via a radiative transition or nonradiatively via the ³H₅ level. The decay patterns obtained at various wavelengths were shown in Figs. 7.1 and 7.2. They present a rise followed by an exponential drop at all temperatures except for the emission at 1.6 μm. This emission shows a double decay at low temperatures and eventually becomes the same as the other patterns obtained at 1.7, 1.8 and 1.9 μm. We believe this emission comes perhaps from a different Tm level. The rise observed in the decay patterns of the different emission lines of the ³F₄ level is due to the ³H₄→³F₄ relaxation, and has the time constant of the ³H₄ level. The exponential part of the pattern corresponds to the ³F₄→³H₆ transition with the time constant equal to the lifetime of the ³F₄ level. The decay pattern of ³F₄ level can then be described by two exponential decay as

$$I(t) \sim \exp(-t/\tau_1) - \exp(-t/\tau_2)$$

where τ_1 is the lifetime of the ³F₄ level, and τ_2 is the lifetime of the ³H₄ level.

9.3 LiYF₄ : Ho³⁺(1%)

Response to pulsed excitation of the ⁵I₇ level was obtained by exciting the system into the ⁵S₂ level of the Ho ion. Emission of this level at 1.9 and 2.1 μm shows similar features(see Fig. 7.5). The rise observed is due to the ⁵I₆ → ⁵I₇ relaxation since the relaxation from ⁵S₂ level to the ⁵I₆ and/or ⁵I₇ levels is much faster than the relaxation from the ⁵I₆ level to the ⁵I₇ level [Ref. 16 of Ch. 4]. The exponential decay is due to the ⁵I₇ → ⁵I₈ transition and shows how the system in the ⁵I₇ level relaxes to the ground state. We believe that the emission lines centered at 1.6 and 1.7 μm are due to the ⁵S₂→⁵I₄ transition having the lifetime of the ⁵S₂ level.

9.4 LiYF₄ : Tm³⁺(5%), Ho³⁺(.2%)

The decay pattern of the emission of LiYF₄ : Tm³⁺(5%), Ho³⁺(.2%) in the 2 μm region was obtained by monitoring the emission at different wavelengths. The emission at low wavelengths (1.7 to 1.8 μm) comes from the ³F₄ level of Tm and the emission at high wavelengths (2.05 to 2.2 μm) comes from the ⁵I₇ level of Ho, and the emission at the intermediate wavelengths (1.8 to 2.0 μm) comes from both ions.

We shall refer mainly to Figures 9.2 a to d, and to the results in Section 6.3. The experimental facts of relevance at this point are :

- 1) The excitation spectrum of the infrared emission is the same regardless of the wavelength monitored, and is made out of bands due to both the Tm and Ho ions.
- 2) The decay patterns at the various wavelengths are different in the early parts of the decay, but eventually become similar.

These two facts seem to indicate that each decay pattern consists of a transient (different for each wavelength) followed by a part that has the same time constant for all the wavelengths and corresponds to a thermalization condition.

We shall use a model similar to the one used by other workers [2] in order to understand the thermalization or approach to equilibrium between the ³F₄ level of Tm and the ⁵I₇ level of Ho. We represent each of the Tm (³F₄) and Ho (⁵I₇) manifolds as a single level with the populations n_1 and N_1 , and consider them connected by forward and backward transfer rate k and k' respectively. The rate equations are then given by

$$\dot{n}_1 = -\frac{n_1}{\tau_{Tm}} - kn_1N_0 + k'n_0N_1 \quad (9.4.1)$$

$$\dot{N}_1 = -\frac{N_1}{\tau_{Ho}} + kn_1N_0 - k'n_0N_1$$

where n_0 and N_0 are the ground state populations of Tm and Ho, and kN_0 and $k'n_0$ equal to p_{23} and p_{32} given in (9.1.1) respectively. By adding these equations we obtain the rate equation for the combined manifolds of Tm and Ho, $N = n_1 + N_1$.

$$\dot{N} = (\dot{n}_1 + \dot{N}_1) = -\left(\frac{n_1}{\tau_{Tm}} + \frac{N_1}{\tau_{Ho}}\right) \quad (9.4.2)$$

This rate is independent of k and k' . At thermal equilibrium since the fraction of excited Tm ions and excited Ho ions remains fixed we can write the following:

$$N_1 = \alpha N, n_1 = \beta N ; \alpha + \beta = 1 \quad (9.4.3)$$

Substituting these relations into equation (9.4.2) we obtain the equation for exponential decay of the combined manifolds of Tm and Ho

$$\dot{N} = (\dot{n}_1 + \dot{N}_1) = -\left(\frac{\beta}{\tau_{Tm}} + \frac{\alpha}{\tau_{Ho}}\right)N \quad (9.4.4)$$

Equation (9.4.4) shows that the decay of the combined system occurs at a rate which is linear combination of the intrinsic Tm and Ho decay rates. We expect that the thermalization within each manifold to be faster than the thermalization between two manifolds, therefore when thermal equilibrium is reached between Tm and Ho ions, the emission across the spectrum should have the same decay

time. In fact equation (9.4.4) agrees with equation (9.1.9). The experimental evidence seems to confirm the validity of the present model which implies the existence of thermalization between the 3F_4 level of Tm and the 5I_7 level of Ho. Indeed, the decay patterns corresponding to the Tm and Ho emissions present different behaviors initially, but after a certain interval of time, become the same, realizing the thermalization condition. The interval of time preceding thermalization decreases with increasing temperature. The common value of the lifetime is close to the one of Ho, implying that $\alpha \approx 1$ and $\beta \approx 0$ in (9.4.4).

The amplitudes of the exponential decays of 1.7 and 2.1 μm emissions vary, as expected, according to the ratio $e^{\Delta E/kT}$ where the effective energy gap was found to be $\Delta E \approx 364 \text{ cm}^{-1}$. At temperatures lower than 100K we observed a deviation from this exponential behavior, which we attributed to the fact that the ions may have been heated by the absorption of light to temperatures greater than that of the lattice.

REFERENCES (Chapter 9)

- 1) Optical Interactions in Solids, B. Di Bartolo, John Wiley and Sons, Publishers, New York, 1968.
- 2) G. Armagan, A. M. Buoncristiani and B. Di Bartolo, Energy Transfer and Thermalization in YAG : Tm, Ho, to appear in J. of Luminescence.

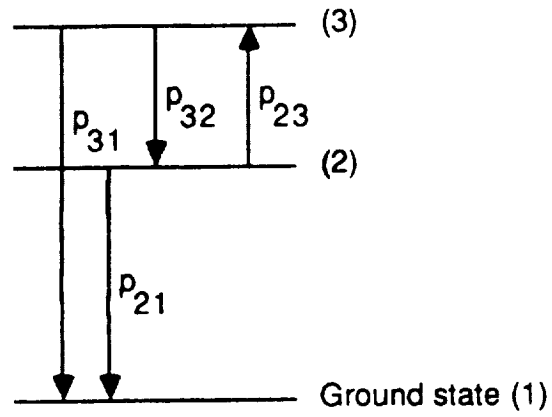


Fig. 9.1 Three level system with two metastable states.

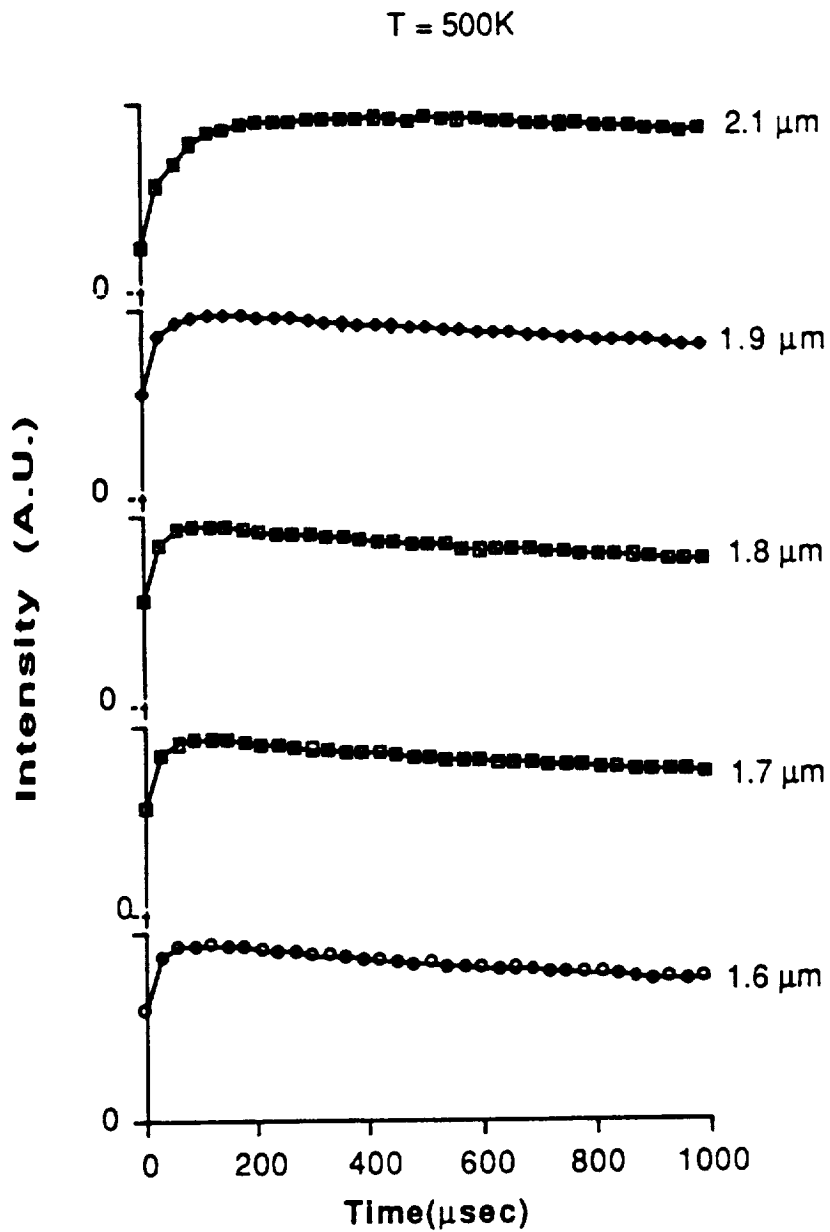


Fig. 9.2 (a) Emission patterns at early times of the decay of the infrared emission of $\text{LiYF}_4 : \text{Tm}^{3+}(5\%), \text{Ho}^{3+}(.2\%)$ at various wavelengths for 500K (excitation is into the $^3\text{H}_4$ level of Tm).

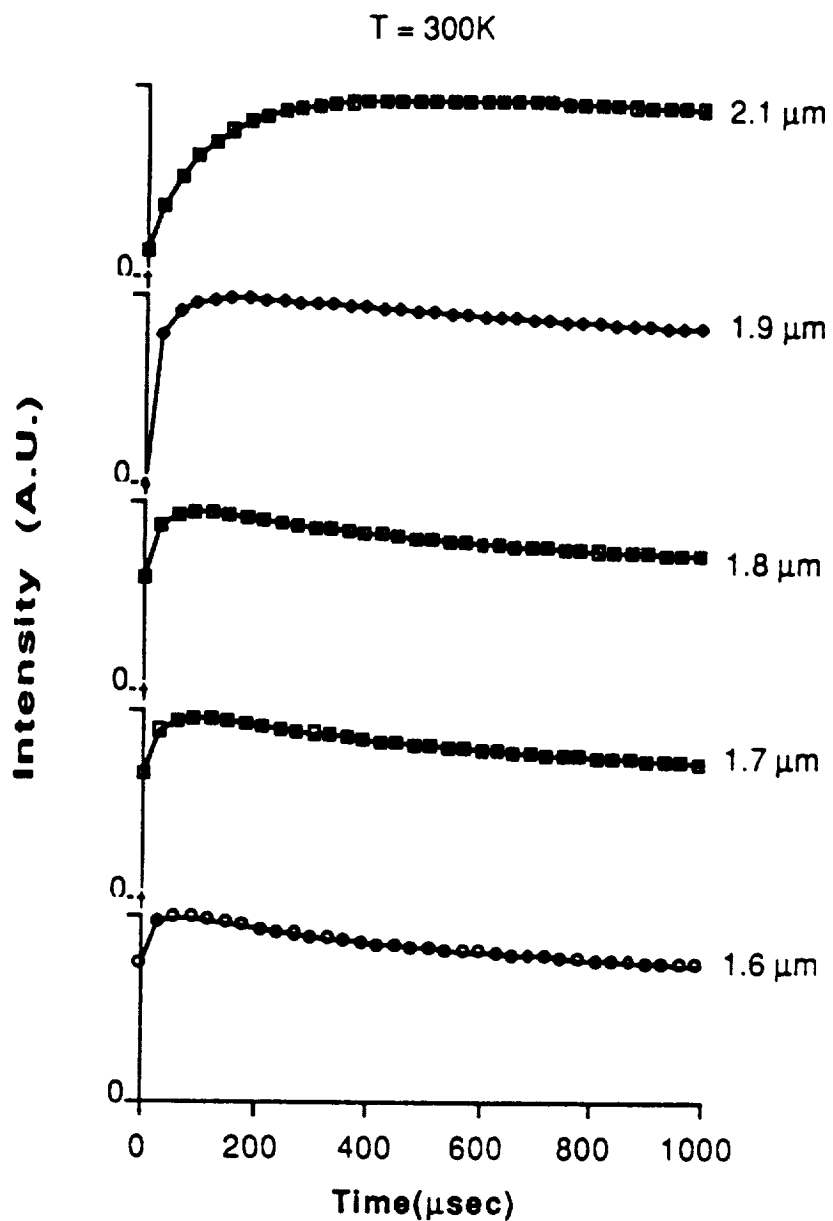


Fig. 9.2 (b) Emission patterns at early times of the decay of the infrared emission of $\text{LiYF}_4 : \text{Tm}^{3+}(5\%), \text{Ho}^{3+}(.2\%)$ at various wavelengths for 300K (excitation is into the $^3\text{H}_4$ level of Tm).

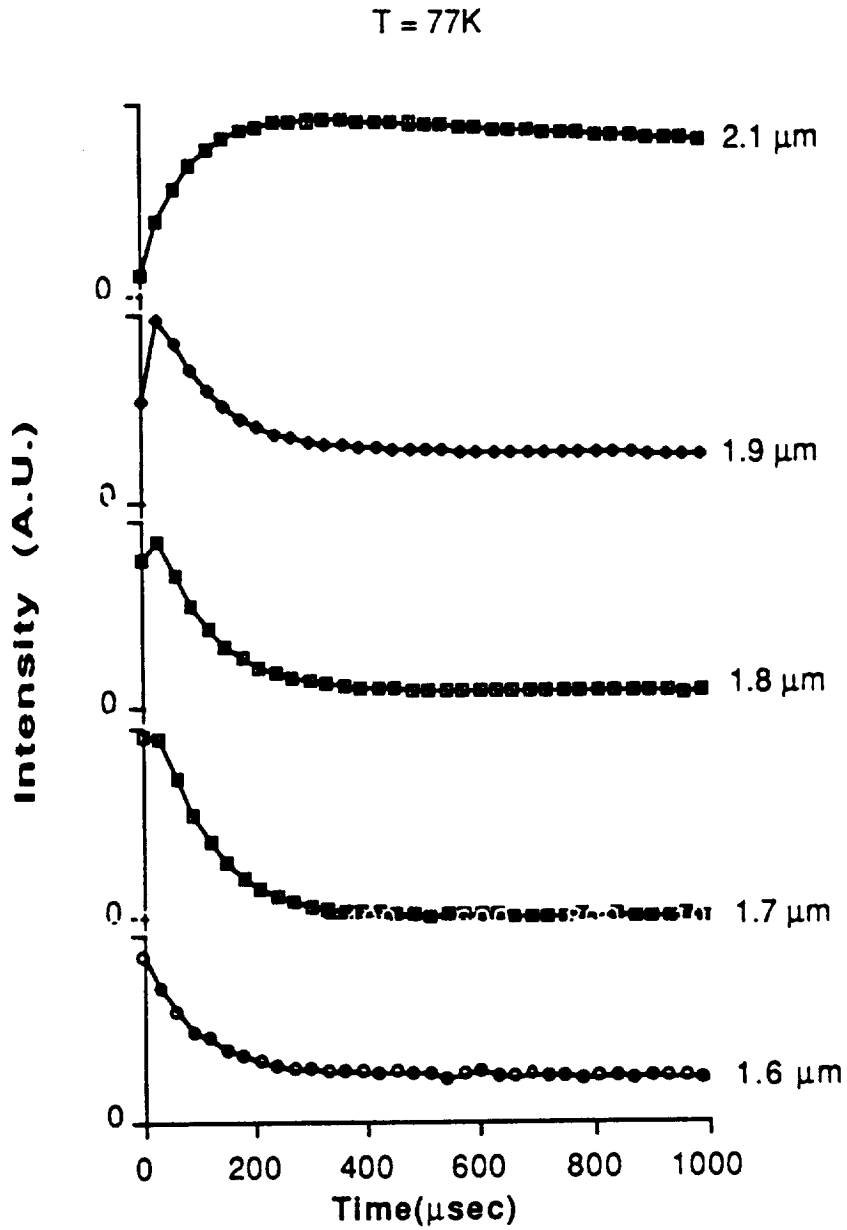


Fig. 9.2 (c) Emission patterns at early times of the decay of the infrared emission of $\text{LiYF}_4 : \text{Tm}^{3+}(5\%), \text{Ho}^{3+}(.2\%)$ at various wavelengths for 77K (excitation is into the $^3\text{H}_4$ level of Tm).

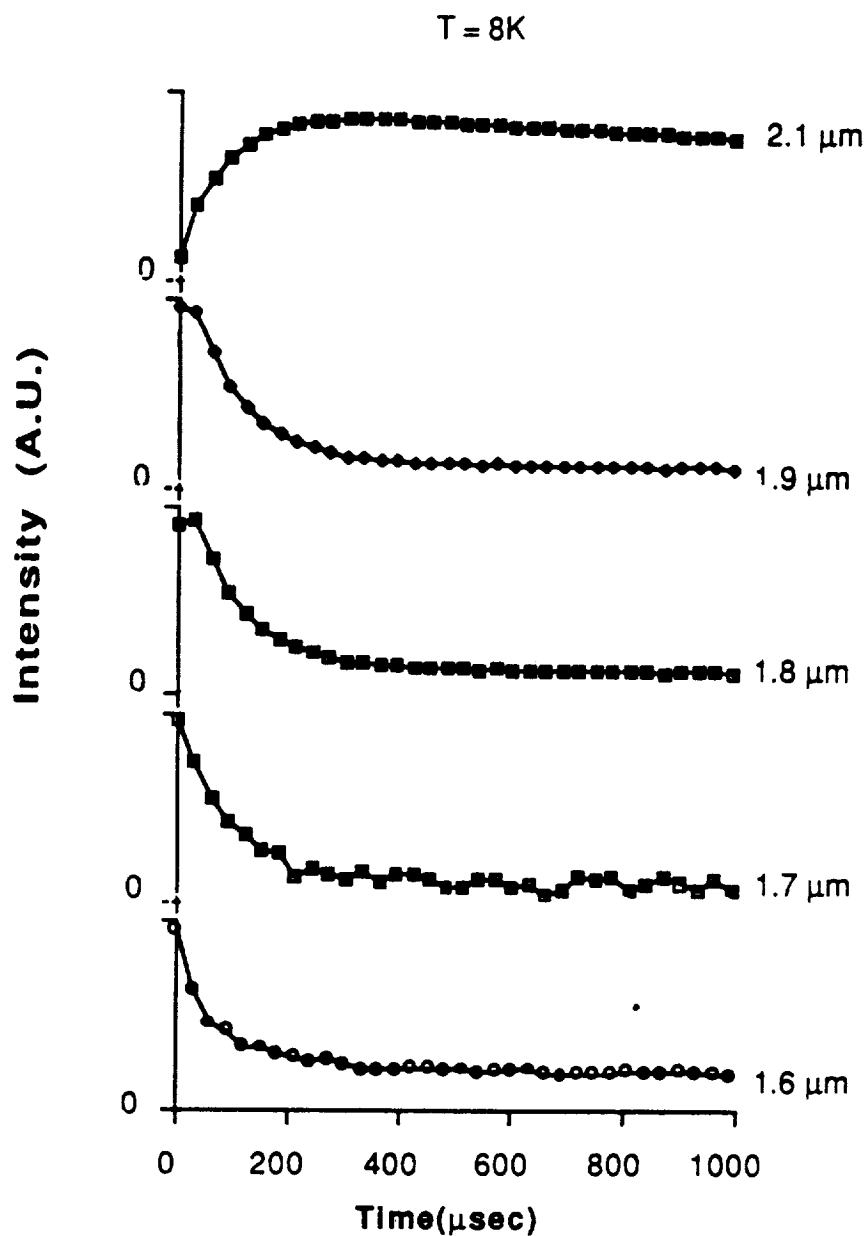


Fig. 9.2 (d) Emission patterns at early times of the decay of the infrared emission of $\text{LiYF}_4 : \text{Tm}^{3+}(5\%), \text{Ho}^{3+}(.2\%)$ at various wavelengths for 8K (excitation is into the $^3\text{H}_4$ level of Tm).

10. CONCLUSIONS AND SUGGESTIONS FOR THE FUTURE WORK

This thesis reports on a study of the temperature dependence of the luminescent characteristics of Tm^{3+} and Ho^{3+} ions in LiYF_4 , and the $(\text{Tm})\ ^3\text{F}_4 \leftrightarrow (\text{Ho})\ ^5\text{I}_7$ energy transfer. The transfer occurs in both directions and thermal equilibrium between the Tm ions in the $^3\text{F}_4$ level and the Ho ions in the $^5\text{I}_7$ level is reached. We observed that the condition for the thermal equilibrium is not achieved immediately upon excitation. The time required for the equilibrium is found to be temperature dependent as shown in Fig. 9.2. During the initial time interval emission at different wavelengths present different patterns, but once the system reaches the thermal equilibrium emission across the spectrum shows the same decay pattern.

We can make the following considerations regarding the nature of the energy transfer process between the Tm and Ho ions. We can safely assume that this transfer is not due to the Dexter-type (reference # 7 of chapter 2) process. The Dexter process, according to our calculations of the previous section, would produce a transfer that accelerates at low temperatures. The experimental evidence provided by Figures 9.2 a to d indicates that the thermalization process sets in at earlier times for higher temperatures. The energy transfer process is therefore controlled by phonon assisted mechanism that responsible for its faster rate at higher temperatures and for the existence of the backward transfer from Ho to Tm. The interplay of the forward and backward transfers determines the thermalization condition observed in this system.

The following tasks are suggested for future work on these materials:

- (1) To make the continuous luminescence and the lifetime measurements by exciting each energy level selectively.
- (2) To make the excitation spectrum measurements at low temperatures, such as liquid nitrogen temperature.
- (3) To make the excitation spectrum under pulsed excitation to get better understanding of the transient features of the decays.
- (4) To study concentration dependence of the $^3F_4 \leftrightarrow ^5I_7$ energy transfer.
- (5) To compare the present measurements with similar measurements made on other crystals, such as YAG (Yttrium Aluminum Garnet) and Germanate crystals, doped with Tm and Ho ions.



Report Documentation Page

1. Report No. NASA CR-187578		2. Government Accession No.		3. Recipient's Catalog No.	
4. Title and Subtitle Energy Transfer Processes Between Tm ³⁺ and Ho ³⁺ in LiYF ₄			5. Report Date July 1991		
			6. Performing Organization Code		
7. Author(s) Gönül Özen			8. Performing Organization Report No.		
			10. Work Unit No. 590-31-31-02		
9. Performing Organization Name and Address Boston College Department of Physics Chestnut Hill, MA 02167-3811			11. Contract or Grant No. NAG1-955		
			13. Type of Report and Period Covered Contractor Report		
12. Sponsoring Agency Name and Address National Aeronautics and Space Administration Langley Research Center Hampton, VA 23665-5225			14. Sponsoring Agency Code		
			15. Supplementary Notes Langley Technical Monitor: Phil Brockman Final Report The information presented in this report was offered as a thesis in partial fulfillment of the requirements for the Degree of Doctor of Philosophy in the Graduate School of Arts and Sciences, Boston College, February 1991.		
16. Abstract This work consists of a detailed study of the spectroscopic properties of the crystal LiYF ₄ doped with Thulium (Tm) and Holmium (Ho) ions. The purpose of this study is to understand the basic processes that regulate the transfer of energy between these two ions in this crystal. In this system Tm is considered the donor ion and Ho the acceptor ion. Spectral data were obtained on three samples available: LiYF ₄ :Tm ³⁺ (.5%), LiYF ₄ :Ho ³⁺ (1%), and LiYF ₄ :Tm ³⁺ (.5%), Ho ³⁺ (.2%). These data, which include absorption, luminescence, excitation and the response to pulsed excitation in a wide range of temperatures, have allowed us to look at the dynamics of the energy transfer process by considering the kinetic evolution of the emission of the two ions (donor and acceptor) involved in the process and the basic spectroscopic properties related to them. This inclusive approach has led to the validation of our physical model. It was of great interest to find that the energy transfer processes between the ³ F ₄ spectral manifold of the Tm ion and the ⁵ I ₇ spectral manifold of the Ho ion cause a thermal equilibration of the excitation in these two manifolds. This fact has important implications for the laser applications of this system.					
17. Key Words (Suggested by Author(s)) Spectroscopy, Tunable Lasers, Laser Materials, Thulium, Holmium			18. Distribution Statement Unclassified - Unlimited Subject Category 36		
19. Security Classif. (of this report) Unclassified		20. Security Classif. (of this page) Unclassified		21. No. of pages 203	22. Price A10



